Rockefeller University
Digital Commons @ RU

Student Theses and Dissertations

2020

A Network Approach to Understanding miRNA Regulation in Adipose Tissue

Sean O'Connor

Follow this and additional works at: https://digitalcommons.rockefeller.edu/student_theses_and_dissertations

 Part of the Life Sciences Commons

A NETWORK APPROACH TO UNDERSTANDING MIRNA REGULATION IN ADIPOSE TISSUE

A Thesis Presented to the Faculty of

The Rockefeller University

in Partial Fulfillment of the Requirements for

the degree of Doctor of Philosophy

by

Sean O'Connor

June 2020

© Copyright by Sean O’Connor 2020

A NETWORK APPROACH TO UNDERSTANDING MIRNA REGULATION IN ADIPOSE TISSUE

Sean O'Connor, Ph.D.

The Rockefeller University 2020

Adipose tissue is a complex organ that is essential for lipid storage and energy homeostasis in mammals. While transcription factors that govern adipogenesis, inflammation, non-shivering thermogenesis, and endocrine function in fat tissue have been well-described, comparatively less attention has been given to post-transcriptional regulators. Here, we employ two contrasting approaches to identify miRNAs that influence adipocyte phenotype. First, miRNAs were sequenced from 6 fat pads, primary preadipocytes, and primary mature adipocytes. Comparative analyses of abundance across adipose tissue type and stage of differentiation revealed a number of miRNAs that influence key metabolic processes. miR-335 inhibited adipogenesis, miR-192 promoted pro-thermogenic and pro-inflammatory pathways, and miR-338 upregulated a variety of genes involved in both lipogenesis and lipolysis/β-oxidation. Although most effects on mRNA abundance were modest, these candidates and others identified in the analysis provide a foundation for further study.

The second portion of this thesis focuses on network-based approaches to describe miRNA regulators in adipose tissue with an emphasis on miRNA binding activity. Most notably, we used Ago HITS-CLIP to comprehensively map mRNA:miRNA interactions in brown and white fat, revealing 21,281 unique miRNA binding sites in 6,717 genes. Most binding sites were shared between brown and white fat, although reads per binding site and reads per gene varied

substantially. Targets for each miRNA were ranked to generate a catalog of miRNA binding activity. The miR-29 family emerged as a top regulator of adipose tissue phenotype with multiple binding sites in the leptin 3'-UTR that were confirmed with luciferase assay validations. miR-29 gain and loss-of-function modulated leptin mRNA and protein levels in primary adipocytes, and miR-29 abundance inversely correlated with leptin levels in adipose tissues. This work represents the only experimentally generated miRNA targetome in adipose tissue and identifies the first known post-transcriptional regulator of leptin.

Dedicated to Nicholas O'Connor

ACKNOWLEDGMENTS

I want to begin by thanking my PhD advisor, Paul Cohen, for the continued mentorship and guidance over the last 5 years. Paul taught me how to ask the right questions, how to design the right experiments, how to stay motivated if those experiments failed, and ultimately how to craft my data into a compelling story. As one of the inaugural members of the Cohen lab, I've had the chance to watch Paul grown the lab from a couple of students and an empty row of benches to what it is today. I'm excited to see what the future holds for Paul and the rest of the team! I also want to thank Jeff Friedman and Charlie Rice, two members of my committee who have provided insight and guidance that played an essential role in my project.

Many of the experiments conducted during my PhD were performed in collaboration with scientists here at Rockefeller, and at outside institutions. The HITS-CLIP work was the result of a multi-year effort with Elisabeth Murphy, a graduate student in Robert Darnell's group. From the moment Elisabeth brought up the idea of using HITS-CLIP on fat tissue during our first year in the program, to the last-minute scrambling to finish figures in time for my final committee meeting, Elisabeth's expertise, skills, and friendship have been instrumental. The miRhub work, and a significant portion of the miRNA analysis and interpretation, was the result of a collaboration with Praveen Sethupathy and Matt Kanke at Cornell University. Without their experience working with miRNAs, both bioinformatically and experimentally, the research presented here would not have been possible.

I also want to thank every member of the Cohen lab, all of whom have influenced my work, either directly or indirectly. François Marchildon provided essential help with bioinformatic analyses, Jingyi Chi and Chan Hee Choi helped to optimize conditions for primary adipocyte experiments, and Sarah Szwed contributed to miRNA luciferase assay validations. The work

presented here would also not have been possible without help from others at Rockefeller, including Tom Carroll from the bioinformatics core, Chingwen Yang at the genome editing center, and Connie Zhao at the genomics resource center. Beyond the direct scientific contributions, members of the Dean's office, including Sidney Strickland, Emily Harms, Cristian Rosario, and Stephanie Fernandez have ensured that Rockefeller is a welcoming and productive place for graduate students.

Lastly, I want to thank my friends and family for encouragement throughout this process. My fellow graduate students, Ryan Farrell, Leo Yuan, Amelia Dunn, Sarah Ackerman, and others have been a great support network over the last 5 years. I also want to thank Yang Ling, my girlfriend, who has had the patience to listen to my failures and successes, and without whom I couldn't imagine making this journey.

TABLE OF CONTENTS

LIST OF FIGURES

LIST OF TABLES

LIST OF ABBREVIATIONS

BMI	Body mass index
BAT	Brown adipose tissue
UCP1	Mitochondrial uncoupling protein 1
WAT	White adipose tissue
sWAT	Subcutaneous white adipose tissue
vWAT	Visceral white adipose tissue
Wt	Wild-type
miRNA	microRNA
pri-miRNA	Primary microRNA
pre-miRNA	Preliminary miRNA
RISC	RNA induced silencing complex
Ago	Argonaute
RBP	RNA binding protein
aWAT	Axillary white adipose tissue
iWAT	Inguinal white adipose tissue
eWAT	Epididymal white adipose tissue
mWAT	Mesenteric white adipose tissue
cWAT	Cold-exposed inguinal white adipose tissue (beige fat)
iBAT	Interscapular brown adipose tissue
HITS-CLIP	High-throughput sequencing of RNA isolated by crosslinking immunoprecipitation
CDS	Coding sequence
3'-UTR	Three prime untranslated region
5'-UTR	Five prime untranslated region
PAR-CLIP	Photoactivatable ribonucleoside-enhanced-CLIP
CLASH	Cross-linking and sequencing of hybrids
iCLIP	Individual-nucleotide resolution-CLIP
CIMS	Cross-linking induced mutation sites
Lep 1	Leptin binding site 1 (miR-29)
Lep 2	Leptin binding site 2 (miR-29)
ECM	Extracellular matrix
GO	Gene ontology

CHAPTER 1: Introduction

1.1 The role of adipose tissue in metabolism

The catabolism of lipids serves as a key source of energy production for most living organisms; however, an excess of free lipids can be toxic (Schaffer, 2003). Vertebrates, and a number of other multicellular animals, have developed specialized cells to sequester surplus lipids, called adipocytes (Ottaviani et al., 2011). During periods of caloric excess, adipocytes take up lipids from the circulation and store them in densely packaged droplets in the form of triglycerides (Olzmann and Carvalho, 2019). When an organism's energy needs increase, triglycerides are mobilized by a series of highly regulated hydrolytic reactions, which liberate free fatty acids to be used an energy substrate (Thompson et al., 2010). Lipid droplets are a remarkably efficient and compact form of energy storage, containing approximately 9 calories per gram, in contrast to glycogen which can only store 4 calories per gram (Kanter, 2018). As a result, a healthy human with 20-25 pounds of fat is provided with well over 1 month of energy reserves.

Adipose tissue is capable of undergoing two types of growth: hypertrophy and hyperplasia. Hypertrophy is the process by which individual fat cells increase in size, and is the predominant form of adipose expansion in humans (Rosen and Spiegelman, 2014). Hyperplasia, by contrast, occurs as progenitor cells differentiate into new, mature adipocytes. In humans, subcutaneous fat has a limited capacity for hyperplasia compared to adipose depots below the waist and in the visceral cavity (Tchoukalova et al., 2010; Drolet et al., 2008). Regardless of the method of expansion, however, excess adiposity has emerged as a global health threat. The rate of obesity in the U.S., defined as a body mass index (BMI) of >30.0 kg/m^2, reached approximately 40% in 2017 (Hales et al., 2017), and continues to increase.

Worldwide, 13% of adults are obese, while 39% are overweight (BMI = 25.0-29.9). Perhaps most indicative of this alarming trend, overweight rates in children have more than quadrupled from around 4% in 1975 to over 18% in 2016 (WHO, 2018).

Obesity lies at the center of a variety of comorbidities, including hypertension, stroke, dyslipidemia, type 2 diabetes, heart disease, stroke, gallbladder disease, osteoarthritis, sleep apnea, respiratory diseases and many types of cancer (Khaodhiar et al., 1999). Obese individuals require, on average, more medication, more hospital visits, and a greater cost of care per visit. Beyond the toll on human wellbeing, the economic cost is significant. As a result of obesity, the U.S spends an additional $147 billion - $210 billion on healthcare per year (Biener et al., 2017), and the average obese employee is less productive by an estimated $506 each year (Cawley et al., 2007; Gates et al., 2008).

1.1.1 Contrasting brown and white fat

For most of recorded human history, it was believed that fat tissue served simply as a reservoir for excess energy, albeit a reservoir that could be detrimental to health when overloaded. In 1969, Smith and Horwitz discovered that a subtype of fat, called brown adipose tissue (BAT), was also capable of producing heat in humans and mice (Smith and Horwitz, 1969). BAT generates heat by expressing a protein called mitochondrial uncoupling protein 1 (UCP1), which shuttles protons across the inner-mitochondrial membrane, an integral component of a process called non-shivering thermogenesis. The release of protons across the membrane generates thermal energy as a byproduct, thereby effectively converting lipids and carbohydrates into heat (Ricquier and Kader, 1976). Under certain conditions, white adipose tissue (WAT) can also contain UCP1 expressing cells, called beige adipocytes. Beige fat is

readily produced in cold-exposed mice, and seems to be similarly activated in humans following cold exposure or catecholamine stimulation (Kiefer, 2017).

In humans, the presence of BAT is correlated with a variety of improved health outcomes. Humans with detectible, active BAT weigh an average of 4 kg less than those without (Lee et al., 2010), and obese humans have reduced BAT compared to lean controls (Orava et al., 2013). BAT is associated with decreased arterial inflammation, reduced liver triglyceride content, and lower levels of atherosclerosis in male patients (Nam and Jun, 2017). Other studies have shown that BAT-positive individuals are less likely to develop type 2 diabetes (Cypess et al., 2009) and have reduced visceral and subcutaneous fat tissue (Brendle et al., 2018). Human derived adipocyte precursors, when differentiated into beige fat cells *in vitro* and transplanted into mice, result in improved glucose tolerance and metabolic function (Min et al., 2016).

In contrast, an excess of WAT is generally associated with negative health outcomes. WAT can be broadly grouped into two categories with differing metabolic behaviors: subcutaneous white adipose tissue (sWAT) and visceral white adipose tissue (vWAT). The contrast between these two types of fat is significant, with vWAT being a far greater culprit in obesity-associated metabolic dysregulation. vWAT expansion is strongly correlated with poor glucose tolerance, hyperinsulinemia, diabetes risk and dyslipidemia (Bjorntorp, 2000; Despres et al., 1985). Humans with vWAT adiposity, but not necessarily sWAT adiposity, are more likely to suffer from a range of cardiovascular diseases, including coronary artery disease, endothelial dysfunction and peripheral arterial disease (Sharma et al., 2001; Planas et al., 2001; Mulyadi et al., 2001). Accordingly, type 2 diabetes and cardiovascular disease correlate much better with vWAT levels than BMI, and adjusting for vWAT levels normalizes the sex-based

difference in cardiovascular disease risk profiles for men and women (Ibrahim, 2010). Fortunately, weight loss in humans tends to occur first, and most dramatically, from vWAT depots (Armellini et al., 1991), which may explain the dramatic health benefits observed following modest weight loss in obese patients (Goodpaster et al., 2010).

At the cellular level, visceral adipocytes tend to be more insulin resistant, larger in size, and less effective at taking up free fatty acids and triglycerides from the circulation (Misra and Vikram, 2003). Visceral adipocytes also secrete free fatty acids more readily than subcutaneous adipocytes, linking enhanced lipolysis to the development of hepatic steatosis via the hepatic portal vein (Imbeault et al., 2000; Rytka et al., 2011). At the molecular level, visceral adipocytes express lower levels of pro-thermogenic transcriptional regulators, including Prdm16 and Pgc1α (Inagaki et al., 2016), and higher levels of pro-inflammatory markers such as Saa3, Retn and Agt (Cohen et al., 2014; Scheja and Heeren, 2019). Visceral adipocytes also contain a higher density of glucocorticoid receptors and androgen receptors (Rebuffe-Scrive et al., 1985; Freedland, 2004), and a lower density of estrogen receptors compared to subcutaneous adipocytes (Pedersen et al., 1996). Variability in the local environment further exacerbates differences in adipocyte function. vWAT depots typically contain an abundance of pro-inflammatory immune cells, including more M1-polarized macrophages (Trim et al., 2018), contributing to a state of chronic inflammation, especially in obese individuals (Weisberg et al., 2003). By comparison, sWAT is more highly innervated, which facilitates the development of beige adipocytes via sympathetic stimulation (Chi et al., 2018).

1.1.2 The adipose secretome

One of the key means by which fat influences whole-body metabolism is the secretion of adipose-derived polypeptides and other signaling factors, called adipokines. In general, brown adipocytes release adipokines with metabolically beneficial effects, while those secreted by visceral adipocytes tend to be metabolically harmful, although this trend does not always hold true. An adipocyte's secretome can be influenced by a number of factors, including adipocyte cell size (Skurk et al., 2007), age (Prostek et al., 2016) and immune environment (Eheim et al., 2014). Several adipokines, many of which are produced by both adipose and other tissues, are reviewed below:

Adiponectin: Adiponectin is a 30 kDa polypeptide produced by both brown and white adipocytes (Wang et al., 2015) that can enter the circulation in several different oligomeric conformations. Large fat cells under obesogenic conditions secrete low levels of adiponectin, while levels are high in lean or fasted animals (Cawthorn et al., 2014). Adiponectin binds to two receptors, AdipoR1 and AdipoR2 to repress gluconeogenesis in liver, increase fatty acid oxidation in skeletal muscle, and reduce inflammation in the vasculature, heart, lung and colon (Fang and Judd, 2018). Adiponectin also preserves insulin sensitivity when over-expressed in obese mice, and conversely, leads to insulin resistance when deleted in lean mice (Scheja and Heeren, 2019).

Leptin: See section 1.1.3

Neuregulin 4 (Nrg4): Nrg4 is a 9 kDa polypeptide, produced primarily by brown adipocytes, that signals to liver to promote insulin sensitivity and reduce hepatic steatosis. Nrg4 binds to Erb3 and Erb4 to regulate the activity of liver X receptor and sterol regulatory element-binding protein (SREBP) (Wang et al., 2014). Nrg4 is also capable of acting in a paracrine fashion on endothelial cells within BAT (Nugroho et al., 2018) and may be involved in enhancing BAT innervation (Christian, 2015).

Fibroblast growth factor 21 (Fgf21): Fgf21 is 22 kDa circulating polypeptide produced by liver that increases hepatic gluconeogenesis and promotes ketogenesis in fasting mice, while also acting on adipose to increase insulin sensitivity (Scheja and Heeren, 2019). Adipocytes also express Fgf21, which can act in a paracrine fashion to increase thermogenesis and promote beige fat cell development in WAT (Huang et al., 2017). Adipose-secreted Fgf21, primarily from brown adipocytes, is also capable of entering the circulation and is thought to contribute to improved glucose tolerance and reduced cardiac hypertrophy (Scheja and Heeren, 2019).

Interleukin (IL-6): IL-6 is a 25 kDa polypeptide produced by several cell types in BAT and WAT that is capable of both pro-inflammatory and anti-inflammatory effects. Adipose-derived IL-6 is increased during obesity and may regulate lipolysis and insulin sensitivity in a paracrine manner (Eder et al., 2009). IL-6 is also capable of acting as an endocrine factor by signaling to the CNS to decrease feeding and improve glucose tolerance (Timper et al., 2017).

Adipsin: Adipsin, the first adipokine discovered in 1987 (Cook et al., 1987), is a 28 kDa polypeptide that improves β-cell function and promotes insulin secretion (Lo et al., 2014).

Adipsin acts, at least in part, by catalyzing the formation of the complement factor C3a, which acts directly on pancreatic islets to stimulate insulin production (Lo et al., 2014).

Retinol-binding protein 4 (RBP4): RBP4 is a 22 kDa polypeptide that is secreted from liver and visceral adipocytes, and to a lesser extent subcutaneous and brown adipocytes (Kloting et al., 2007). RBP4 induces insulin resistance and inflammation in muscle and fat by two primary mechanisms. The first involves signaling to NF-κB and MAPK in adipose-resident macrophages to increase T-cell activation (Moraes-Vieira et al., 2016), and the second is by binding to the STRA6 receptor which causes downstream insulin resistance (Berry et al., 2013). It is unclear to what extent adipose secreted RBP4 acts in an endocrine role, since mice with a liver-specific deletion of RBP4 seem to lack circulating RBP4. However, direct modulation of RBP4 in adipocytes significantly influences insulin sensitivity and inflammation in adipose tissue, indicating the importance of RBP4's paracrine action (Scheja and Heeren, 2019).

Resistin: Resistin is a 12.5 kDa polypeptide secreted from monocytes and visceral adipocytes, and to a lesser extent subcutaneous and brown adipocytes, that signals to a variety of organs to cause insulin resistance (Steppan and Lazar, 2004). Resistin levels are increased in obese humans and mice, although secretion in humans appears to arise largely from monocytes rather than adipocytes (Schwartz and Lazar, 2011). Resistin acts, in part, by binding to TLR4, causing increased lipid storage and inflammation in liver (Tan et al., 2015).

Tumor necrosis factor α (TNFα): TNFα, a 25.6 kDa polypeptide, was one of the earlier adipokines to be discovered. TNFα induces a state of insulin resistance and poor glucose metabolism in adipose tissue and has a generally pro-inflammatory effect (Hotamisligil et al., 1993). Both macrophages and adipocytes are capable of producing and secreting TNFα; however, tissue resident macrophages appear to be responsible for most of the increase of TNFα in obesity. Interestingly, when TNFα was ablated in mouse macrophages, mice were still insulin resistant, suggesting that adipocyte-derived TNFα plays an important role in paracrine signaling (Cawthorn and Sethi, 2008).

Monocyte chemoattractant protein-1 (MCP1): MCP1 is a 13 kDa chemokine that is secreted from a variety of tissues, including adipocytes. Expression and secretion are highest in visceral adipocytes, followed by subcutaneous and brown adipocytes (Bruun et al., 2005). MCP1 acts as a chemotaxic factor that binds to the CCR2 receptor to recruit monocytes to sites of inflammation (Deshmane et al., 2009). Obesity in humans, particularly visceral obesity, increases MCP1 mRNA levels and corresponding tissue macrophage and monocyte infiltration (Harman-Boehm et al., 2007). Increased circulating MCP1 has been shown to correlate with a number of poor metabolic health outcomes, including type II diabetes, cardiovascular disease, poor glucose metabolism and dyslipidemia (Panee, 2012).

12,13-dihydroxy-9Z-octadecenoic acid (12,13-diHOME): 12,13-diHOME is a lipid based signaling molecule, or lipokine, that is produced by brown adipocytes and acts in both a paracrine and endocrine manner (Scheja and Heeren, 2019). In mice and humans, 12,13-diHOME levels are increased in response to cold and appear to facilitate lipid uptake into

brown adipocytes by increasing translocation of fatty acid transporters into the cellular membrane. Injection of exogenous 12,13-diHOME reduces circulating lipid levels in mice (Lynes et al., 2017). Additionally, 12,13-diHOME secretion from brown adipocytes increases in response to exercise, leading to enhanced fatty acid uptake and oxidation in muscle (Stanford et al., 2018).

Palmitoleate: Palmitoleate is a lipokine, secreted primarily by white adipocytes, that is produced in conjunction with de-novo lipogenesis in adipocytes (Cao et al., 2008). Palmitoleate acts, in part, by integrating into the endoplasmic reticulum (ER) of macrophages, resulting in a decreased sensitivity to ER stress (Cimen et al., 2016). Palmitoleate also signals through AMP-activated protein kinase to increase the expression of anti-inflammatory genes, decrease the expression of pro-inflammatory genes, and shift macrophages towards an M2 state (Chan et al., 2015). Dietary supplementation of palmitoleate in mice is associated with reduced liver inflammation, increased glucose sensitivity and reduced atherosclerosis (Guo et al., 2012; Cao et al., 2008; Cimen et al., 2016).

1.1.3 What we know about leptin

In 1950, an obese strain of mice was discovered in the lab of George Snell. The obese phenotype was attributed to a recessive mutation in an unknown gene that Snell's group named *obese*, or *ob* (Ingalls et al., 1950). 16 years later, a similar obese strain of mice with rapid onset of diabetes was discovered by Doug Coleman (Hummel et al., 1966). This strain, and the gene responsible, was named *diabetes*, or *db*. Coleman's lab proceeded to conduct a series of parabiotic experiments in which the circulations of mice from different genetic backgrounds

were linked together. They found that blood from lean wild-type (Wt) and *db/db* mice could dramatically reduce food intake and body weight of *ob/ob* mice. In experiments linking *db/db* mice to lean Wt mice, hypophagia in the Wt mice led to starvation and death (Coleman, 1978). Based on these findings, Coleman hypothesized that the *ob* gene encoded a circulating, anti-obesity factor, and that this factor's receptor was absent in the *db* mice. Previous studies had shown that rats with lesions in certain hypothalamic regions were unable to properly regulate food intake, hinting that *ob* could be functioning as an endocrine factor that signaled to the central nervous system by binding to *db* receptors in the hypothalamus (Hervey, 1959).

Years later, Jeffrey Friedman's lab at The Rockefeller University employed a system of positional cloning that identified the precise location of the *ob* gene. Friedman's group discovered an adipose-specific mRNA originating from the *ob* locus and showed that the *ob* gene in mutant mice contained a nonsense mutation in the 105th amino acid that caused a premature stop codon (Zhang et al., 1994). Injection of recombinant *ob* gene product, later named leptin, had a dramatic weight-lowering effect on *ob* mutant mice, but not *db* mutant mice (Halaas et al., 1995). Over the next several years, it was confirmed that *db* encoded leptin's receptor, Ob-R, a member of the gp130 family of cytokine receptors (Vaisse et al., 1996). As hypothesized earlier, the mutant isoform responsible for obesity in *db/db* mice, the Ob-Rb receptor, is highly expressed in several hypothalamic nuclei that influence hunger and satiety in mammals (Fei et al., 1997; Vaisse et al., 1996).

Leptin's best described role is that of a physiological rheostat, regulating feeding behavior and energy expenditure via the central nervous system (Kelesidis et al., 2010). In the arcuate nucleus of the hypothalamus, leptin binds to the Ob-Rb receptor and stimulates anorexigenic POMC neurons, promoting the synthesis of α-MSH which binds to melanocortin

receptors to decrease body weight (Zhou and Rui, 2013). In parallel, leptin inhibits production of neuropeptide Y in orexigenic AgRP neurons (Morris and Rui, 2009). Outside of the hypothalamus, leptin acts as a pro-inflammatory cytokine by binding to receptors on monocytes, neutrophils, natural killer cells and other immune cells (Fernandez-Riejos et al., 2010). Leptin receptors are found on a variety of peripheral tissues, including skeletal muscle, pancreas and adipose tissue, although evidence of metabolically relevant signaling in these tissues is limited (Guo et al., 2007).

In general, increased adiposity is associated with increased circulating leptin, and white adipocytes secrete more leptin than brown adipocytes (Perdikari et al., 2018). Leptin levels, however, can change rapidly under certain physiological conditions, and expression is not strictly tied to fat mass (Ahima, 2008). Fasting causes a dramatic decrease in circulating leptin, while re-feeding after a fast results in a rapid rebound that surpasses baseline levels (Kmiec et al., 2005). Likewise, moderate weight loss can induce a significant reduction in circulating leptin, disproportionate to the loss of adipose tissue (Thompson et al., 2015). Independent of adipose tissue mass, leptin levels are influenced by inflammation, showing an increase in response to inflammatory stimuli including IL-1 and lipopolysaccharide (Faggioni et al., 1998; Iikuni et al., 2008). Taken together, these observations suggest a sophisticated set of regulatory mechanisms that control leptin abundance.

Thus far, several transcription factors that modulate leptin transcription have been characterized. AP-2β binds to the leptin promoter, 34-42 bp upstream of the transcriptional start site, and represses expression, resulting in lowered leptin mRNA and protein levels (Fuke et al., 2010). SREBP1 also binds the leptin promoter, 59-64 bp upstream of the transcriptional start site, causing increased transcription (Kim et al., 1998). Additionally, Fosl2 and CEBPα

activate leptin transcription by binding to an enhancer region 4.5 kb upstream of the promoter and a region 217 bp upstream of the transcriptional start site, respectively (Wrann et al., 2012; Miller et al., 1996). While important discoveries, AP-2β, SREBP1, Fosl2, and CEBPα exert only modest changes in leptin transcription, and are likely not the primary drivers controlling leptin abundance.

Recently, a long-noncoding RNA (lncRNA) with more powerful effects on leptin transcription was identified by two groups in parallel. The first group, Lo et al., used RNAseq to identify adipose-specific lncRNAs that were differentially expressed in obesity across several adipose depots (Lo et al., 2018). They identified lnc-leptin, which was necessary for adipogenesis and leptin expression in primary adipocytes *in vitro. In vivo*, mouse iWAT depots injected with ASOs targeting lnc-leptin had reduced leptin mRNA levels compared to controls (Lo et al., 2018). These findings were confirmed by Jeffrey Friedman's lab, who identified the same lncRNA in parallel, which they named lncOb. The study from Friedman's lab generated a lncOb knockout mouse and observed increased weight gain in lean mice and mice with diet induced obesity (DIO), with a corresponding decrease in leptin mRNA and protein levels. Using human GWAS data, they identified a variant in the lncOb genetic locus that correlated with decreased leptin expression and increased BMI in human patients (Dallner et al., 2019). Both studies showed that lnc-leptin/lncOb interacts with LE1, an enhancer region 16 kb upstream of leptin's transcriptional start site that controls leptin expression, in part by binding PPARγ/RXRα (Zhang et al., 2018). These recent studies on lncRNAs, combined with previous work on transcription factors that regulate leptin, demonstrate various mechanisms by which adipocytes can modulate leptin transcription in response to physiological conditions. To date, however, no post-transcriptional regulators of leptin have been identified.

1.2 MicroRNAs

In 1993, Rosalind Lee, Rhonda Feinbaum and Victor Ambros discovered microRNA (miRNA) in C. elegans by identifying two non-protein coding transcripts arising from the *lin-4* locus that regulated *Lin-14*, a gene involved in larval development (Lee et al., 1993). They found that lin-14 protein, but not transcript levels, decreased temporally during larval development, and that the 3'-UTR acted as a crucial negative regulatory element (Wightman et al., 1993). After cloning the *lin-4* locus, they observed that the two *lin-4* transcripts shared complementarity with a region in the 3'-UTR of *lin-14,* suggesting an antisense mechanism of RNA-based post-transcriptional regulation (Lee et al., 1993). Later work, carried out in the labs of David Bartel, Thomas Tuschl, and others, revealed that the *lin-4* transcripts belonged to a large class of small RNAs that were expressed in both invertebrates and vertebrates (Lagos-Quintana et al., 2001; Lau et al., 2001). Furthermore, they found that the sequences of many of these miRNAs were well conserved across a number of species, hinting at their broadly conserved regulatory power (Lau et al., 2001).

Most miRNAs target a wide range of mRNAs, and the effect on each individual target is generally subtle. The significance of a miRNA's regulatory function arises, in many cases, from the ability to regulate multiple members of cellular pathways (Bartel, 2018). The power of a miRNA's regulatory role is most evident in whole-body knockout experiments. A large study conducted by Stephen Cohen's lab showed that knockouts of each of the abundant miRNA families in fruit flies induced an observable phenotype in greater than 80% of mutants (Chen et al., 2014b). Individual studies in mice have shown similar results, with many miRNAs being required for viability. For example, of the 27 best conserved murine miRNA families,

knockout of miR-1, miR-9, miR-34, and miR-124 caused postnatal lethality in most animals (Heidersbach et al., 2013; Shibata et al., 2011 ; Song et al., 2014; Sanuki et al., 2011), while knockout of miR-29, miR-92, and miR-219 caused embryonic lethality in many or most animals (Sassi et al., 2017; Penzkofer et al., 2014; Wang et al., 2017). Of the remaining 27 families, most caused non-lethal phenotypic changes when ablated (Bartel, 2018).

1.2.1 miRNA biogenesis, regulation and decay

MiRNAs are located throughout the genome. About half occur as standalone genes with individual promoters and regulatory regions, and half occur within introns of protein coding genes (Ha and Kim, 2014). MiRNAs are first transcribed by RNA polymerase II (or in some limited cases, RNA polymerase III) to give rise to primary miRNAs (pri-miRNAs), which are several hundred base pairs long (Lee et al., 2004). Pri-miRNAs are then cleaved by a complex of two proteins, Drosha and DGCR8, to produce preliminary miRNAs (pre-miRNA), which are exported into the cytoplasm (O'Brien et al., 2018). Once in the cytoplasm, pre-miRNAs are cleaved by dicer, leaving a mature, double stranded miRNA sequence of approximately 22 base pairs (Lund and Dahlberg, 2006). The final stage in miRNA processing is the loading of one of the two miRNA strands onto the RNA induced silencing complex (RISC) via association with Argonaute (Ago) (O'Brien et al., 2018). Since a mature miRNA duplex is double stranded, only one of two strands loads per RISC. Typically, the strand which has lower thermodynamic stability at the 5’ end is loaded onto Ago and the alternative strand is degraded (Krol et al., 2004; Khvorova et al., 2003). The determination of which strand is preferentially loaded can vary, however, and for some miRNAs both duplex sequences are biologically active (O'Brien et al., 2018).

The biogenesis of miRNAs is regulated by a variety of factors. Transcription of standalone miRNAs is usually controlled by individual promoters, much like any protein coding gene. Other miRNAs are found within polycistronic regions under the control of a single promoter (Lee et al., 2002). Those localized to intronic regions of protein coding genes typically follow the transcriptional pattern of their host gene (Bartel, 2018); however, in some cases these miRNAs can also have their own, distinct promoters (Monteys et al., 2010). Once transcribed, RNA binding proteins (RBPs) are capable of binding to both pri-miRNAs and pre-miRNAs to influence processing by Drosha/DGCR8 and Dicer (Treiber et al., 2017). MiRNAs themselves can bind to pre-miRNAs, their own or others, to enhance or inhibit processing (Zisoulis et al., 2012). Another form of general regulation arises from modulation of the miRNA processing machinery. For example, Drosha/DCGR8 localization (Tang et al., 2010), activity (Wada et al., 2012) and stability (Herbert et al., 2013) can be impacted by posttranslational modifications, resulting in global changes in miRNA levels.

In general, miRNAs are very stable, with an average half-life approximately 10-fold greater than the average mRNA (Gantier et al., 2011). Stability varies by individual miRNA, however, and pulse chase experiments in mammalian cells have suggested that up to 20% of miRNAs have short half-lives (Marzi et al., 2016). There have been several identified mechanisms of miRNA decay. In some cases, exonucleases recognize specific mature miRNA sequences, a process that has been demonstrated in the degradation of miR-382 by RRP41 and XRN1 (Bail et al., 2010). In other cases, exonucleases recognize miRNAs that have been tagged for degradation. This occurs in mouse embryonic stem cells where let-7 family members are tagged with uridine tails, causing recognition by the exonucleases Dis3L2 (Chang et al., 2013). Adenosine tags on the 3’ends of miRNAs can cause either increased stability, or

increased turnover, as seen with mono-adenylated miR-122 stabilization in liver (Boele et al., 2014) and polyadenylated miR-21 degradation (Katoh et al., 2009). Another mechanism of miRNA turnover is caused by Target RNA-Directed MicroRNA Degradation (TDMD), which occurs when a miRNA binds certain targets with high complementarity. In TDMD, the miRNA is typically altered by 3' trimming, or by polyadenylation/polyurdinylation (Fuchs Wightman et al., 2018). In mouse cerebellum, miR-29 has been shown to undergo TDMD after binding to a complementarity region of the *Nrep* transcript (Bitetti et al., 2018).

1.2.2 miRNA target recognition and repression

Canonical binding of miRNAs to targets is driven by a core seed sequence that consists of nucleotides 2-7 of the miRNA, which forms a 6-mer pair with its target. A 7-mer beginning from nucleotide 1 of the miRNA is called a 7-mer-A1 (provided that the first base of miRNA is a T), a pairing of nucleotides 2-8 is called a 7-mer-m8, and a pairing with nucleotides 1-8 is called an 8-mer. 7-mers and 8-mers are more likely to bind with high affinity and confer a high level of repression, although many 6-mers are also physiologically relevant (Bartel, 2018). Beyond the seed sequence, complementarity with downstream regions of the miRNA can also impact affinity, although these regions have only a minor influence on miRNA binding activity (Friedman et al., 2009).

miRNAs are also capable of binding to non-canonical sites, which are defined as sites lacking full complementarity with nucleotides 2-6 of the miRNA. Typically, a large degree of additional nucleotide pairing, outside of the seed, is present in non-canonical sites (Bartel, 2018). Data from a number of Ago-crosslinking experiments, in which miRNAs and their targets are immuneprecipitated, suggest that a large portion of miRNA associations occur with

non-canonical targets (Chi et al., 2009; Spengler et al., 2016; Boudreau et al., 2014; Grosswendt et al., 2014). It appears, however, that most of these non-canonical sites are not functional since miRNA binding events do not typically result in reduced abundance of target genes (Agarwal et al., 2015). There are notable exceptions; however, it is likely that many identified non-canonical sites are the results of transient interactions between miRNAs and potential targets rather than fully functional sites (Chandradoss et al., 2015).

Once a miRNA binds to its target, there are several mechanisms by which that target can be repressed, degraded or sliced (Hausser et al., 2013). When imperfect nucleotide pairing occurs, which is the case for the vast majority of miRNAs in humans and mice, Ago recruits TNRC6. TNRC6 associates with the CCR4-NOT complex, which is directly responsible for deadenylating the mRNAs poly(A) tail and causing degradation (Kuzuoglu-Ozturk et al., 2016). Additionally, the CCR4-NOT complex is capable of recruiting DDX6 and 4E-T, which can act by several mechanisms to inhibit translation (Kuzuoglu-Ozturk et al., 2016; Kamenska et al., 2014; Kamenska et al., 2016). When miRNAs bind 3'-UTR targets, mRNA destabilization appears to be the predominant mechanism-of-action; although, miRNAs binding CDSs are more likely to act via translational inhibition (Hausser et al., 2013). In some cases, miRNAs can also mediate the direct cleavage of their targets by endonuclease activity (Shin et al., 2010; Park and Shin, 2014). In mammals, Ago2 is the only Ago family member that is capable of endonuclease activity, and cleavage generally requires a high degree of complementarity (Jung et al., 2017). Thus far, target cleavage by miRNAs has been described for approximately 20 mRNAs (Bartel, 2018); however, that number is continuing to grow as methods for determining miRNA mechanism-of-action are becoming more sophisticated.

1.2.3 miRNA in adipose tissue

A number of essential cellular processes in adipocytes are regulated, directly or indirectly, by miRNAs. In work from Ronald Kahn's lab, dicer was deleted from adipocytes using an adiponectin-CRE driven conditional knockout (KO) model. KO mice were viable but suffered from lipodystrophy and significantly altered gross morphology (Mori et al., 2014). Interestingly, effects of miRNA ablation varied by adipose depot, with a dramatic reduction in vWAT, a moderate reduction in sWAT, and an increase in BAT, indicating that the role of miRNAs in adipocytes varies by fat depot. In addition, mice were highly insulin resistant, and despite the increase in BAT mass, were unable to produce heat via non-shivering thermogenesis (Mori et al., 2014). Future studies found that adipose specific KO of dicer accelerated aging and contributed to type II diabetes development, in part, by altering adipose-derived metabolites in the circulation (Reis et al., 2016).

In the last decade, many studies have focused on the role of individual miRNAs in regulating adipocyte phenotype. Some of these have focused on the vWAT/BAT metabolic axis, and the ability of miRNAs to induce or inhibit thermogenesis, while others have focused on miRNAs that regulate other metabolic processes, including adipogenesis. Several of the best characterized miRNAs are described below:

MiR-133: MiR-133 was found to decrease significantly in BAT and WAT following cold exposure in mice (Trajkovski et al., 2012). *In vitro* studies found that miR-133 binds to and represses PRDM16, and that gain-of-function in brown preadipocytes blocks the development of thermogenic gene expression following differentiation (Trajkovski et al., 2012). A double knockout of miR-133a1 and miR-133a2 caused mice to develop beige sWAT and led to

increased cold-induced thermogenesis in BAT and sWAT (Liu et al., 2013). Mice were also more glucose tolerant and insulin sensitive, consistent with the metabolic effects seen in other genetic models that induce beige fat development (Seale et al., 2011).

MiR-196a: MiR-196a is induced in white preadipocytes by β-adrenergic stimulation or cold exposure. MiR-196a upregulation leads to adipocyte browning via the repression of *Hoxc8* which causes a downstream increase in C/EBPβ activity (Mori et al., 2012). Mice with transgenic over-expression of miR-196a show increased non-shivering thermogenesis, increased energy expenditure, and a resistance to weight gain (Mori et al., 2012).

MiR-30: The miR-30 family, which consists of miR-30a – miR-30e, is an inducer of adipogenesis in human and mouse preadipocytes, likely via repression of the transcription factor Runx2 (Mao et al., 2018). In addition to their role in adipogenesis, members of the miR-30 family promote thermogenic gene expression. Gain-and-loss of function studies in primary murine adipocytes demonstrate miR-30's ability to cause beiging of WAT and to reduce thermogenesis in primary brown adipocytes (Hu et al., 2015). These effects are likely due to miR-30's role in repressing RIP140, which blocks miR-30's induction of *UCP1* and *Cidea* (Hu et al., 2015). Like many miRNAs expressed in adipocytes, miR-30 is also expressed in adipose resident macrophages. Here, miR-30 works to inhibit inflammation by targeting a ligand of Notch1. Knockdown of miR-30 caused increased production of pro-inflammatory cytokines and increased M1 polarization of macrophages in mice (Miranda et al., 2018).

MiR-378: MiR-378 is a BAT and muscle enriched miRNA that lies within an intron of Pgc1-β. In a transgenic mouse model overexpressing miR-378 under the control of the ap2 promoter, BAT mass is increased while iWAT and eWAT depots are both reduced in size (Pan et al., 2014). This effect was attributed to an increase in proliferation of BAT adipocytes, rather than cellular hypertrophy, and a decrease in adipocyte cell size within the WAT depots. Interestingly, miR-378 decreases *Prdm16* and *Ucp1* mRNA in sWAT, an effect that seems to contradict miR-378's role in expanding BAT (Pan et al., 2014). This disparity may be caused by miR-378 targeting *Pde1b* in BAT but not WAT, indicative of the impact of cellular microenvironment on miRNA binding activity.

MiR-146a: MiR-146a is reduced in obesity in mice and humans and is involved in suppressing pro-inflammatory pathways. Gain-of-function in cultured human adipocytes found that miR-146a suppresses inflammation by targeting *Iraf1* and *Traf6*, leading to a reduction in *IL-6* and *Mcp1* (Roos et al., 2016). In a whole-body mouse knockout (KO) model, loss of miR-146a causes increased weight gain on HFD, accompanied by poor glucose tolerance and increased liver triglyceride levels. These effects were attributed to miR-146's role in suppressing the NF-κB pathway in combination with modulation of mTOR signaling (Runtsch et al., 2019).

1.2.4 Exosomal miRNAs

In addition to regulating adipose metabolism within adipocytes, miRNAs can be secreted in exosomes to signal to distal tissues as endocrine or paracrine factors. A study conducted in obese human patients found that circulating exosomal miRNAs were altered in comparison to lean patients, and that these miRNAs were likely to influence inflammatory and

fibrotic pathways (Ferrante et al., 2015). In mice, recent work with the adipose-specific dicer KO line showed that a significant portion of circulating exosomal miRNAs are derived from adipose tissue, and that exosomal miRNAs can regulate gene expression in distal organs (Thomou et al., 2017). A few individual exosomal miRNAs have been characterized in more depth. MiR-34 is increased in obese mice and is transferred from adipocytes to macrophages via exosomes. Ablation of miR-34 causes an increase in M2 macrophage polarization (Pan et al., 2019). MiR-155 is secreted in exosomes from adipose tissue resident macrophages in obese mice, causing inhibition of Ppargγ, insulin resistance and glucose intolerance (Ying et al., 2017). Despite these studies, there is still controversy over whether or not exosomal miRNAs can reach sufficient levels in target tissues to significantly modulate mRNA levels (Bartel, 2018). Further work is necessary to explore the full potential, and limitations, of this mode of inter-organ communication.

CHAPTER 2: Profiling miRNA in Adipose

2.1 Introduction

To date, most work on miRNAs in adipose tissue has focused on identifying regulators of thermogenic genes, or other determinants of brown and beige adipocyte identity (Goody and Pfeifer, 2019). Comparatively fewer studies have investigated miRNAs that contribute to phenotypic differences between the two subcategories of WAT: vWAT and sWAT. To address this, we began by comprehensively measuring miRNA expression throughout a range of adipose depots in mice under normal physiological conditions. Specifically, we sequenced BAT, beige fat, 2 vWAT, and 2 sWAT depots. The rationale for isolating multiple depots of each WAT subcategory was twofold: first, to increase sample number and robustness for the

two major WAT subcategories, and second, to filter out miRNAs that are specific to one particular depot. This approach allowed us to avoid identifying candidates with functions related to body segmentation and anatomical position while focusing on miRNAs that are most responsible for contributing to phenotypic differences between adipose tissue types. Of the candidates that emerged from the profiling screen, expression under a variety of physiological conditions was assessed by qPCR. Finally, candidates were overexpressed in cultured primary adipocytes using viral vectors to assess impact on adipogenic, pro-inflammatory and pro-thermogenic pathways.

In addition to sequencing miRNAs from mouse tissue, we also profiled miRNAs from vWAT and sWAT preadipocytes and their mature counterparts. Many of the most significant mediators of adipocyte identity and function have been identified by profiling genes induced during the course of adipocyte differentiation. These include *Ppargγ*, which was discovered as a differentiation enriched activator of *aP2* (Tontonoz et al., 1994), and adiponectin, which was

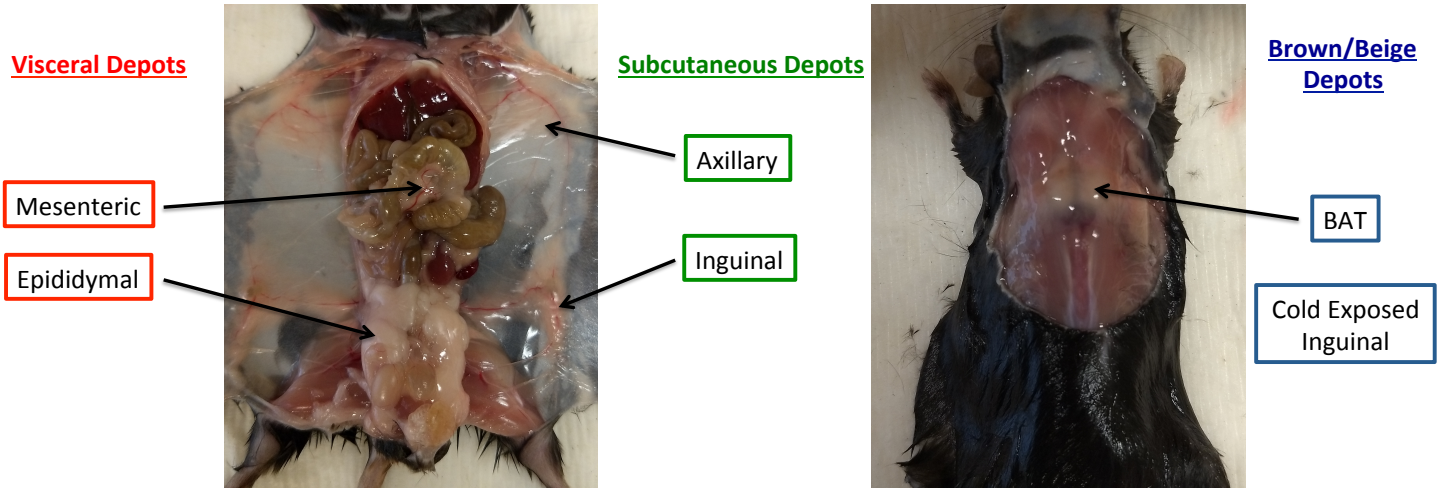

Figure 2.1 Adipose depots used for sequencing
vWAT depots isolated for sequencing consisted of mWAT and eWAT. sWAT depots consisted of aWAT and iWAT with lymph nodes removed. iBAT was dissected from the interscapular region, and beige fat consisted of inguinal fat from cold exposed mice.

identified by screening a cDNA library from differentiating 3T3-L1 adipocytes (Scherer et al., 1995). Thus far, there has been limited use of the same approach to study miRNAs that contribute to adipocyte identity. The screen performed here identified a number of candidates with the potential to control adipocyte function, including miR-218 and miR-708. Future studies will explore the full functional roles of these candidates *in vitro* and *in vivo*.

2.2 Results: *In vivo* miRNA seq

Small RNAs from 6 different mouse adipose depots were profiled by miRNAseq. The depots sequenced were as follows: two sWAT depots, axillary (aWAT) and inguinal (iWAT), two vWAT depots, epididymal (eWAT) and mesenteric (mWAT), iBAT and cWAT (iWAT from cold exposed mice) (Figure 2.1). A total of 653 unique miRNAs mapped to the mouse genome, and most were expressed in all 6 depots (Figure 2.2). From these, a variety of criteria were applied to identify miRNAs that are likely to mediate phenotypic differences between vWAT and sWAT. First, differential abundance was analyzed between sWAT (iWAT and aWAT combined reads) and vWAT (eWAT and mWAT combined reads). 37 miRNAs had a fold change of greater than 2 or less than 0.5 in the sWAT/vWAT comparison (note: an exception was made for the vWAT enriched miR-10 due to highly abundant total read counts). Next, a threshold of 330 normalized reads was applied to eliminate miRNAs with low relative abundance, leaving 19 candidates (note: an exception was made for the vWAT enriched miR-375 due to a high vWAT/sWAT fold change). Of these 19 miRNAs, 5 were eliminated due to depot-specific enrichment that was not shared by the other adipose depot of the same subcategory (e.g. high abundance in iWAT and low expression in aWAT). Several of the

remaining 14 miRNAs were removed from the candidate list because of a failure to validate by qPCR, or because they had been previously studied in adipose tissue (Figure 2.2).

The remaining 8, novel candidates include 4 that are enriched in sWAT and 2 that are enriched in vWAT. The miR-183/96/182 family is most abundant in iBAT, with roughly 8-fold lower abundance in both sWAT depots and 25-fold lower abundance in both vWAT depots (Figure 2.3A). Expression of miR-183 did not differ between iWAT and cWAT, although miR-182 levels were slightly increased, and miR-96 levels were slightly decreased in cWAT. miR-338 is about 3-fold more abundant in the two sWAT depots than the two vWAT depots, and interestingly, is least abundant in iBAT (Figure 2.3B). miR-10b, the most highly expressed of the candidates by normalized read counts, is most abundant in both vWAT depots, with roughly 60% lower abundance in sWAT (Figure 2.4A). miR-192 is enriched in vWAT by about 2.5-fold compared to sWAT (Figure 2.4B), while miR-375 is nearly undetectable in non-vWAT depots and only modestly abundant in eWAT and mWAT (Figure 2.4 C). Enrichment of miR-335 in vWAT was driven almost entirely by eWAT, and average vWAT abundance was about 3-fold that of sWAT (Figure 2.4 D).

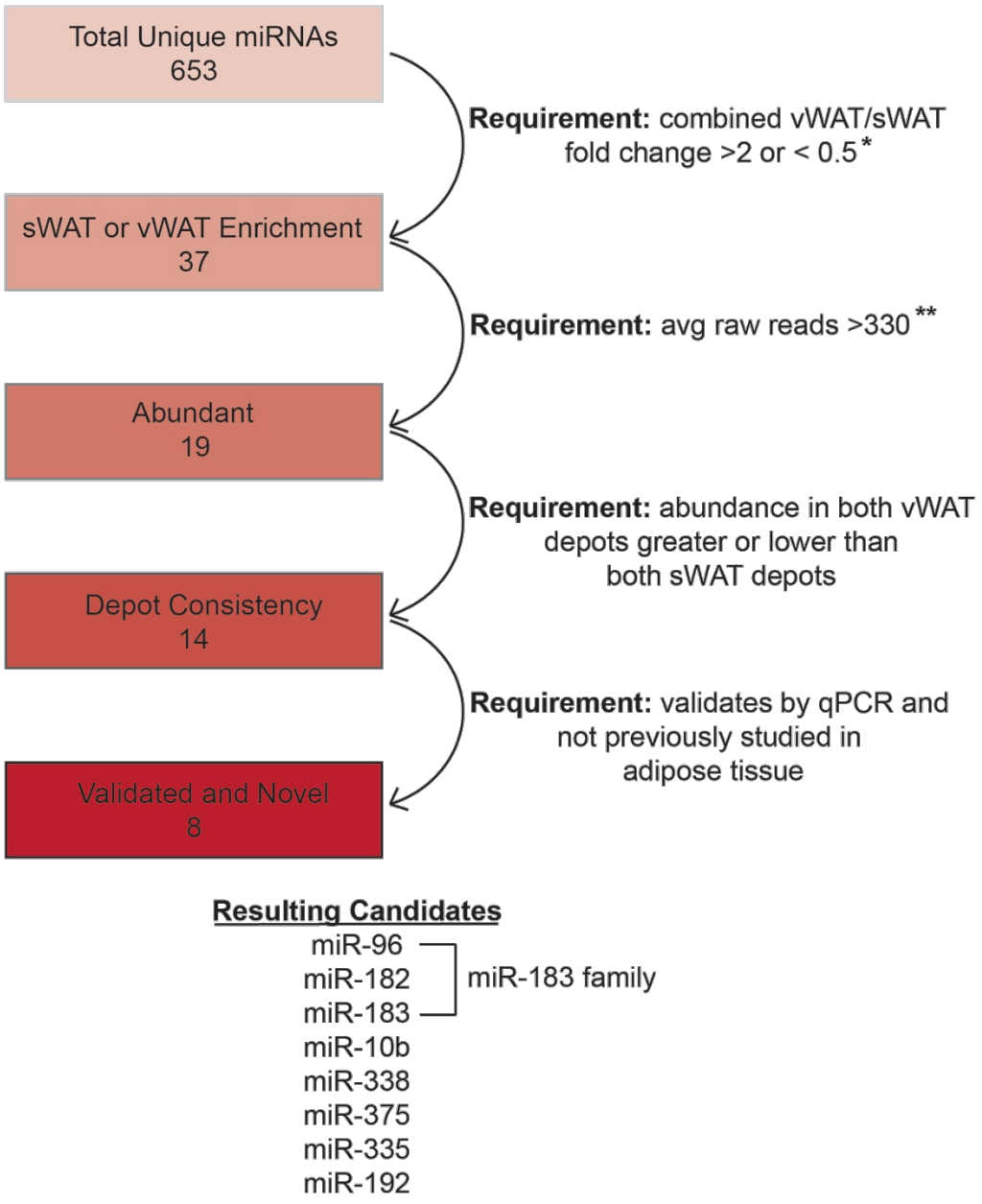

Figure 2.2 Schematic of criteria applied to identify miRNA candidates from *in vivo* screen

* an exception was made for miR-10b

** an exception was made for miR-375

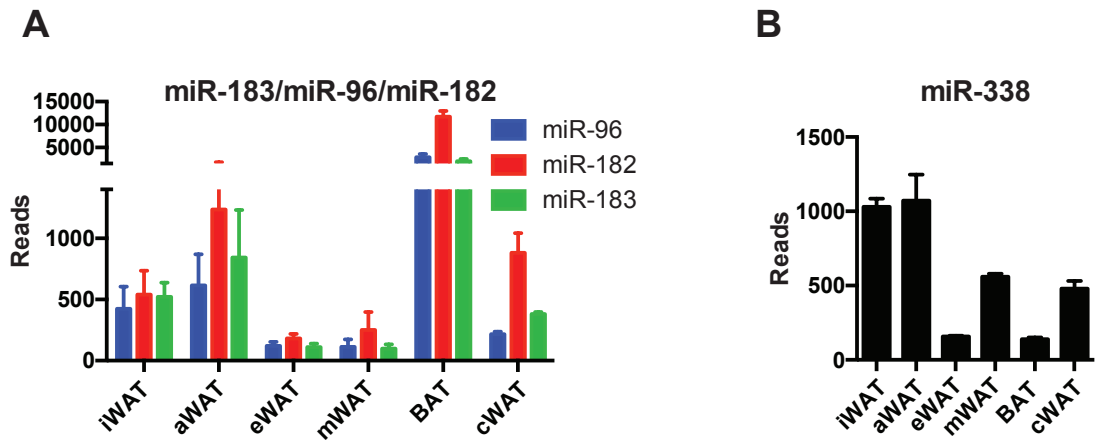

Figure 2.3 RNAseq reads of sWAT enriched miRNA candidates
(A and B) DEseq normalized read counts of the miR183/96/182 family (A) and miR-338 (B).

All results are presented as mean ±SEM

To further characterize the 8 miRNA candidates, abundance was measured by qPCR in a variety of conditions. First, primary preadipocytes isolated from mouse eWAT and iWAT were differentiated into mature adipocytes over the course of 7 days. RNA was collected immediately prior to differentiation, as well as 2 days, 3 days, 4 days, 5 days and 7 days post-induction.

Of the sWAT enriched miRNAs, miR-96, miR-182, and miR-183 all showed a robust increase over the course of differentiation (Figure 2.5A-2.5C). At day 7, miR-182 and miR-183, but not miR-96, were somewhat more abundant in iWAT than eWAT primary cells, although not to the extent seen *in vivo*. miR-338 levels decreased modestly following induction and were roughly equivalent in mature eWAT cells compared to mature iWAT cells (Figure 2.5D).

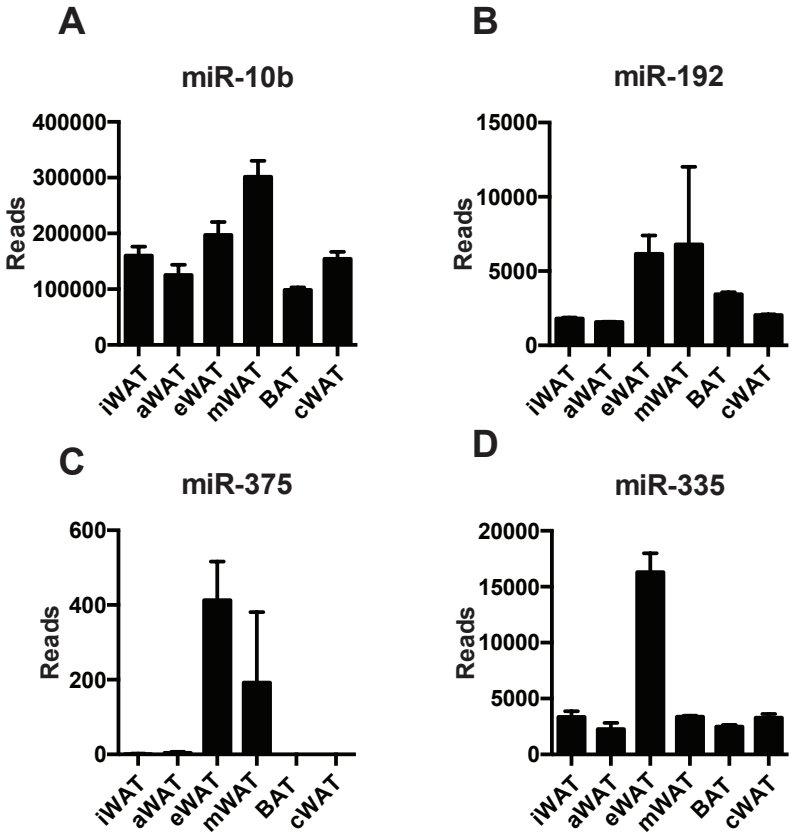

Figure 2.4 RNAseq reads of vWAT enriched miRNA candidates
(A-D) DEseq normalized read counts of miR-10b (A), miR-192 (B), miR-375 (C) and miR-335 (D).

All results are presented as mean ±SEM

Among the vWAT enriched miRNAs, both miR-335 and miR-192 showed strong differentiation dependent increases in abundance (Figure 2.6A and 2.6D), while miR-375 and miR-10b did not (Figure 2.6B and 2.6C). miR-335 and miR-10b were significantly enriched in eWAT cells compared to iWAT cells, while miR-192 was eWAT enriched in mature cells. Surprisingly, miR-375 abundance was dramatically lower in eWAT compared to iWAT, a reversal of the pattern seen *in vivo*.

Next, miRNA candidate abundance was measured in a cohort of diet-induced obese (DIO) mice fed high-fat diet (HFD) for 24 weeks and compared to chow-fed littermate controls. Samples from the 5 major depots (excluding beige fat) were dissected, and miRNA levels were measured by qPCR to assess obesity-dependent changes in abundance. Additionally, miRNA levels were compared to those in 13-week old chow-fed mice to determine the consistency of depot specificity at different ages. In general, variability in miRNA abundance in 30-week mice was high compared to the variability in younger mice; however, non-significant trends emerged with many of the miRNA candidates.

Of the 4 sWAT enriched candidates, miR-96, miR-182 and miR-183 showed a HFD-dependent decrease in abundance in 3 or more depots each, although this decrease was not necessarily statistically significant (Figure 2.7A – 2.7C). Interestingly, while miR-96 and miR-183 both decrease significantly in iBAT of HFD mice, miR-182 levels remained unchanged. The sWAT enrichment of the miR-183/96/182 family was not well maintained at 30 weeks, especially for miR-182. By comparison, miR-338 did retain its sWAT enrichment and trended modestly towards decreased abundance in obese mice compared to lean controls (Figure 2.7D).

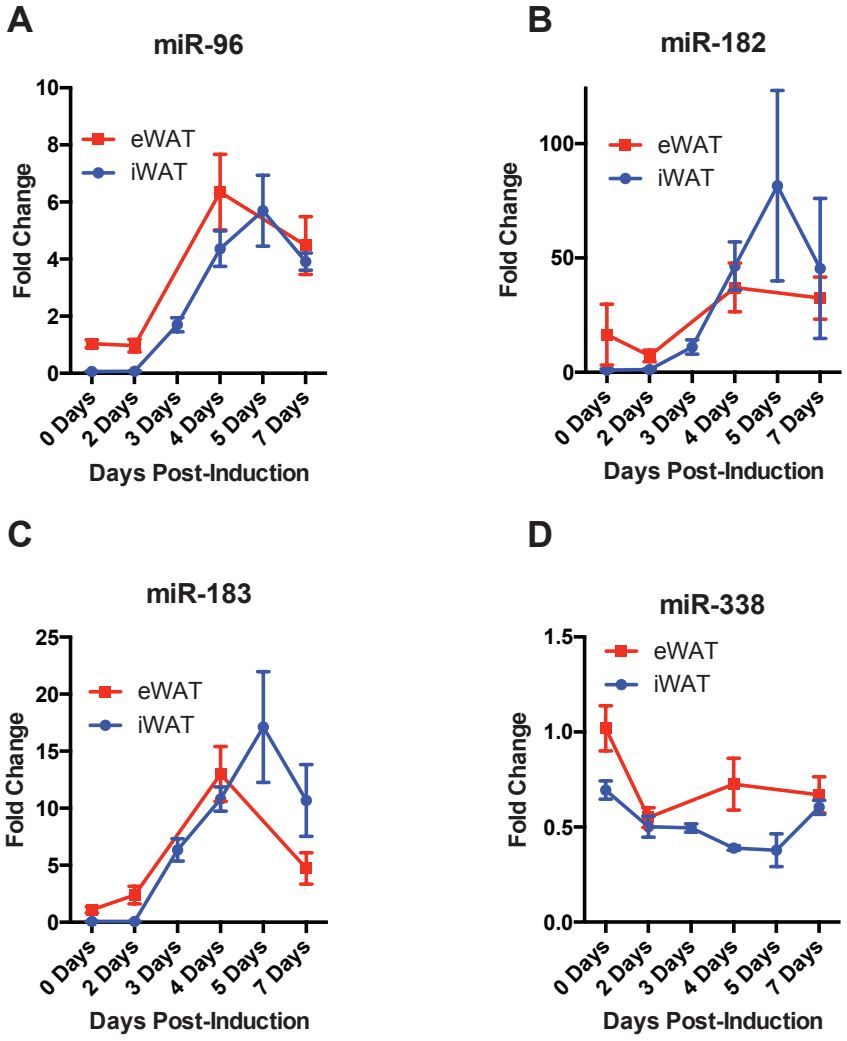

Figure 2.5 Abundance of vWAT enriched miRNA candidates in differentiating primary adipocytes

qPCR was used to measure miRNA expression of miR-96 (A), miR-182 (B), miR-183 (C) and miR-338 (D) in primary eWAT and iWAT adipocytes at various stages of differentiation.

All results are presented as mean ±SEM

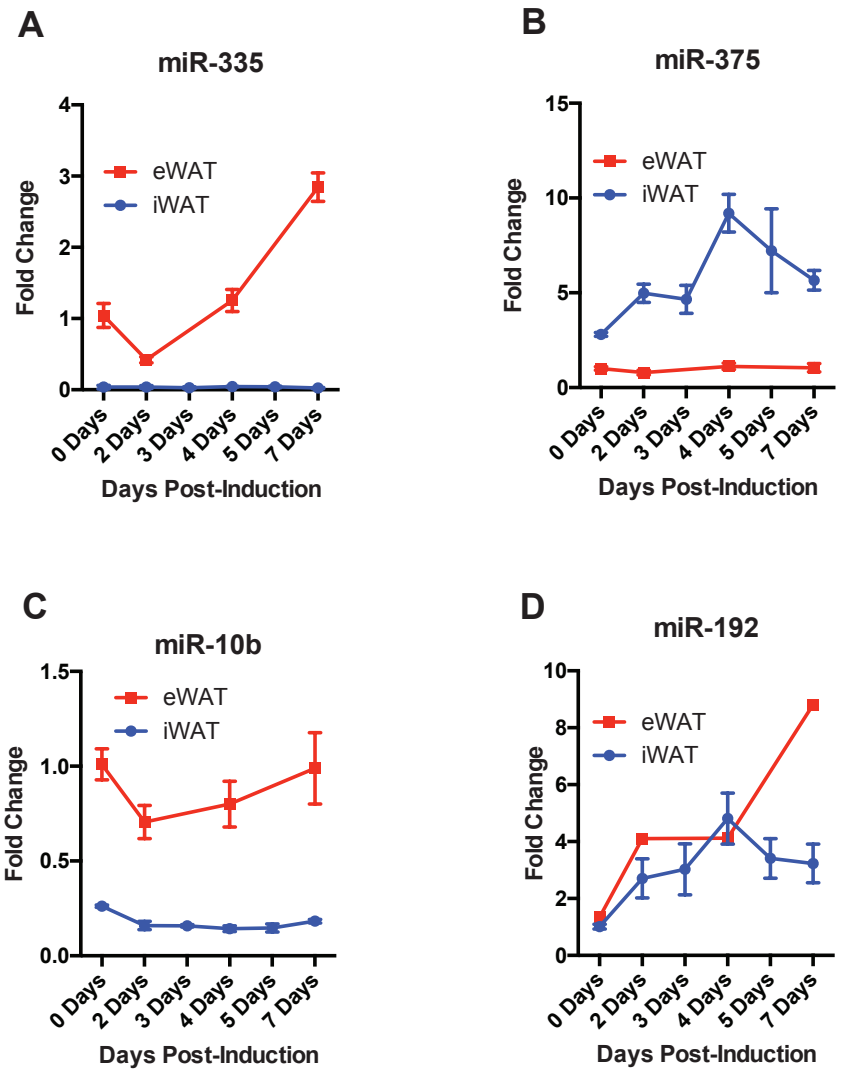

Figure 2.6 Abundance of vWAT enriched miRNA candidates in differentiating primary adipocytes

qPCR was used to measure miRNA expression of miR-335 (A), miR-375 (B), miR-10b (C) and miR-192 (D) in primary eWAT and iWAT adipocytes at various stages of differentiation.

All results are presented as mean ±SEM

Among the vWAT enriched miRNAs, miR-335 showed a strong increase in abundance in DIO mice in both sWAT depots, with no change in either vWAT depot or iBAT (Figure 2.8A). In lean mice, visceral enrichment was well maintained at the 30-week time point. miR-375 also retained visceral enrichment at 30 weeks in lean mice, but miRNA levels in DIO mice moved in the opposite direction, decreasing by about 10-fold (Figure 2.8B). miR-10b levels did not change dramatically in obese mice, and depot specificity was maintained, albeit weakly (Figure 2.8C). miR-192 levels were vWAT enriched at 30-weeks in lean mice, although obese mice had roughly equivalent abundance in all 5 depots (Figure 2.8D).

Next, candidates were prioritized to identify those miRNAs that were most likely to contribute to phenotypic differences between sWAT and vWAT. A point system was used to grant either 1, 0.5 or 0 points to each candidate for each of the four physiological states measured. Specifically, a point was awarded to candidates that increased in abundance over the course of differentiation, maintained depot specificity (either vWAT or sWAT enriched) in primary cells, increased or decreased in obese mice relative to controls (in at least 2 depots), and maintained depot specificity in 30 week-old control mice.

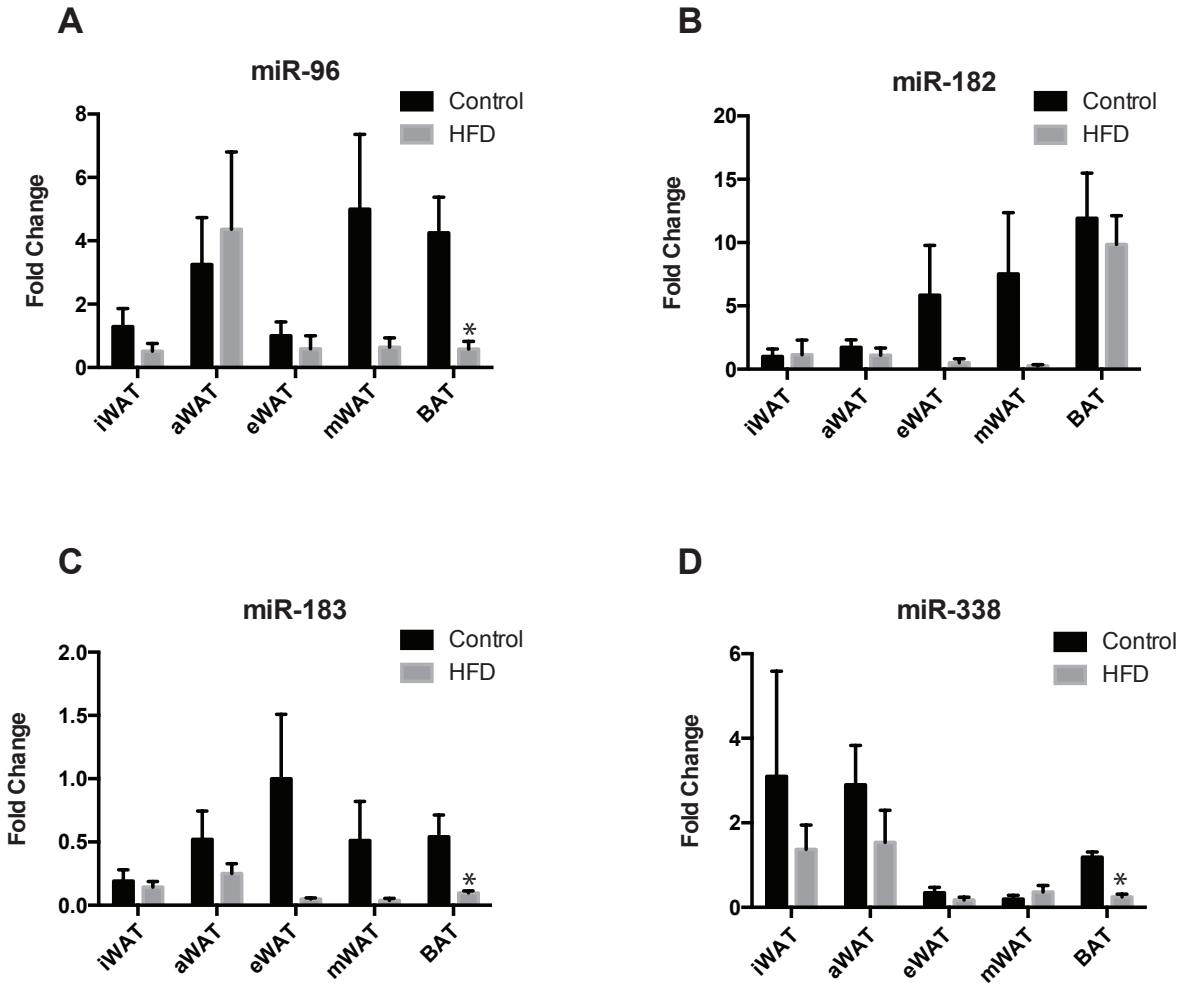

Figure 2.7 Obesity-dependent changes in abundance of sWAT enriched candidates
(A-D) qPCR was used to quantify abundance of miR-96 (A), miR-182 (B), miR-183 (C) and miR-338 (D) in 5 adipose depots from 30-week old mice. Mice were fed either a standard chow or 60% HFD diet, beginning at 6 weeks of age.

All results are presented as mean ±SEM. Student's t test for HFD vs. control (*$p < 0.05$, **$p < 0.005$, ***$p < 0.0005$, ****$p < 0.00005$)

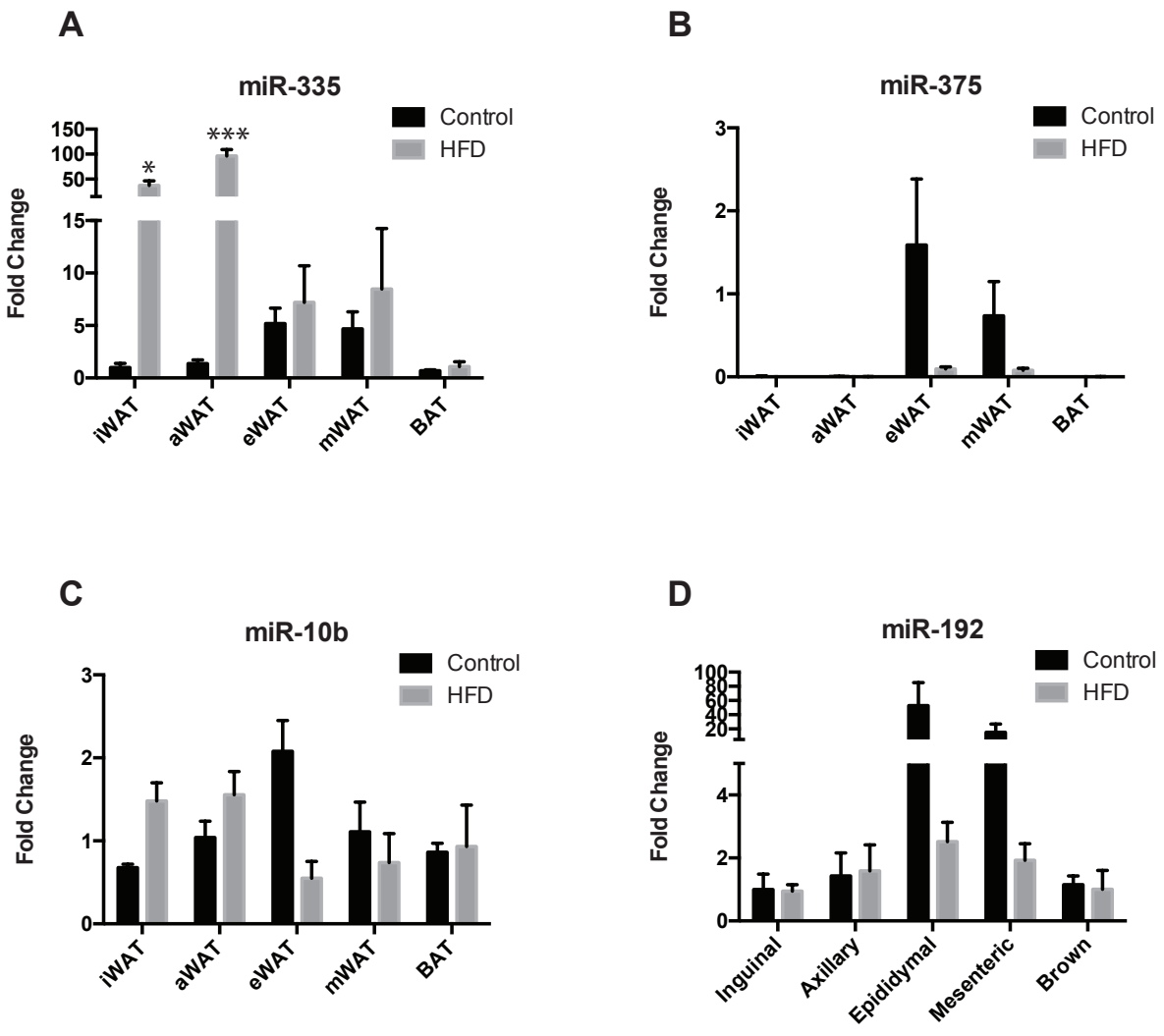

Figure 2.8 Obesity-dependent changes in abundance of sWAT enriched candidates
(A-D) qPCR was used to quantify abundance of miR-335 (A), miR-375 (B), miR-10b (C) and miR-192 (D) in 5 adipose depots from 30-week old mice. Mice were fed either a chow diet or a 60% HFD diet, beginning at 6 weeks of age.

All results are presented as mean ±SEM. Student's t test for HFD vs. control (*$p < 0.05$, **$p < 0.005$, ***$p < 0.0005$, ****$p < 0.00005$)

Interestingly, all four vWAT enriched candidates scored higher than the sWAT enriched candidates. miR-335, in particular, matched the pattern expected of a vWAT enriched miRNA that contributes to a more visceral adipose phenotype *in vivo* and *in vitro*. The large obesity-dependent increase in iWAT and aWAT hints at a potential role for miR-335 in mediating the 'visceralization' of mouse sWAT under obesogenic conditions. *In vitro*, miR-335 was nearly undetectable in primary sWAT cells, and expression increased significantly throughout differentiation in primary vWAT, suggesting that miR-335 plays an important role in mature vWAT biology. miR-192 abundance also changed in HFD fed mice; however, the direction of change was inconsistent with a more 'visceralized' phenotype. In primary cells, miR-192 increased throughout differentiation, but the depot specificity was not as stark as that of miR-335. Both miR-375 and miR-10b displayed some of the expression patterns expected of visceral enriched miRNAs, but depot abundance was reversed in miR-375 *in vitro*, and miR-10b did not increase over the course of differentiation.

Table 1: Summary of miRNA candidates

miRNA	Enriched depot	Differentiation dependent expression change	Depot specificity maintained in primary cells	Obesity dependent expression change	Depot specificity maintained at 30 weeks	Score
miR-183/96/182	sWAT	1	0	0.5	0	1.5
miR-338	sWAT	0	0	0.5	1	1.5
miR-375	vWAT	0.5	0	1	1	2.5
miR-10b	vWAT	0	1	0.5	1	2.5
miR-192	vWAT	1	0.5	1	1	3.5
miR-335	vWAT	1	1	1	1	4

2.2.1 Gain and loss-of-function with *in vivo* candidates

To directly study the functional role of miRNAs in adipocyte biology, candidates were overexpressed in a cell culture model. Genes involved in adipogenesis, non-shivering thermogenesis, and inflammation were measured by qPCR to assess phenotypic shifts along the vWAT/BAT axis. Specifically, genes analyzed for differentiation were *Pparγ2* (Mueller et al., 2002), *aP2* (Sun et al., 2003) and *Adipoq* (Wang et al., 2015); pro-thermogenic genes were *Prdm16* (Seale et al., 2011), *Pgc1α* (Liang and Ward, 2006), *Cidea* (Fischer et al., 2017), and *Ucp1* (Ricquier and Kader, 1976); pro-inflammatory genes were *Agt* (Ailhaud et al., 2000), *Saa3* (Sanada et al., 2016), *Opgn* (Aronis et al., 2012), *Bnc1* (Cohen et al., 2014), *Hif1α* (Krishnan et al., 2012), and *Retn* (Steppan and Lazar, 2004).

For the first two candidates, miR-335 and miR-192, pri-miRNA loci were cloned into retroviral vectors containing GFP. An immortalized line of mouse preadipocytes, 3T3-F442A cells, were transduced with multiple rounds of retrovirus, then differentiated into mature adipocytes. Either transduction with GFP alone or with GFP/miR-335 resulted in robust induction of GFP by fluorescence microscopy, with nearly 100% of cells GFP positive (Figure 2.9A and 2.9B). MiR-335, which was expressed endogenously at very low levels in 3T3-F442A cells, was dramatically induced in GFP/miR-335 transduced cells (Figure 2.9C). Differentiation appeared to be slightly inhibited, with a modest decrease in *Pparγ2* and *aP2* levels, and a significant decrease of about 40% in *Adipoq* (Figure 2.9D). Thermogenic gene expression remained largely unchanged, aside from a small decrease in *Cidea*. Several vWAT markers showed altered abundance in GFP/miR-335 transduced cells, including a decrease in angiotensinogen and an increase in *Saa3* by 40% and 75%, respectively.

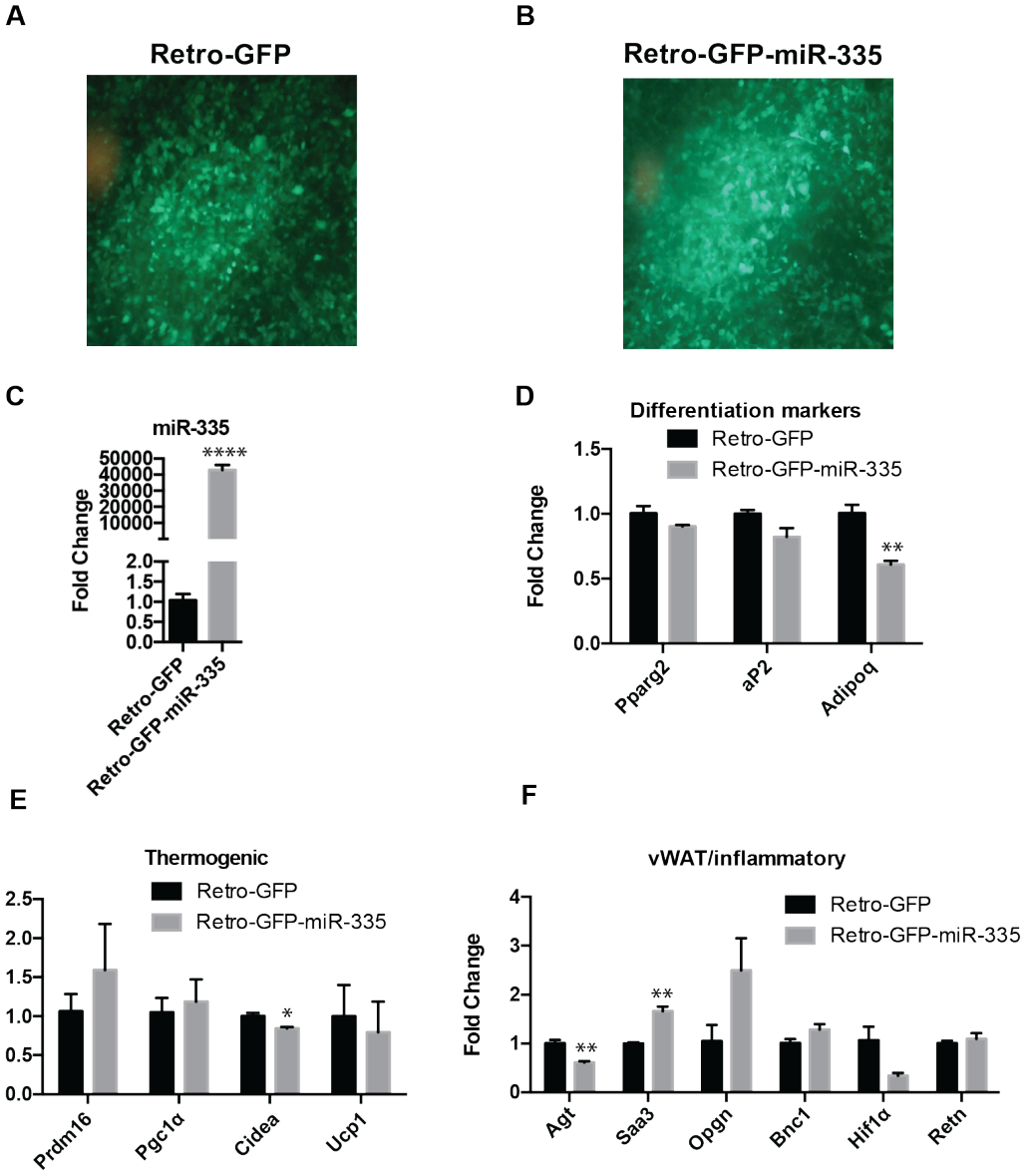

Figure 2.9 miR-335 modestly represses adipogenesis in 3T3-F442A cells
(A and B) 3T3-F442A preadipocytes were transduced with a retrovirus containing GFP only. (A) or GFP and miR-335 (B). GFP was imaged by fluorescence microscopy.
(C) miRNA-based qPCR of miR-335.
(D-F) mRNA-based qPCR for differentiation markers (D), pro-thermogenic/BAT identity. genes (E), and pro-inflammatory/vWAT identity genes (F).

All results are presented as mean ±SEM. Student's t test for HFD vs. control (*$p < 0.05$, **$p < 0.005$, ***$p < 0.0005$, ****$p < 0.00005$).

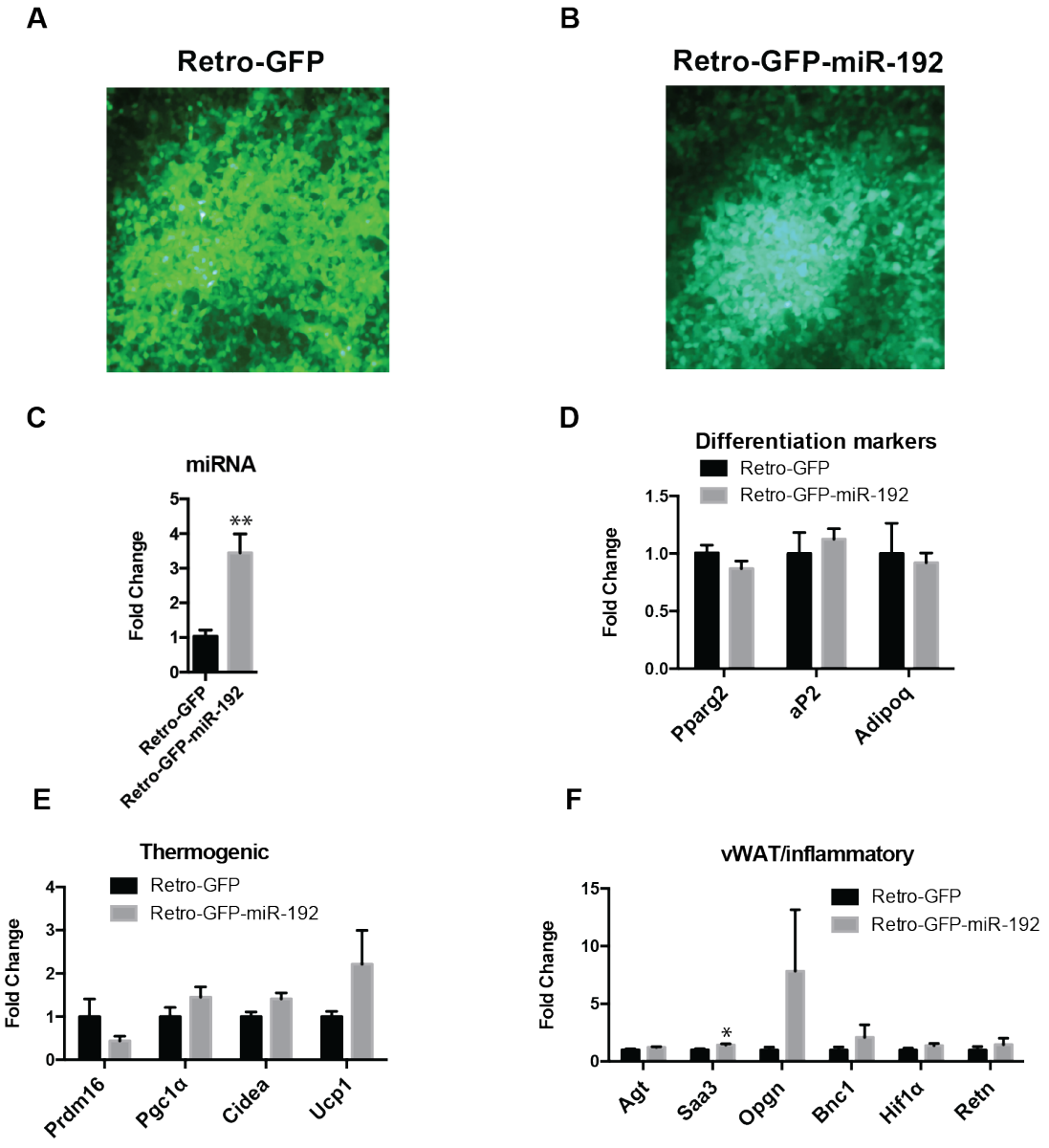

Figure 2.10 miR-192 modestly increases pro-thermogenic and pro-inflammatory gene abundance in 3T3-F442A cells

(A and B) 3T3-F442A preadipocytes were transduced with a retrovirus containing GFP only (A) or GFP and miR-192 (B). GFP was imaged by fluorescence microscopy.

(C) miRNA-based qPCR of miR-192.

(D-F) mRNA-based qPCR for differentiation markers (D), pro-thermogenic/BAT identity genes (E), and pro-inflammatory/vWAT identity genes (F).

All results are presented as mean ±SEM. Student's t test for HFD vs. control (*$p < 0.05$, **$p < 0.005$, ***$p < 0.0005$, ****$p < 0.00005$).

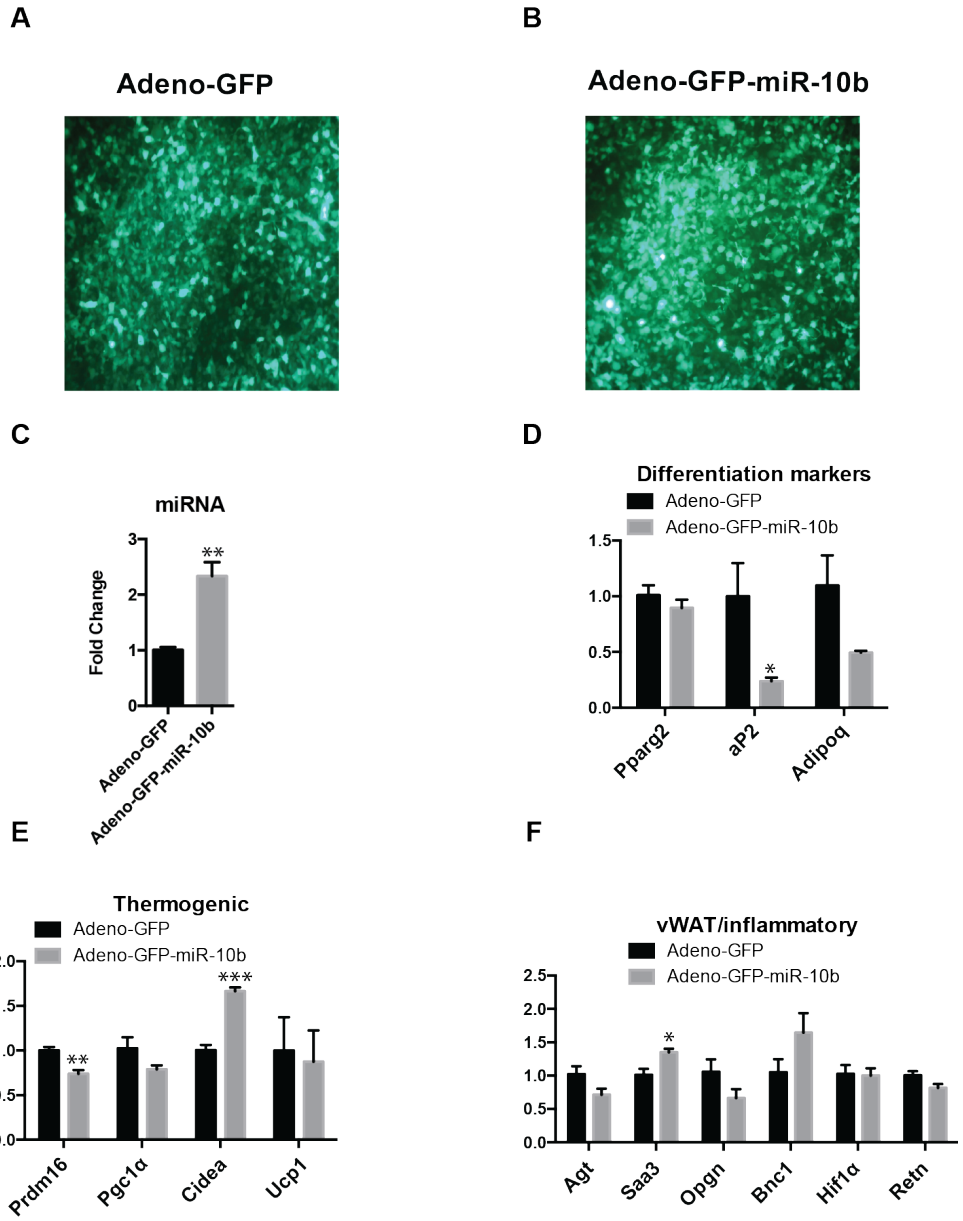

Figure 2.11 miR-10b may repress adipogenesis in 3T3-F442A cells
(A and B) 3T3-F442A adipocytes were transduced on the fourth day of differentiation with an adenovirus containing GFP only (A) or GFP and miR-10b (B). GFP was imaged by fluorescence microscopy.
(C) miRNA-based qPCR of miR-10b.
(D-F) mRNA-based qPCR for differentiation markers (D), pro-thermogenic/BAT identity genes (E), and pro-inflammatory/vWAT identity genes (F).

All results are presented as mean ±SEM. Student's t test for HFD vs. control (*$p < 0.05$, **$p < 0.005$, ***$p < 0.0005$, ****$p < 0.00005$).

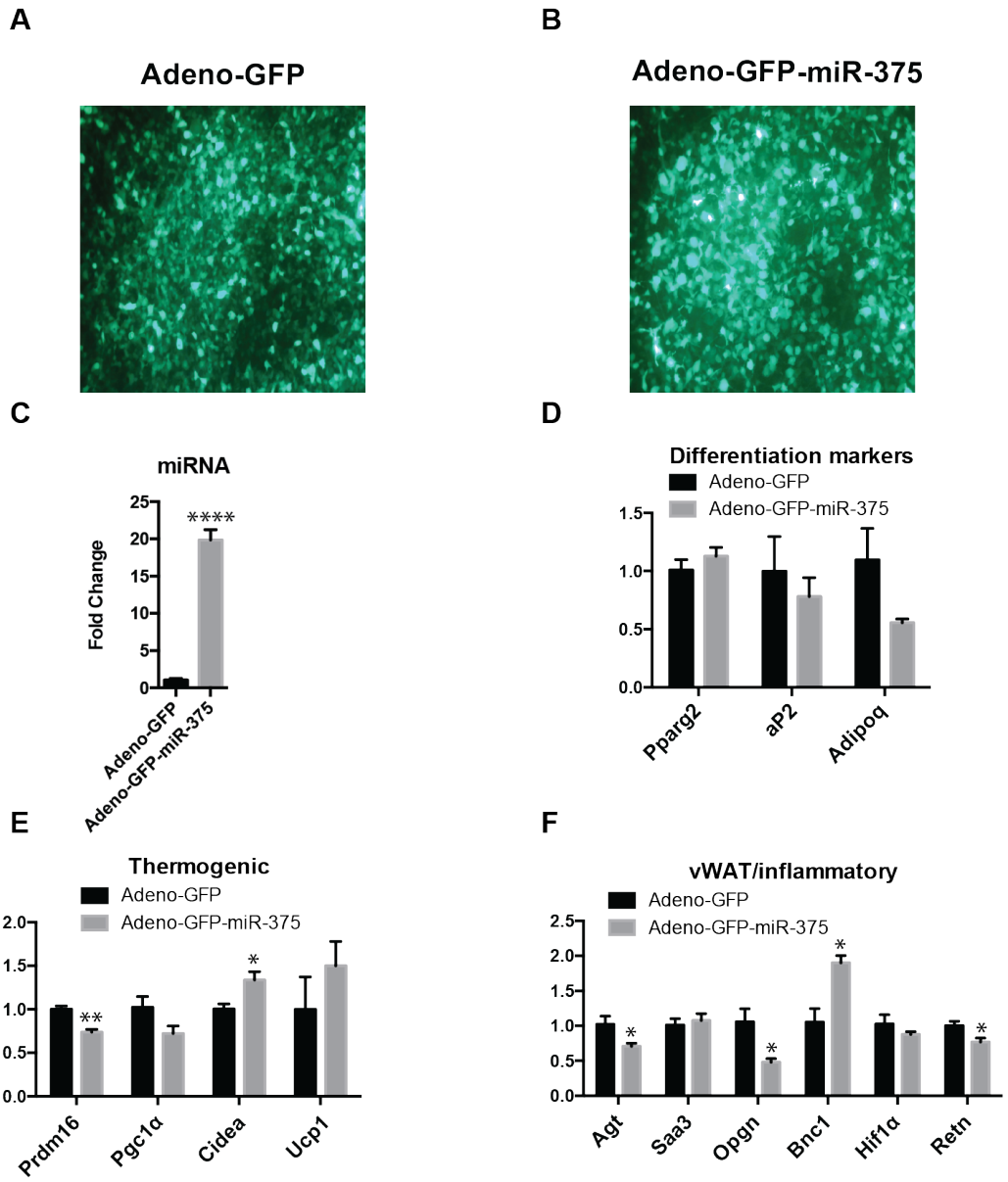

Figure 2.12 miR-375 impacts abundance of several genes in 3T3-F442A cells
(A and B) 3T3-F442A adipocytes were transduced on the fourth day of differentiation with an adenovirus containing GFP only (A) or GFP and miR-375 (B). GFP was imaged by fluorescence microscopy.
(C) miRNA-based qPCR of miR-375.
(D-F) mRNA-based qPCR for differentiation markers (D), pro-thermogenic/BAT identity genes (E), and pro-inflammatory/vWAT identity genes (F).

All results are presented as mean ±SEM. Student's t test for HFD vs. control (*$p < 0.05$, **$p < 0.005$, ***$p < 0.0005$, ****$p < 0.00005$).

In summary, miR-335 may play a minor role in inhibiting differentiation; however, no clear pattern emerged with regards to shifting fat cell identity along the iBAT/vWAT axis.

3T3-F442A cells transduced with miR-192 retrovirus or GFP control showed strong expression of GFP by fluorescence microscopy (Figures 2.10A and 2.10B), although the corresponding induction of miR-192 was only 3-4 times above control levels due to the higher baseline level of miR-192 expression in 3T3-F442As (Figure 2.10C). No changes were observed in the three differentiation markers (Figure 2.10D). Given that miR-192 is a vWAT enriched miRNA, we hypothesized that pro-thermogenic gene abundance would decrease with overexpression; however, *Pgc1α*, *Cidea,* and *Ucp1* all trended towards increased abundance (Figure 2.10E). Of the panel of vWAT/inflammatory genes, *Saa3* was induced significantly by about 40%, and all other genes were non-significantly induced (Figure 2.10F). In summary, miR-192 may confer a modest pro-thermogenic and pro-inflammatory phenotype without contributing to a clear shift along the iBAT/vWAT axis.

Next, the third and fourth-ranked candidates, miR-10b and miR-375, were cloned into an adenoviral backbone containing GFP. Wildtype 3T3-F442A cells were differentiated in culture and transduced with adenovirus after 4 days. When cells reached maturity on day 7, GFP was imaged by fluorescence microscopy and RNA was collected for qPCR. Cells transduced with control virus or with GFP/miR-10b showed a robust induction of GFP (Figure 2.11A and 2.11B). Given the high levels of endogenous miR-10b, miRNA levels were increased by only about 2-3-fold, representing a fairly small relative increase, but a large absolute increase (Figure 2.11C). *aP2* and *Adipoq* levels were reduced by 75% and 60%, respectively, but *Pparγ2* remained unchanged (Figure 2.11D). Among thermogenic and vWAT/inflammatory gene panels, the abundances of several individual mRNAs were altered,

but no clear pattern emerged. *Prdm16* and *Pgc1α* abundances were decreased by 15-20%, while *Cidea* levels increased by 60% and no change was observed for *Ucp1* (Figure 2.11E). Among pro-inflammatory genes, *Saa3* and *Bnc1* were increased, and *Agt* and *Opgn* were modestly decreased (Figure 2.11F).

In 3T3-F442A cells transduced with an adenovirus expressing miR-375, GFP was visible in close to 100% of cells imaged (Figures 2.12A and 2.12B), and miR-375 was robustly induced (Figure 2.12C). There were no significant changes in the abundance of differentiation makers, although *aP2* and adiponectin trended lower (Figure 2.12D). Similar to miR-10b gain-of-function, no clear pattern was observed in thermogenic genes. *Prdm16* and *Pgc1α* abundances were decreased by 20-30%, and *Cidea* and *Ucp1* abundances were increased by 30-40% (Figure 2.12E). Among the pro-inflammatory genes, levels of *Agt*, *Opgn*, and *Retn* were significantly decreased. *Bnc1* levels, however, were increased by 90%, consistent with the expected metabolic impact of a vWAT enriched miRNA and negating the anti-inflammatory trend (Figure 2.12F).

One of the disadvantages of working with immortalized cell lines is that gene expression and function do not fully represent the phenotype of adipocytes in an *in vivo* setting. Primary adipocytes, while not a perfect model of adipocytes *in vivo*, are a closer representation. For the final candidate tested, miR-338, preadipocytes were isolated from the stromal vascular fraction (SVF) of mouse sWAT and differentiated into mature adipocytes over the course of 7 days. On the fourth day, adipocytes were transduced with adenovirus expressing either GFP alone or GFP/miR-338. RNA was collected on the 7th day, and RNA abundance was measured by qPCR. In addition to the panel of genes in figures 2.9 – 2.12, several other genes involved in thermogenesis, vWAT/pro-inflammatory pathways and lipid metabolism were measured.

Specifically, *Dio2* (de Jesus et al., 2001), *Cox8b* (Garcia et al., 2016), *Ehmt1* (Ohno et al., 2013), *Ebf2* (Rajakumari et al., 2013), and *Elovl3* (Shapira and Seale, 2019) are associated with BAT identity and/or correlate in expression with canonical, non-shivering thermogenic activity. *Ckmt1* and *Gatm* are both involved in an alternative thermogenic pathway that utilizes a futile phospho-creatine cycle (Kazak et al., 2015), and *Atp2a2* is involved in an endoplasmic reticulum-based alternative thermogenic pathway (Ikeda et al., 2017). *Wt1* (Chau and Hastie, 2015), *Raldh2* (Cohen et al., 2014), *Tnfα* (Treede et al., 2009), and *Tle3* (Villanueva et al., 2013) are associated with WAT cell identify and/or negatively correlate with thermogenesis. Of the lipid metabolic genes, *Pparα* (Corrales et al., 2018), *Acox1* (Varanasi et al., 1994), and *Atgl* (Morak et al., 2012) are involved in lipolysis and/or oxidation of fatty acids, while *Fasn* (Smith et al., 2003), *Acc1* (Tong, 2005), *Scd1* (Flowers and Ntambi, 2008), and *Fsp27* (Grahn et al., 2014), are involved in fatty acid synthesis or lipid storage.

MiR-338 was robustly induced in primary adipocytes transduced with GFP/miR-338 (Figure 2.13A), and while *Pparγ2* and *aP2* levels remained unchanged, adiponectin was reduced by 80% (Figure 2.13B). Among genes involved in the canonical thermogenic pathway, *Pgc1α*, *Cidea*, and *Ucp1* were induced 2-3-fold, while *Dio2* and *Elovl3* were repressed (Figure 2.13C). Given that *Ucp1* is most directly involved in thermogenesis, the functional impact of the decrease in *Dio2* and *Elovl3* is unclear. Additionally, *Atp2a2* mRNA was increased significantly, and *Ckmt1* and *Gatm* levels were modestly induced, suggesting that miR-338 may be increasing thermogenic activity through several pathways in parallel. Of the pro-inflammatory genes, there was a general trend towards decreased abundance, with *Saa3*, *Raldh2,* and *Wt1* decreasing 90%, 80%, and 55%, respectively (Figure 2.13D). *Agt* and *Hif1α*, were both decreased modestly, and *Tnfα* and *Tle3* increased by 100% and 75%, respectively.

Interestingly, mRNA for all genes related to lipid metabolism, except *Scd1*, increased significantly (Figure 2.13E). Given that several of these genes are involved in de novo lipogenesis, and others are involved in oxidation of lipids, these results are somewhat paradoxical. It may be that miR-338 works by increasing the general metabolic activity of adipocytes rather than shifting cells towards either a more anabolic or catabolic state. In summary, miR-338 appears to increase cellular metabolism by promoting thermogenesis and lipid processing, while potentially promoting a more iBAT-like identity by down-regulating many genes involved in pro-inflammatory pathways.

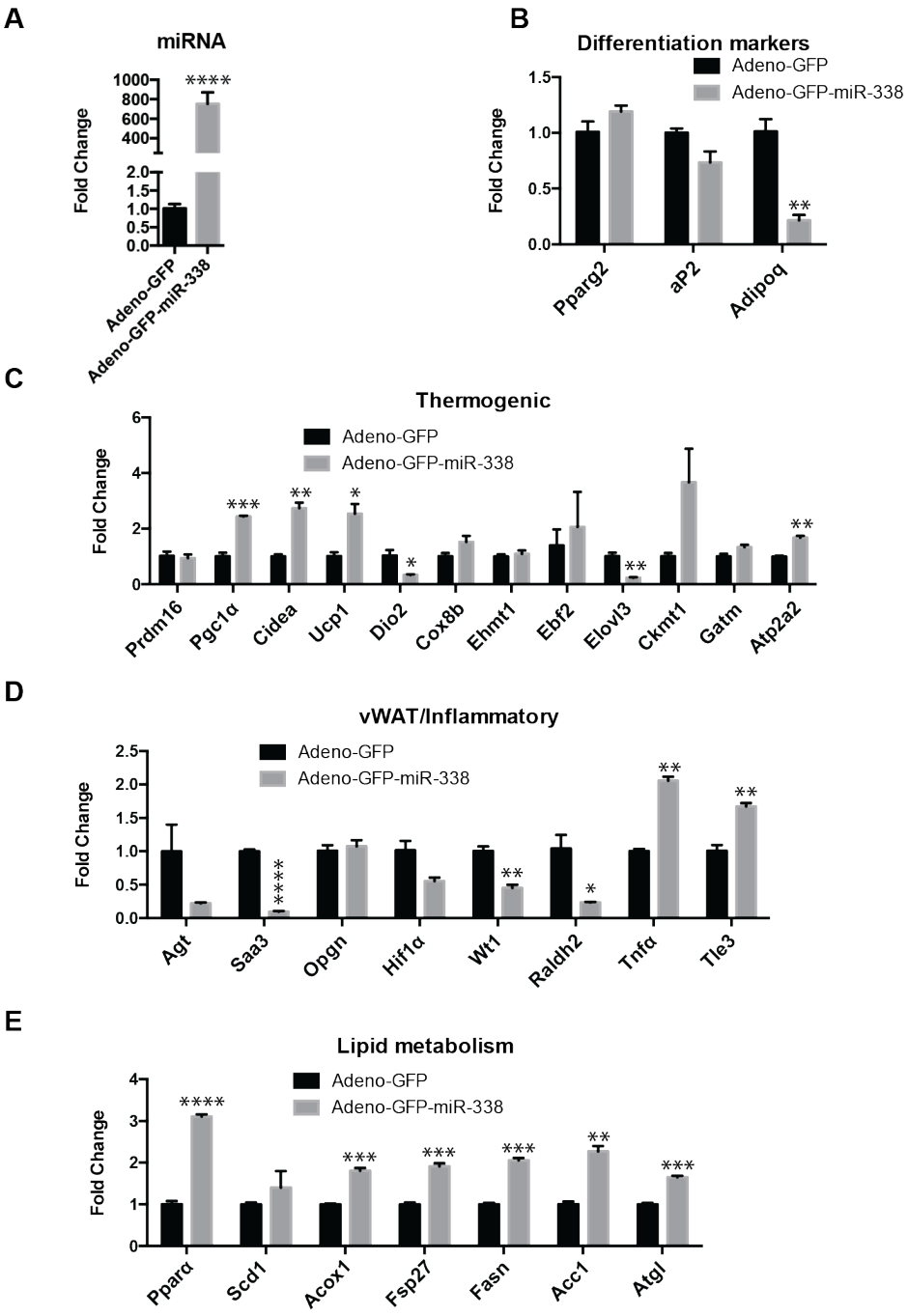

Figure 2.13 miR-338 increases thermogenic and lipid metabolic genes in primary adipocytes

(A) miRNA-based qPCR of miR-375.

(B-E) mRNA-based qPCR for differentiation markers (B), pro-thermogenic/BAT identity genes (C), pro-inflammatory/vWAT identity genes (D), and genes involved in lipid metabolism (E).

All results are presented as mean ±SEM. Student's t test for HFD vs. control (*$p < 0.05$, **$p < 0.005$, ***$p < 0.0005$, ****$p < 0.00005$)

2.3 Results: *in vitro* miRNAseq

The strategy used thus far to identify miRNA candidates has focused on differences in abundance between adipose depots *in vivo*. This approach risks filtering out miRNA candidates that significantly impact cellular function but are expressed at equivalent levels across adipose depots. Additionally, the *in vivo* screen does not distinguish between miRNAs expressed by adipocytes vs. non-adipocyte cell types within adipose tissue. As an alternative approach, we cultured primary adipocytes from iWAT and eWAT and collected total RNA for miRNA sequencing before and after differentiation. In addition, we sequenced miRNAs from mature iWAT adipocytes treated with the β3-agonist CL-316,243 which induces non-shivering thermogenesis *in vivo* and *in vitro* (Himms-Hagen et al., 1994; Li et al., 2017b). CL-316,243 activates adenylyl cyclase, generating cyclic AMP (cAMP) which leads to downstream transcription of thermogenic genes (Harms and Seale, 2013). Many of the intracellular events following CL-316,243 agonism, however, have not been fully characterized. Studying changes in miRNA abundance following CL-316,243 treatment could provide new insights into thermogenic gene activation.

To begin, miRNA abundance was compared between preadipocytes and mature adipocytes isolated from either iWAT or eWAT. In eWAT derived cells, 58 miRNAs had p-values < 0.01, 183 had p-values < 0.05, and 316 miRNAs had p values < 0.1. All miRNAs were visualized on volcano plots and those with p-values <0.05 and a fold change of >2 or < 0.5 were highlighted blue to indicate preadipocyte enrichment or red to indicate mature adipocyte enrichment (Figure 2.14A). The top 20 candidates, ranked by p-value, are shown in Table 2. Many of the top candidates were very low in abundance, including miR-6922, miR-6901, and miR-404. Several of the top, more abundant miRNAs have been described

previously as key regulators of adipocyte function. miR-143, which is increased in obese mice (Takanabe et al., 2008), targets members of the MAPK pathway and influences adipocyte differentiation (Chen et al., 2014a). MiR-30 influences inflammation and insulin sensitivity in adipose tissue (Koh et al., 2018), while let-7 represses thermogenic pathways in sWAT (Giroud et al., 2016). Notably, miRNAs that have been well characterized in the literature are all increased in mature adipocytes compared to preadipocytes. Several miRNAs showing the reverse pattern, including miR-31 and miR-451, have not been extensively studied, and may represent potential modulators of adipogenesis or other adipocyte functions.

In iWAT derived cells there were 51 miRNAs with p-values < 0.01, 187 with p-values < 0.05, and 343 with p values < 0.1. miRNAs are plotted in Figure 2.14B and those with p-values <0.05 and a fold changes of >2 or < 0.5 are highlighted. Among the top 20 candidates shown in Table 3, several of the mature adipocyte-enriched candidates overlap with miRNAs from the eWAT comparison, including miR-143 and miR-30. Several miRNAs have been described previously, including miR-365, which interacts with Ppargγ to promote adipogenesis and thermogenesis (Shamsi et al., 2017), and miR-93, which targets Tbx3 and Sirt7 to suppress adipogenesis (Cioffi et al., 2015). miR-31 and miR-541 were also enriched in mature iWAT compared to iWAT preadipocytes, although they did not rank in the top 20 by p-value.

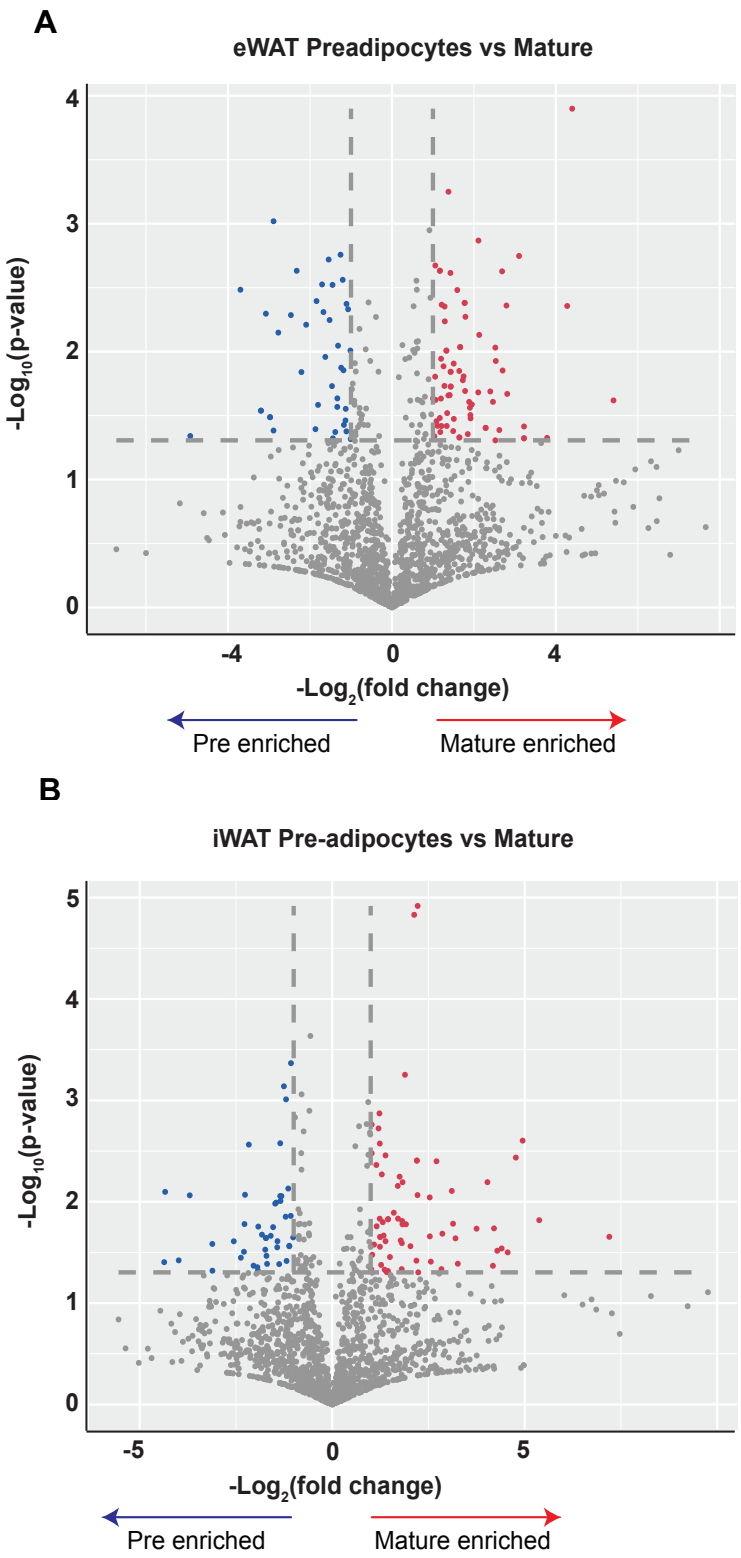

Figure 2.14 miRNA abundance is differentiation-dependent in primary WAT adipocytes
(A and B) Volcano plot of eWAT (A) and iWAT (B) derived preadipocytes compared to mature adipocytes. Horizontal and vertical dashed lines represent $p < 0.05$ and fold change > 2 or < 0.5, respectively.

Table 2: Top miRNAs by p-value: eWAT preadipocytes vs. eWAT mature adipocytes

miRNA	Enriched	Fold Change	p-value	Pre reads	Mat reads
miR-6922	Mature	21.08	1.26E-04	0	9
miR-143	Mature	2.60	5.62E-04	833	2,167
miR-31	Pre	0.13	9.57E-04	7,854	1,060
miR-30d	Mature	1.89	1.13E-03	120	225
miR-6901	Mature	4.32	1.36E-03	4	18
miR-424	Pre	0.42	1.75E-03	123	51
miR-203	Mature	8.58	1.79E-03	2	14
miR-665	Pre	0.34	1.91E-03	830	284
miR-30b	Mature	2.08	2.12E-03	18,072	37,613
miR-4335-	Mature	2.25	2.33E-03	5	11
miR-4335-	Mature	2.25	2.33E-03	5	11
miR-667	Pre	0.20	2.33E-03	28	6
miR-3963	Mature	6.44	2.36E-03	9	56
miR-2478	Mature	2.69	2.43E-03	81	218
miR-541	Pre	0.43	2.75E-03	8,431	3,665
miR-93a	Mature	1.51	2.79E-03	24	36
miR-370	Pre	0.31	2.98E-03	190	58
miR-409	Pre	0.37	3.01E-03	1,993	729
miR-7093	Pre	0.08	3.28E-03	3	0
let-7d	Mature	1.52	3.28E-03	38,635	58,844

Table 3: Top miRNAs by p-value: iWAT preadipocytes vs. iWAT mature adipocytes

miRNA	Enriched	Fold Change	p-value	Pre reads	Mat reads
miR-365	Mature	4.66	1.21E-05	3,584	16,704
miR-30c	Mature	4.38	1.48E-05	13,977	61,170
miR-16a	Pre	0.68	2.32E-04	283	191
miR-431	Pre	0.48	4.30E-04	61	29
miR-30a	Mature	3.71	5.60E-04	1,251	4,639
miR-125a	Pre	0.42	7.27E-04	429	180
miR-379	Pre	0.58	8.72E-04	5,713	3,292
miR-667	Pre	0.44	9.78E-04	437	190
miR-425	Mature	1.91	1.04E-03	1,899	3,631
miR-434	Pre	0.66	1.27E-03	6,010	3,988
miR-30b	Mature	2.34	1.35E-03	1,471	3,444
miR-299a	Pre	0.51	1.47E-03	856	439
miR-6990	Mature	NA	1.53E-03	0	1
miR-93	Mature	1.86	1.71E-03	5,758	10,703
miR-744	Mature	2.04	1.73E-03	2,093	4,265
miR-143	Mature	1.62	1.80E-03	1,171	1,899
miR-30b	Pre	2.30	1.89E-03	20,615	47,482
miR-329	Mature	0.60	2.03E-03	2,744	1,641
miR-30e	Mature	1.97	2.08E-03	1,346	2,654
miR-4510	Mature	1.99	2.17E-03	1	2

Next, a second set of volcano plots were generated to visualize changes in miRNA abundance following CL-316,243 treatment. The number of miRNAs with p-values <0.05 and a fold change of >2 or < 0.5 was significantly lower than in the preadipocyte to mature adipocyte comparisons (Figure 2.15A). Only 5 miRNAs had p-values < 0.01, while 36 had p-values < 0.05, and 78 miRNAs had p values < 0.1. The top 20 candidates, ranked by p-value, are listed in Table 4. Notably, all of the miRNAs with p-values < 0.01 had normalized read counts of < 20 per sample in both the control group and the CL-316,243 group. The only abundant miRNA, miR-872, was decreased by only 11% in CL-316,243 treated cells. In summary, while CL-316,243 treatment strongly induces thermogenesis, changes in miRNA abundance do not appear to mediate this effect.

A comparison of miRNAs in mature iWAT vs. mature eWAT (Figure 2.15B) resulted in 14 miRNAs with p-values < 0.01, 80 miRNAs with p-values < 0.05, and 160 miRNAs with p values < 0.1. Of the top-ranked miRNAs shown in Table 5, several have been shown to mediate differences in phenotype between BAT and WAT, or between sWAT and vWAT. MiR-196a promotes BAT/beige identity by suppressing the WAT-associated gene *Hoxc8* (Mori et al., 2012). Mice overexpressing miR-196a have increased beige fat and are resistant to obesity. miR-195a targets zfp423, a transcription factor that promotes vWAT phenotype and inhibits adipogenesis (Yun et al., 2015). miR-199a, which did not rank in the top 20 candidates, has been shown to inhibit thermogenesis by suppressing the mTOR signaling pathway (Gao et al., 2018) and by targeting *Pgc1α* and *Prdm16* (He et al., 2018). MiR-199b, which has not been thoroughly investigated in adipose tissue, ranks 18th by p-value and may play a similarly important role in regulating adipocyte phenotype.

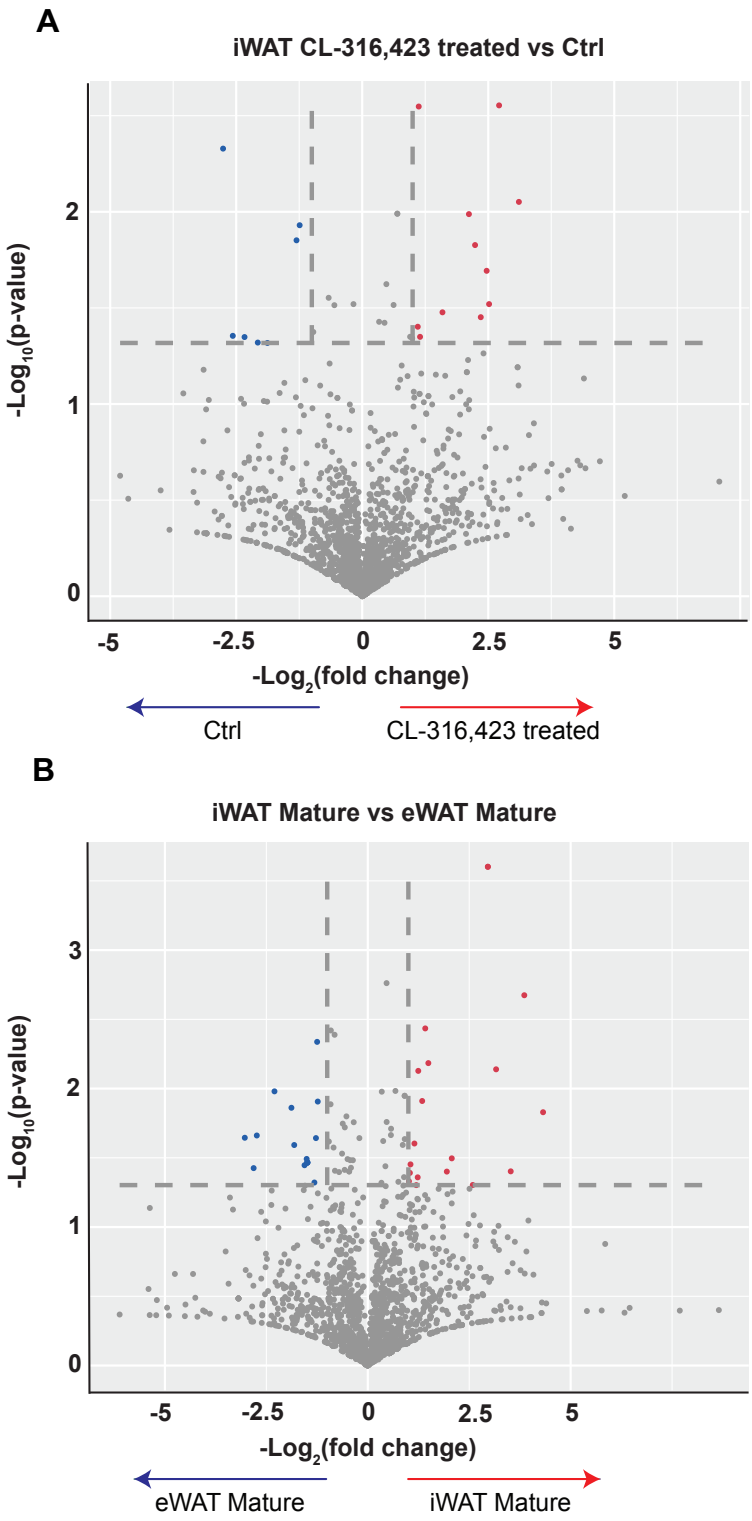

Figure 2.15 miRNA abundance is moderately depot dependent and only minimally impacted by CL-316,243 treatment

(A and B) Volcano plot of miRNA abundance in CL-316,243 treated iWAT compared untreated iWAT (A) and mature iWAT compared to mature eWAT (B). Horizontal and vertical dashed lines represent $p < 0.05$ and fold change > 2 or < 0.5, respectively.

Table 4: Top miRNAs by p-value: CL-316,243 treated iWAT

miRNA	Enriched	Fold Change	p-value	Ctrl reads	CL reads
miR-76871	CL-316,243	NA	1.74E-03	0	2
miR-7054	CL-316,243	6.57	2.79E-03	1	8
miR-103	CL-316,243	2.18	2.83E-03	7	15
mIR-4335	Ctrl	0.15	4.69E-03	5	1
miR-450b	CL-316,243	NA	8.00E-03	0	2
miR-8097	CL-316,243	8.62	8.88E-03	0	3
let-7f	CL-316,243	1.62	1.02E-02	10	16
let-7f (R+3)	CL-316,243	1.62	1.02E-02	10	16
miR-200b	CL-316,243	4.34	1.03E-02	1	5
miR-6236	Ctrl	0.42	1.17E-02	18	8
miR-3061	Ctrl	0.41	1.41E-02	10	4
miR-6395	CL-316,243	4.72	1.49E-02	1	4
miR-186	CL-316,243	5.54	2.03E-02	1	6
miR-135a	CL-316,243	1.39	2.38E-02	24	33
miR-218	Ctrl	0.63	2.80E-02	30	19
miR-1668	CL-316,243	5.72	3.02E-02	1	5
miR-872	Ctrl	0.89	3.02E-02	1,749	1,551
miR-506	CL-316,243	1.54	3.05E-02	21	33
miR-500	Ctrl	0.68	3.06E-02	62	43
miR-20864	Ctrl	NA	3.25E-02	3	0

Table 5: Top miRNAs by p-value: mature iWAT vs. mature eWAT

miRNA	Enriched	Fold Change	p-value	iWAT reads	eWAT reads
miR-196b	iWAT	7.78	2.50E-04	7	57
miR-196c	iWAT	7.78	2.50E-04	7	57
miR-490	iWAT	NA	1.53E-03	0	1
miR-6950	iWAT	NA	1.53E-03	0	1
miR-320	iWAT	1.38	1.73E-03	5,093	7,019
miR-196a	iWAT	14.50	2.12E-03	481	6,973
miR-497a	iWAT	2.67	3.68E-03	3,077	8,214
miR-181d	eWAT	0.53	3.80E-03	521	277
miR-674	eWAT	0.57	4.09E-03	1,721	976
miR-181c	eWAT	0.42	4.60E-03	613	258
miR-195a	iWAT	2.81	6.55E-03	4,687	13,189
miR-196b	iWAT	8.96	7.26E-03	917	8,211
miR-378b	iWAT	2.37	7.45E-03	57	136
miR-9298	eWAT	NA	7.61E-03	1	0
miR-30b	iWAT	1.60	1.04E-02	2,148	3,444
miR-9993b	eWAT	0.20	1.05E-02	4	1
miR-9226	iWAT	1.27	1.05E-02	1,727	2,193
miR-199b	iWAT	1.88	1.13E-02	38,046	71,416
miR-190a	iWAT	2.53	1.23E-02	260	657
miR-181c	eWAT	0.43	1.24E-02	41	17

Next, the individual comparisons made in figures 2.14 and 2.15 were combined to identify miRNA candidates that were moderately abundant, depot-specific and differentiation dependent in primary adipocytes. All 815 unique miRNAs mapping to the mouse genome were filtered by abundance, leaving 414 miRNAs with normalized read counts > 100 (Figure 2.16). 106 of these miRNAs were differentiation dependent, defined as having greater abundance in mature adipocytes vs. preadipocytes for both eWAT and iWAT, and a p-value < 0.1. Then, candidates were restricted to those showing depot dependence with either >2-fold change or < 0.67-fold change in eWAT vs. to iWAT, leaving 14 miRNAs. 12 of these 14 candidates had either been previously characterized in the literature, were identified in section 2.3, or were not detectable in primary adipose tissue by qPCR. The resulting two candidates were miR-708 and miR-218. MiR-708 is highly differentiation dependent, with 25-30-fold higher expression in both mature iWAT and mature eWAT compared to preadipocytes from either depot. miR-708 is 2-fold more abundant in mature adipocytes from iWAT than eWAT, although this difference is not maintained *in vivo*. Levels of miR-218 are increased by differentiation in both iWAT and eWAT cells, by 45% and 65%, respectively. *In vitro* and *in vivo*, miR-218 is roughly 50% more abundant in eWAT than iWAT, and *in vivo* abundance is roughly 7-fold higher in iBAT than eWAT.

2.5 Summary

A combination of the two screening approaches used in this chapter, the first *in vivo* and the second *in vitro*, provides a comprehensive overview of miRNA abundance under various conditions in adipocytes. *In vivo*, miRNA levels vary significantly between the three

major adipose types (vWAT, sWAT, and iBAT), with the most significant variability arising between iBAT and vWAT. miRNA levels were less variable between multiple depots of the same category (eWAT/mWAT, iWAT/aWAT), and between cWAT (beige) and iWAT. *In vitro*, miRNA profiles differ greatly between preadipocytes and mature adipocytes for both eWAT and iWAT. Top differentiation dependent candidates include miR-31 and miR-541, both of which were more abundant in preadipocytes. There were fewer miRNAs that varied

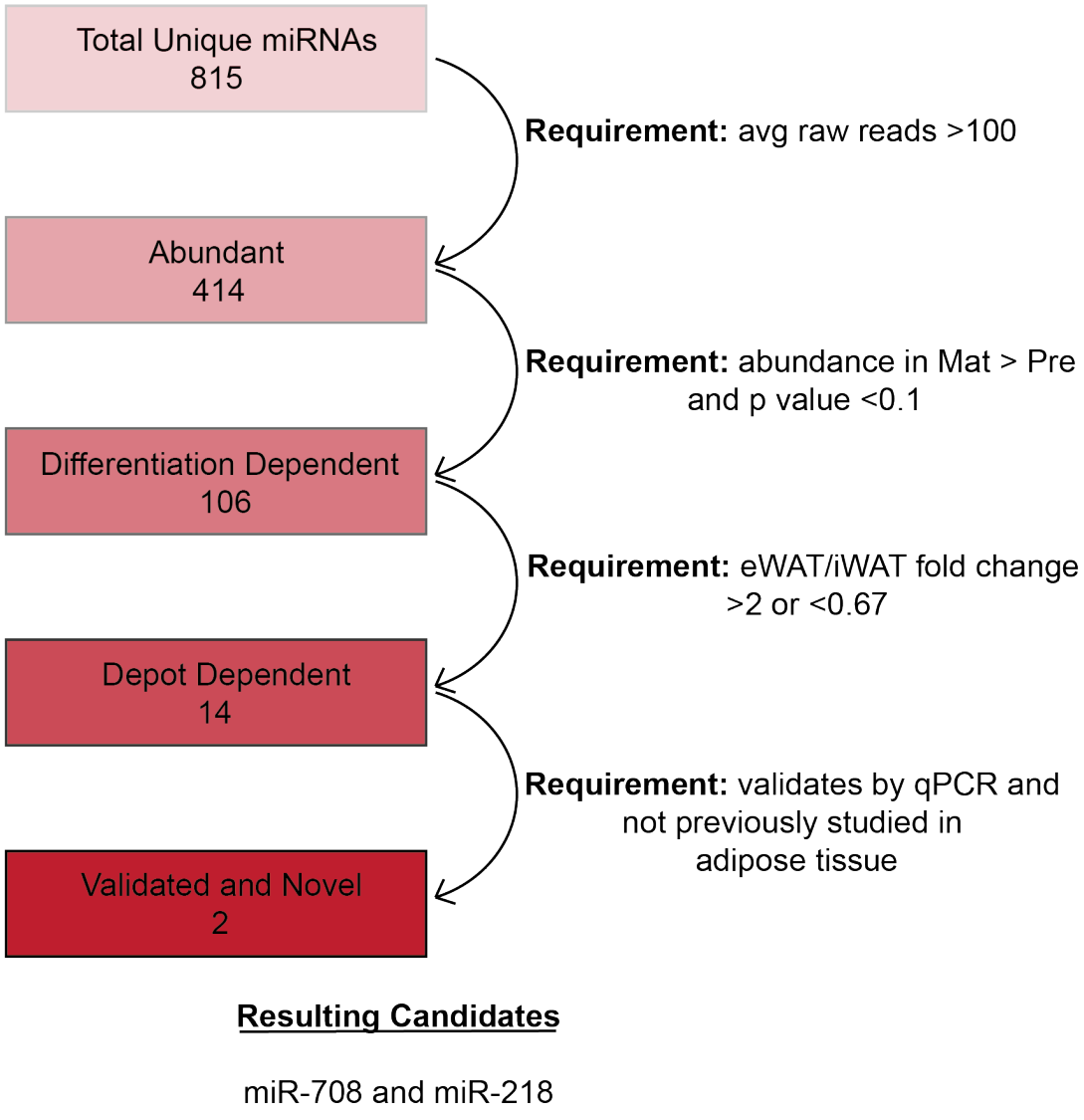

Figure 2.36 Schematic of criteria applied to identify miRNA candidates from *in vitro* screen

between eWAT and iWAT, and almost no abundant species with a strong fold change between CL-316,243 treated iWAT and control iWAT. Taken together, these results suggest that miRNAs play an important role in contributing to differences among adipose tissue depots, but do not play as central of a role in mediating cold or CL-316,243 induced beiging of iWAT.

For both profiling experiments, a series of filters were applied to identify candidates that had the greatest potential to mediate adipose identity and function. In general, miRNAs with higher absolute abundance and high differential expression between vWAT and sWAT were selected. Given the similarity in approach, many of the candidates that emerged from the *in vitro* screen had previously been identified *in vivo*, including the miR-183 family, miR-378, members of the miR-30 family, and others. Of the candidates from the *in vivo* screen, abundance was measured in primary cells and obese mice to further characterize expression behavior. Candidates were then ranked to prioritize consistency between abundance in primary cells and adipose tissue, and by significant changes under obesogenic conditions.

Several viral-vector based strategies were used to perform gain-of-function of miRNA candidates *in vitro*. For the top 2 ranked candidates, retroviruses were used to generate stable lines of 3T3-F442A cells overexpressing miR-335 or miR-192. The results of these two experiments were underwhelming, with miR-335 seeming to modestly inhibit differentiation while miR-192 caused a slight increase in pro-thermogenic and pro-inflammatory gene expression. Neither of these phenotypic changes represents a clear shift towards a 'visceralized' pattern of gene expression as initially hypothesized. For the second 2 candidates, miR-10b and miR-375, adenoviruses were used to drive expression. In these experiments, miR-10b slightly inhibited differentiation, and miR-375 repressed the abundance of some pro-inflammatory genes. Again, neither of these miRNAs resulted in a clear trend towards a

'visceralized' phenotype. For the final candidate tested, miR-338, primary cells were used, and a more substantial effect on gene expression was observed. The abundance of several thermogenic genes increased, and many pro-inflammatory genes were repressed. While these trends match the hypothesized effects of a sWAT enriched candidate, some genes in both thermogenic and pro-inflammatory pathways changed in the opposite direction (e.g. *Dio2*, *Elovl3*, *Tle3*). Unexpectedly, many genes involved in lipid metabolism were also impacted by miR-338. Here, 8/8 mRNAs increased, with 7/8 reaching statistical significance. Paradoxically, these genes span both lipogenic and lipolytic/β-oxidative processes, indicating that miR-338 increases activity across contrasting metabolic pathways within adipocytes. Further studies will be needed to more thoroughly characterize miR-338's role, both *in vitro* and *in vivo*.

Between the two candidates from the *in vitro* screen, miR-708 showed particularly robust differentiation-dependent induction. In B-cells, miR-708 was found to promote Wnt/β-Catenin signaling by targeting *Dkk3*, a suppressor of Wnt signaling that is also enriched in eWAT (Zhang et al., 2017). Wnt signaling in adipocytes has been found to inhibit adipogenesis (Ross et al., 2000), which would seemingly contradict the observed increase in miR-708 during adipogenesis *in vitro*. Interestingly, the HITS-CLIP experiments performed in chapter 3 identified several novel miR-708 targets involved in adipogenesis, including *aP2* and *Ncoa6* (Qi et al., 2003). These targets suggest that, perhaps, miR-708 acts to halt further increases in adipogenic gene expression as preadipocytes reach maturity. Other miR-708 targets from HITS-CLIP are genes involved in lipid synthesis, including *Acaca* and *Fasn*. Further studies are needed to fully characterize the role of miR-708 in these pathways and others.

There are several limitations to the work presented in this chapter. First, the 3T3-F442A cell line, while more convenient to work with, does not accurately model the phenotype of adipocytes *in vivo*. Even for experiments conducted with primary cells, there are significant differences in gene expression between adipocytes *in vitro* and *in vivo*. Second, gain-of-function experiments typically push miRNA expression beyond physiological levels, which can result in repression of non-traditional targets. Loss-of-function experiments are therefore often more effective at revealing physiologically relevant phenotypic effects of an endogenous miRNA. Additionally, gain-of-function may not result in any impact on a target mRNA if that mRNA is already fully 'saturated' with miRNA. For this reason, both gain and loss-of-function are necessary to fully probe a miRNA's physiological function. Moving forward, the next chapter will explore an alternative approach to characterizing miRNAs in adipose tissue that emphasizes miRNA targets in addition to expression levels.

CHAPTER 3: A network approach to studying miRNAs in adipose tissue

3.1 Introduction:

Most miRNA studies begin with profiling miRNA abundance among different cell types or tissues or across different physiological conditions. While this approach has yielded a number of important miRNA regulators in adipose tissue, including many of those described in chapter 1, expression levels alone do not indicate that a miRNA is associated with a particular biological role. Indeed, the results from chapter 2 demonstrate that many differentially abundant miRNA candidates do not significantly influence adipogenic, pro-thermogenic or pro-inflammatory pathways, at least in immortalized adipocyte cell lines. As an alternative approach, the following two chapters will focus on miRNA target recognition as

a starting point. Since many of the key proteins and transcriptional regulators that influence adipocyte metabolism have been well described previously, this approach takes advantage of well-defined gene networks associated with adipocyte identity.

MiRNAs often influence cellular phenotype by targeting multiple members of a particular gene pathway, exerting a subtle effect on each target (Bartel, 2018). As such, focusing exclusively on an individual target can overlook powerful cumulative effects. For this reason, we utilized two network-based methods to identify and characterize miRNAs that contribute to iBAT vs. eWAT identity. The first of these approaches, miRhub, is a computational program that focuses on network-effects of miRNAs using a Monte Carlo simulation to identify regulatory hubs for a particular gene set of interest. 3 primary pieces of information are needed: (1) the gene set of interest, (2) predicted miRNA/target pairs as determined by TargetScan, and (3) gene interactions based on protein association in the STRING 9.0 database (Rutledge et al., 2015; Baran-Gale et al., 2013). The algorithm selects miRNAs with abundances that are inversely correlated with their targets and incorporates data on the centrality of their targets to gene networks in the tissue of interest. Because iBAT and vWAT lie at opposite ends of a metabolic spectrum regarding thermogenic potential (Ye et al., 2013), chronic inflammation (Ziegler et al., 2019), insulin sensitivity (Janochova et al., 2019), and adipokine secretion (Scheja and Heeren, 2019), we began by defining our gene set of interest to be mRNAs with differential abundance between iBAT and eWAT.

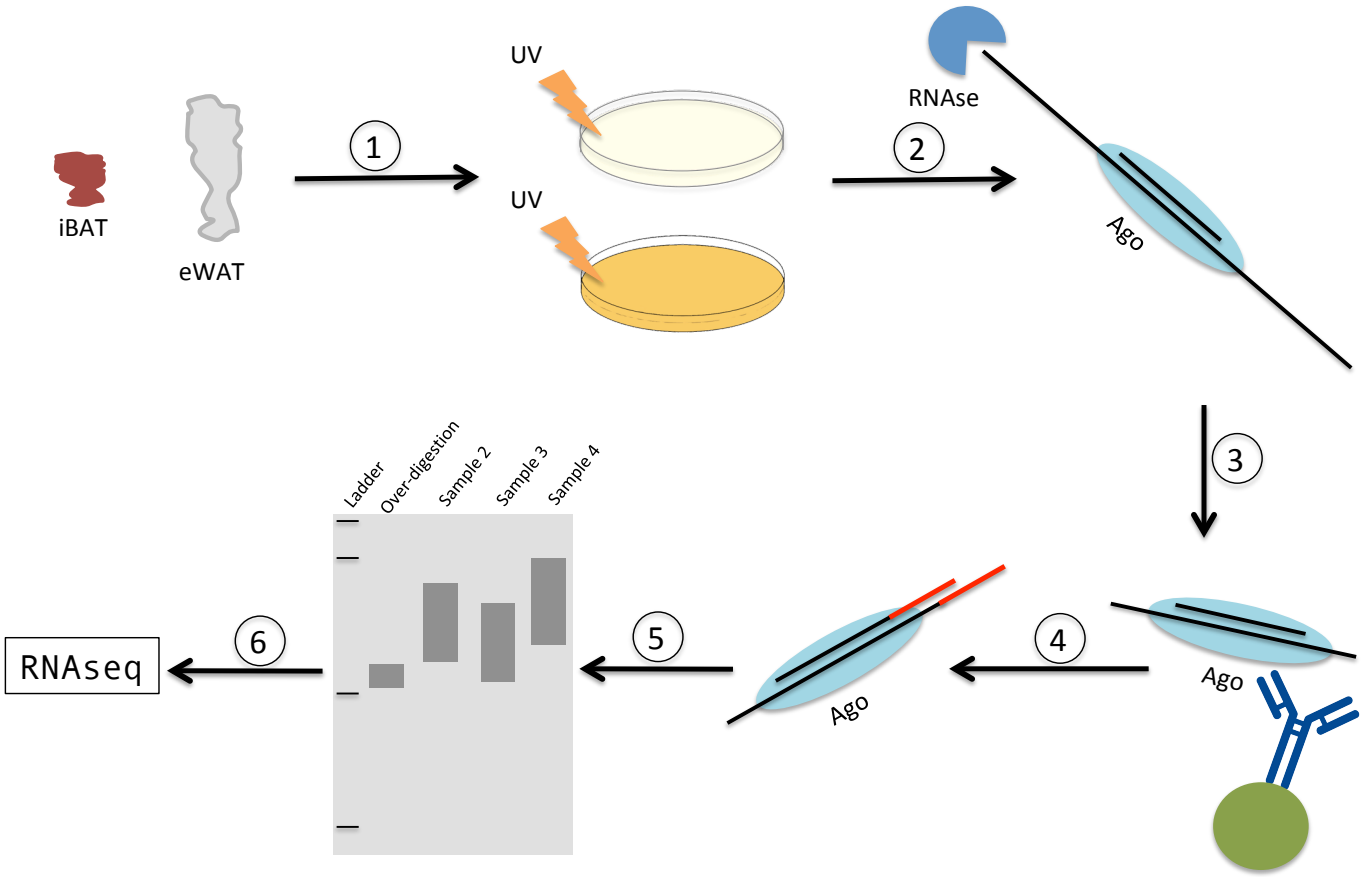

Figure 3.1 Overview of HITS-CLIP experimental workflow
(1) iBAT and eWAT are flash frozen, ground to a fine powder with mortar and pestle, then irradiated with UV light to crosslink RNA and proteins.
(2) The irradiated samples are dissolved in lysis buffer then RNAse is used to digest regions of unprotected RNA. RNA bound tightly by Ago is not protected.
(3) Ago:RNA complexes are immuneprecipitated using an anti-Ago2 antibody.
(4) Radiolabeled linkers are added to the overhanging 3' ends of miRNA and mRNA fragments.
(5) Ago:RNA complexes are run on a gel, transferred to a membrane, then exposed to film to generate an autoradiograph.
(6) The Ago protein is digested with protease to release RNA, which is then sequenced.

The second network-based approach, high-throughput sequencing of RNA isolated by crosslinking immunoprecipitation (HITS-CLIP), is a powerful technique capable of identifying tens of thousands of miRNA binding sites within a tissue of interest (Chi et al., 2009). The technique involves crosslinking Argonaute (Ago) with associated RNA, including miRNAs and miRNA targets. Following immunoprecipitation, RNA is sequenced, and miRNAs are

matched with their targets across the transcriptome. An overview of the technique, which can be divided into 6 broad steps, is presented in Figure 3.1. HITS-CLIP belongs to a family of high-throughput crosslinking techniques, including PAR-CLIP (photoactivatable ribonucleoside-enhanced-CLIP), CLASH (cross-linking and sequencing of hybrids) and iCLIP (individual-nucleotide resolution-CLIP). PAR-CLIP uses nucleoside analogs that readily crosslink to RNA, leaving distinct mutations that can be used to precisely locate Ago binding sites (Hafner et al., 2010). The major drawback to PAR-CLIP is the inability to use tissue samples as starting material (Hafner et al., 2010). CLASH unambiguously identifies miRNA targets, including non-canonical sites, by ligating mRNA/miRNA fragments. Protocols typically use an ectopically expressed Ago that, while helpful for immunoprecipitation, introduce artifacts by altering endogenous Ago/miRNA behavior (Helwak et al., 2013). iCLIP differs in the way that cDNA libraries are reverse transcribed before sequencing. Unlike most CLIP protocols, iCLIP captures cDNAs that would otherwise be truncated at mutation sites by ligating an adapter and circularizing at the site of truncation (Huppertz et al., 2014). It is unclear if this circularization step induces or removes bias in generating libraries for sequencing. In summary, while each high-throughput protocol has advantages and disadvantages, HITS-CLIP remains the most robust and proven technique to identify miRNA binding sites *in vivo*.

3.2 Results: miRhub identifies potential regulatory hubs in adipose tissue

To identify post-transcriptional determinants of brown vs. white fat identity, we utilized the *in vivo* small RNAseq data presented in chapter 2 to compare iBAT and eWAT and found substantial variance by principal component analysis (PCA; Figure 3.2A). Of the 378 miRNAs with >100 reads, the levels of 105 were significantly different between iBAT and

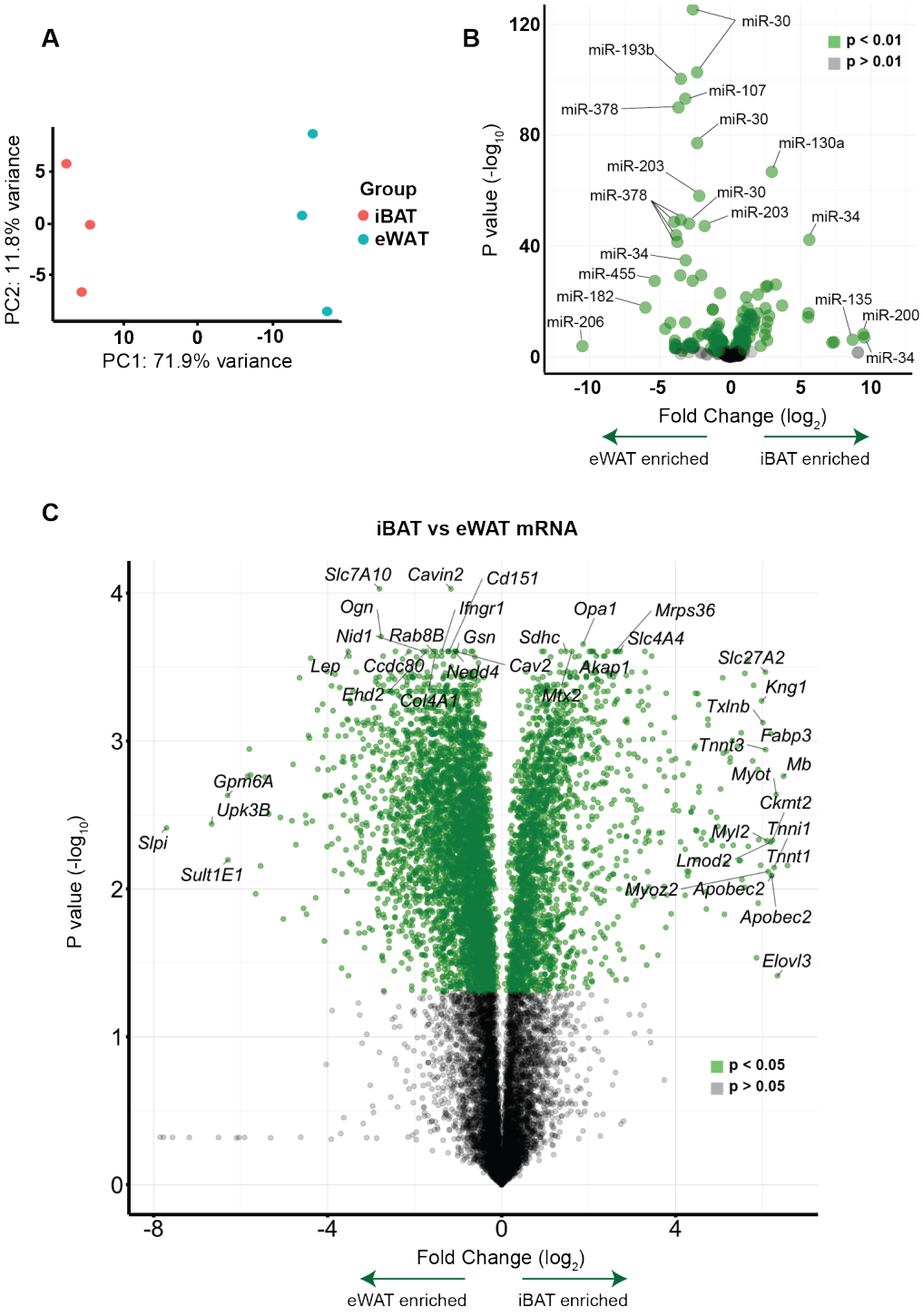

Figure 3.2 Differential abundance of mRNAs and miRNAs in iBAT and eWAT
(A) PCA analysis of small RNA sequencing of iBAT and eWAT from 13-week old male mice (3 mice pooled per group, n=3).
(B) Volcano plot showing miRNAs enriched in iBAT vs. eWAT (3 mice pooled per group, n = 3).
(C) Volcano plot showing mRNAs enriched in iBAT vs. eWAT (n = 3).

eWAT (p-value <0.01; Figure 3.2B). A number of the most differentially expressed miRNAs have been shown to play important roles in adipocyte function, including miR-30 (Hu et al., 2015), miR-193b (Sun et al., 2011), miR-378 (Pan et al., 2014) and miR-130 (Kim et al., 2013). Next, mRNA levels were compared between iBAT and eWAT using previously generated microarray data (Cohen et al., 2014; GEO accession GSE53307), identifying 2,693 genes with absolute $\log_2$ fold change >2 and $p < 0.05$ (Figure 3.2C).

To identify miRNAs that act as regulatory hubs in adipose tissue, we used miRhub as previously described (Baran-Gale et al., 2013). We defined the gene set of interest as mRNAs with a fold change > 4 or < 0.25 and a p-adj < 0.05 between iBAT and eWAT. The miRNAs analyzed were those with differential abundance between iBAT and eWAT, defined as having DEseq normalized read counts greater than 100 and $p < 0.01$. The analysis resulted in 3 iBAT enriched candidates with p-values < 0.05, and an additional 5 eWAT and 3 iBAT enriched candidates with p-values between 0.05 and 0.2 (Figures 3.3A and 3.3B). miR-133 and miR-328 have been previously described as regulators of iBAT identity and function (Trajkovski et al., 2012; Oliverio et al., 2016), while the role of miR-29 in adipose tissue has not been thoroughly characterized. MiR-29 levels were measured in the iBAT and eWAT of several

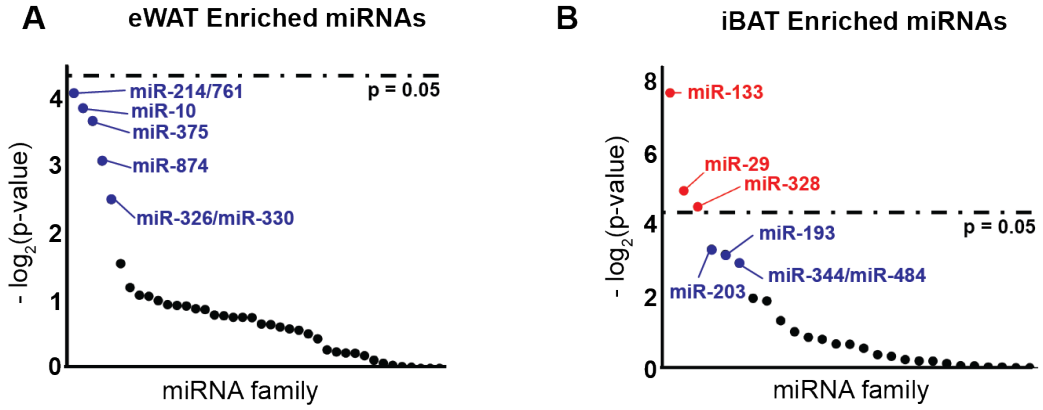

Figure 3.3 MiRhub analysis identifies 11 potential miRNA regulatory hubs
(A) MiRhub results for eWAT enriched miRNAs (blue = 0.05 < p < 0.2).
(B) MiRhub results for iBAT enriched miRNAs (red = p < 0.05, blue = 0.05 < p < 0.2).

cohorts of mice of varying ages, as well as primary cells isolated from iBAT and eWAT. The iBAT enrichment of miR-29 from the miRNA sequencing experiment was not consistent across all conditions *in vivo* and *in vitro* (data not shown). These results suggest that miR-29 may act as a regulatory hub to promote BAT identity under certain conditions; however, future studies are needed to fully characterize miR-29 expression and function.

3.3 Results: HITS-CLIP reveals miRNA binding sites in iBAT and eWAT

While miRhub is a powerful tool for studying miRNA binding at the network level, it relies on bioinformatic target predictions, which have a high false-positive rate (Pinzon et al., 2017). Therefore, to identify adipose-specific miRNA binding activity based on *in vivo*, biochemical interactions, we used Ago HITS-CLIP on iBAT and eWAT. Following UV crosslinking, Ago:RNA complexes were immunoprecipitated (Figure 3.4A) and separated by gel electrophoresis to produce an autoradiograph of labeled RNA (Figure 3.4B). After sequencing Ago-associated RNAs, iBAT and eWAT samples separated effectively by PCA (Figure 3.5A) and showed low inter-sample variability by Pearson correlation (Figure 3.5B). Non-miRNA reads were clustered into peaks using Homer motif analysis, revealing a total of 21,281 unique peaks across 6,717 genes. The majority of peaks, ~53%, fell within mRNA 3'-untranslated regions (UTRs), ~40% within coding sequences (CDS) and the remaining 7-8% within 5'-UTRs, introns and other regions (Figure 3.5C). Total sample reads and unique peaks were higher in iBAT than eWAT, although the proportions of reads mapping to the 3'-UTR vs. CDS was roughly equivalent in both depots (Figure 3.5D). A differential analysis between eWAT and iBAT was performed on reads per peak and reads per gene (Figures 3.6A and 3.6B).

Several genes, including *Ccdc80*, *Abcd2,* and *Lep* were among the most differentially regulated.

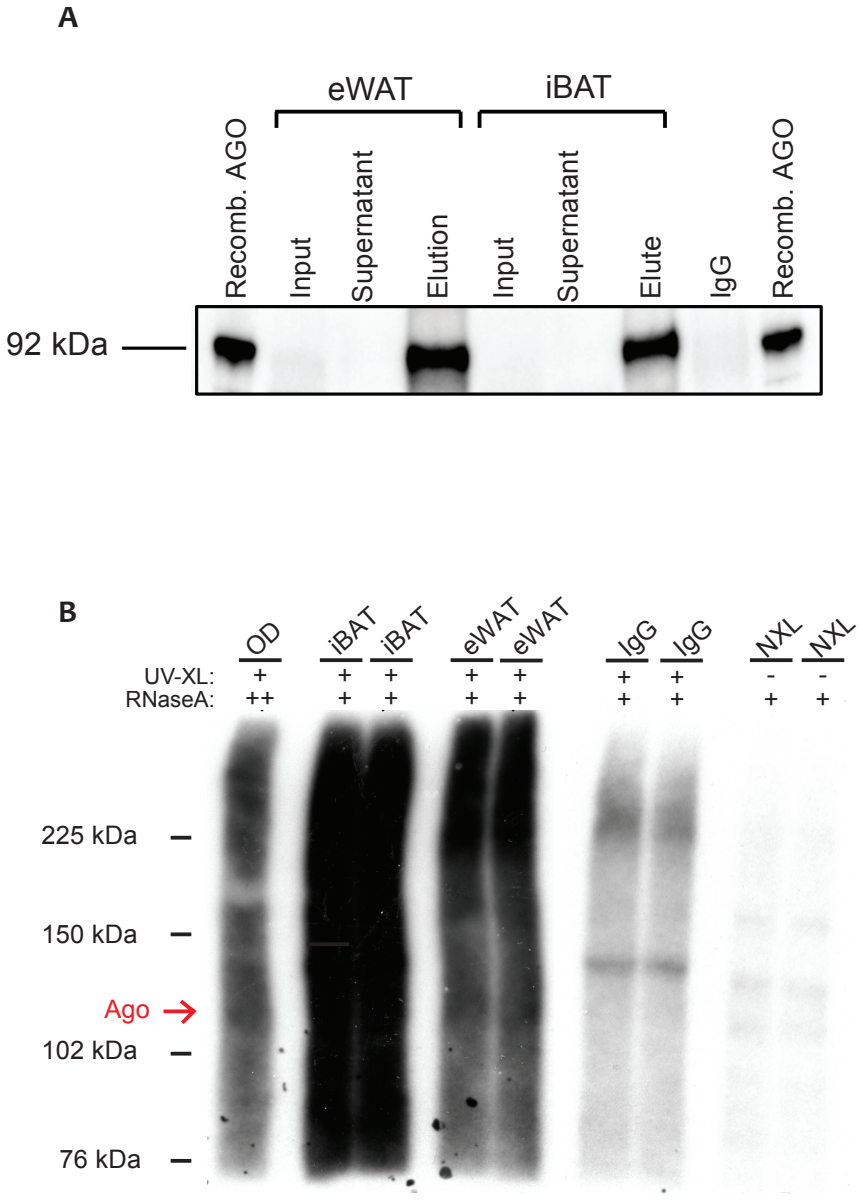

Figure 3.4 Ago immunoprecipitation and Autoradiograph
(A) Immunoprecipitation of Ago from eWAT and iBAT.
(B) Representative autoradiograph of an over-digested control (OD), iBAT, eWAT, an IgG control and a no-crosslink control (NXL).

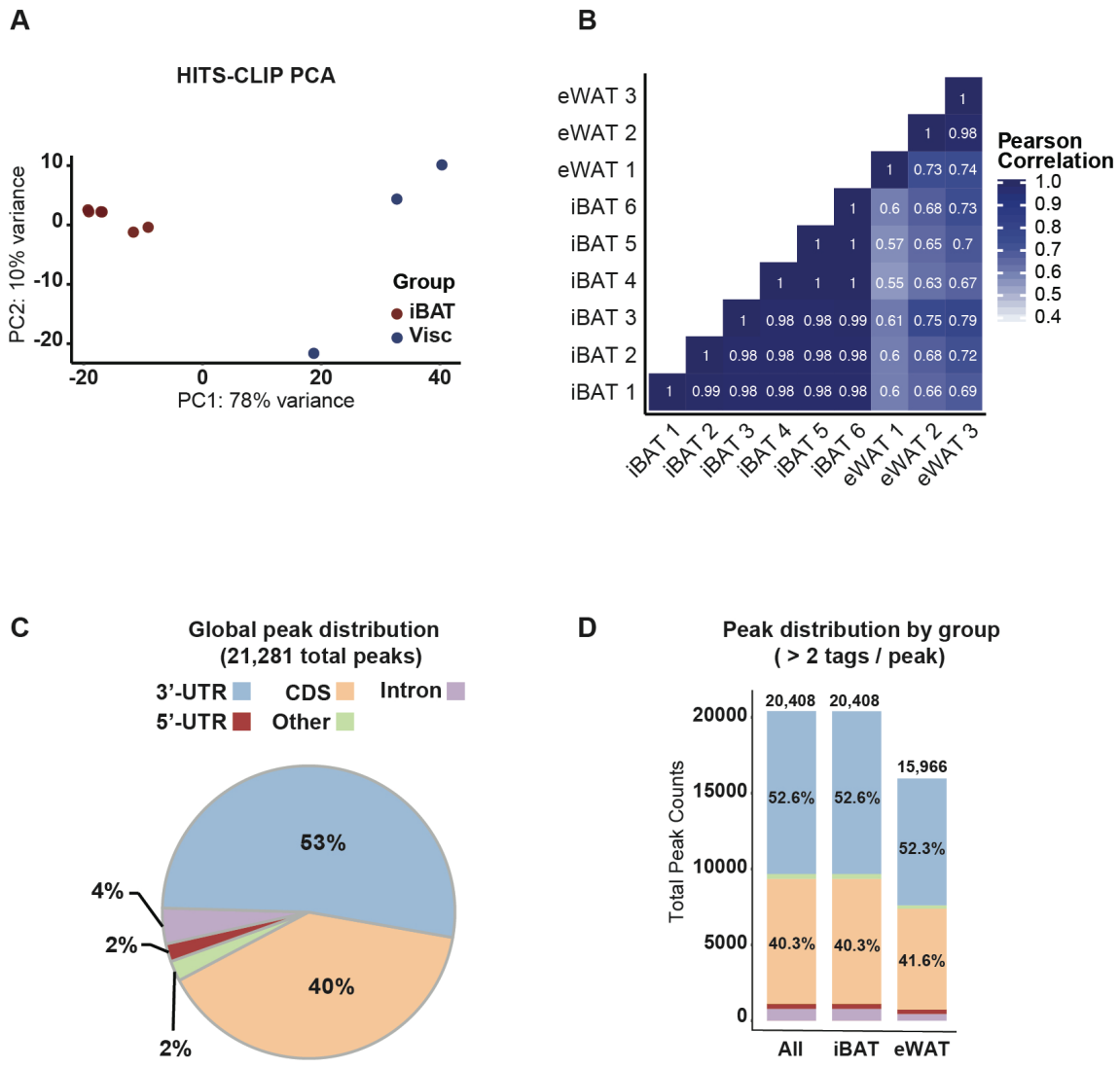

Figure 3.5 A majority of peaks fall within mRNA 3'-UTRs
(A) PCA analysis of HITS-CLIP on iBAT and eWAT from 13-week old male mice (2 mice pooled per group, n = 6 for iBAT, n = 3 for eWAT).
(B) Pearson correlations for 6 iBAT and 3 eWAT samples.
(C) Global peak distribution, averaged across all samples.
(D) Total peak counts, by annotated region, for iBAT and eWAT.

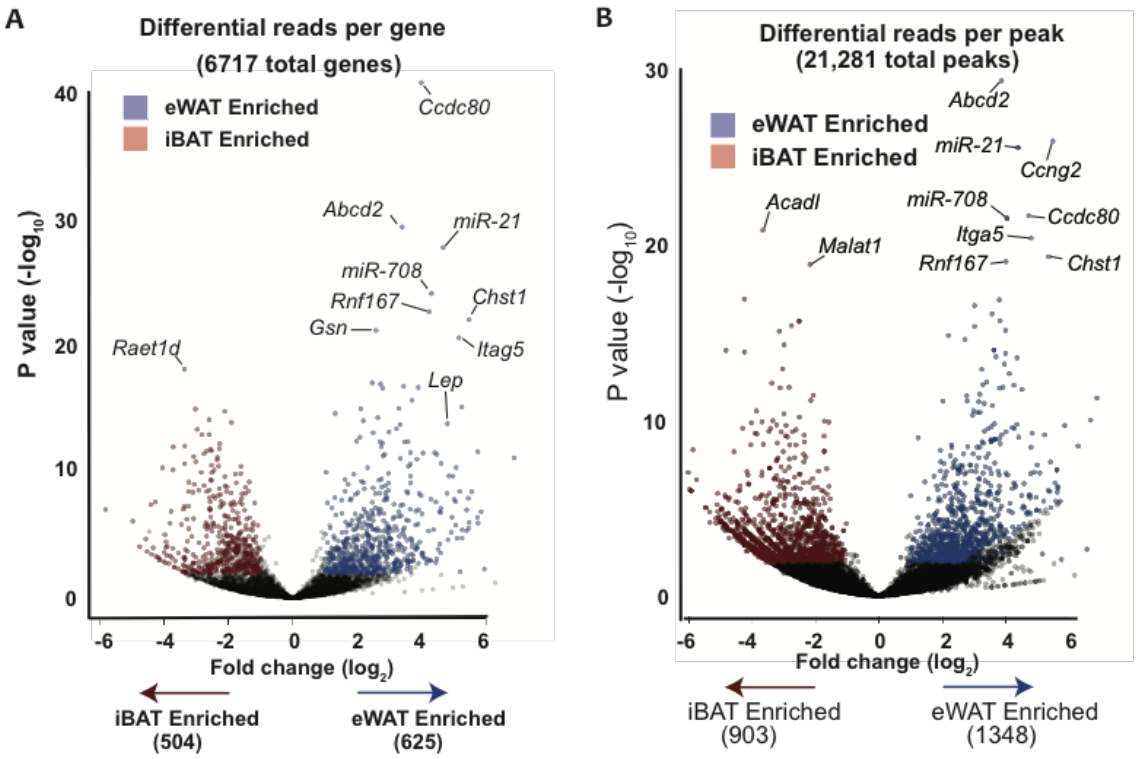

Figure 3.6 miRNA binding varies between iBAT and eWAT
(A and B) Volcano plot of miRNA binding sites of differential read counts in iBAT and eWAT, grouped by gene (A) and by peak (B).

Ago-associated reads were next mapped to a library of mature miRNAs, resulting in 193 unique miRNAs. After clustering by family, we restricted our focus to abundant miRNA families with normalized reads > 0.5% total miRNA (Figure 3.7A). The iBAT vs. eWAT enrichment of Ago-associated miRNAs correlated well with total miRNA abundance by small RNAseq (Figure 3.7B), indicating that Ago loading is primarily influenced by miRNA abundance in adipose tissue.

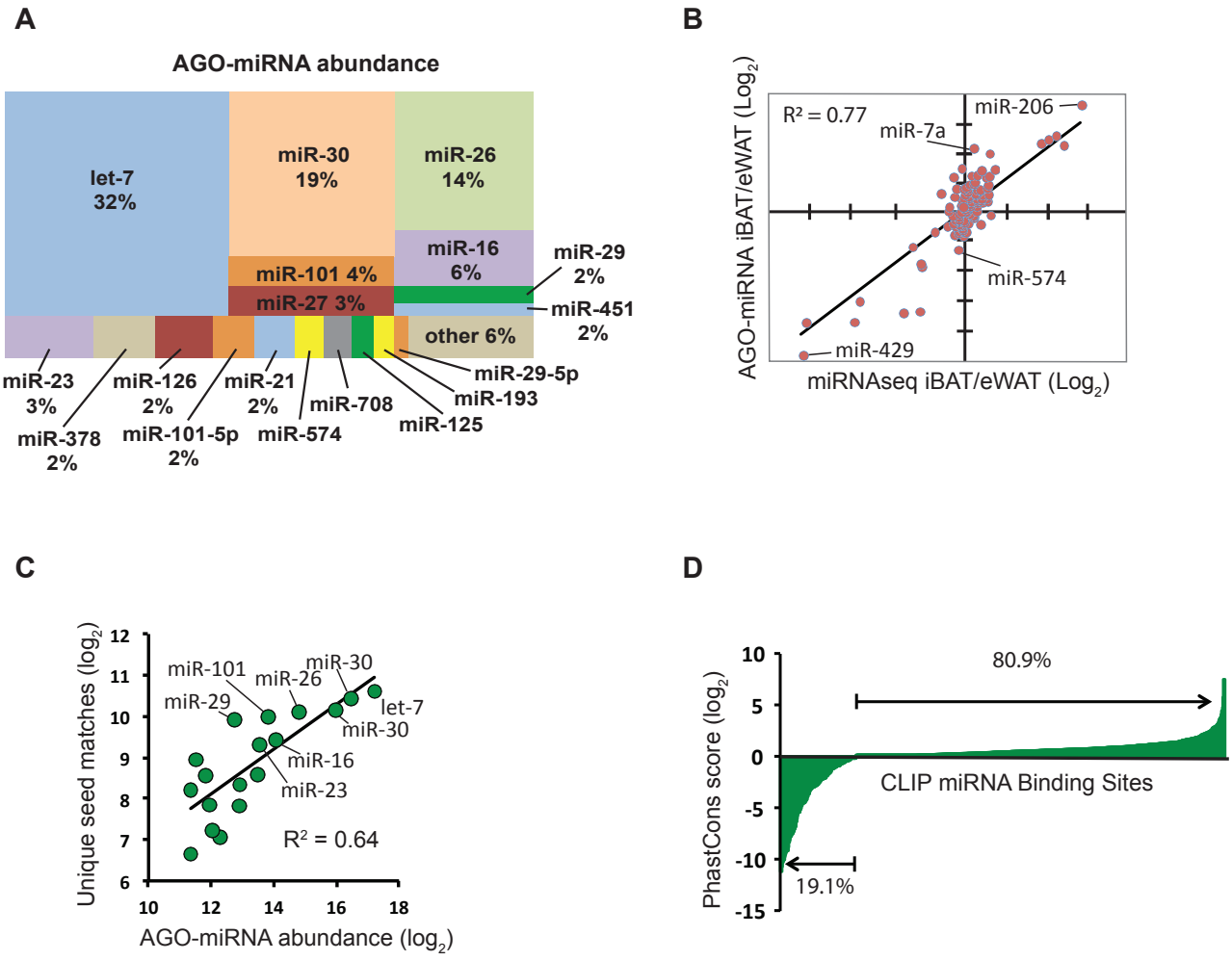

Figure 3.7 Most miRNA binding sites are well-conserved
(A) Most abundant Ago-associated miRNA families, grouped by 6-mer.
(B) Relative depot enrichment of HITS-CLIP miRNA reads to small RNA sequencing miRNA reads.
(C) Linear regression of miRNA abundance and unique seed matches.
(D) Histogram of top 1000 peaks ranked by ascending PhastCons score.

Next, Ago-associated miRNAs were matched with binding sites by searching for seed sequence complementarity within statistically significant peaks. Among the most abundant miRNA families, there was a strong correlation between miRNA reads and unique seed matches, consistent with previously published HITS-CLIP results (Figure 3.7C; Chi et al., 2009). With a minimum seed length of 6 nucleotides, however, simply matching seed

sequences to peaks is likely to generate a high number of false positives. To address this, PhastCons scores (Siepel et al., 2005) for each binding site were calculated by measuring the conservation of each HITS-CLIP generated miRNA binding site relative to 200 base pairs of flanking DNA. Of the top 1000 binding sites by peak height, 80.9% were well conserved across the 28 species included in the analysis (Figure 2D). We then generated a match score for each miRNA binding site based on (1) peak height, (2) PhastCons score and (3) length of seed sequence complementarity. The match score is not an indication of affinity between a miRNA and its target *per se* but is rather a prediction of confidence for each miRNA/target pair.

To identify miRNAs most responsible for impacting gene regulation in adipose tissue, miRNAs were ranked by the sum of total binding events across all targets, referred to here as seed match total reads. The top 3 ranked candidates by seed match total reads, miR-30, let-7 and miR-26 have been thoroughly studied in adipose tissue, both *in vivo* and *in vitro* (Hu et al., 2015; Koh et al., 2018; Ventayol et al., 2014; Giroud et al., 2016; Karbiener et al., 2014; Acharya et al., 2019). For this reason, we decided to focus on miR-29, the fourth-ranked candidate (Figure 3.8A). miR-29 has been described previously as a regulator of the glucocorticoid receptor in adipocytes (Glantschnig et al., 2019), but has otherwise not been investigated in depth. Interestingly, when seed match total reads were plotted against Ago-associated miRNA reads, we found that miR-29 matched more targets than expected (Figure 3.8B). Considering that only a fraction of Ago:miRNA complexes are associated with target mRNAs (La Rocca et al., 2015), these findings suggest that miR-29 is disproportionately active in adipose tissue.

A

miRNA	Seed match total reads
miR-30	10,117
miR-26	10,085
let-7	9,394
miR-29	8,131
miR-16	5,648
miR-27	5,332
miR-101	4,493
miR-125	4,463

B

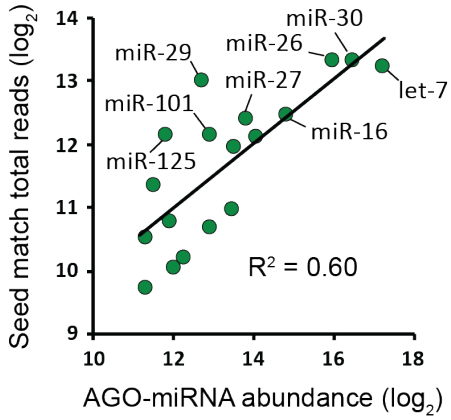

Figure 3.8 miR-29 is a highly active miRNA in adipose tissue
(A) miRNAs ranked by seed match total reads.
(B) Linear regression of Ago-miRNA abundance and seed match total reads.

3.4 Summary

The two network-based approaches used in this chapter highlight different rationales for identifying miRNA regulators. MiRhub focused on miRNAs that repress gene networks associated with iBAT/eWAT identity, while HITS-CLIP prioritized candidates based on the sum of total binding events. Of the three miRhub candidates with $p < 0.05$, miR-29 was by far the most abundant by total reads. Interestingly, among miR-29's top 100 targets are several WAT identity markers from the BATLAS gene set (Perdikari et al., 2018), suggesting that miR-29 is a miRNA hub that promotes BAT identity and/or represses WAT identity in adipocytes. These findings, however, are complicated by the fact that miR-29 does not appear to be consistently enriched in iBAT depots of mice. It may be that miR-29 is upregulated in iBAT at certain ages or under certain physiological conditions in order to repress eWAT identity. The conditions impacting miR-29 expression, and the mechanism by which miR-29 represses eWAT gene programs, should be investigated in future studies.

Interestingly, we found that miR-29 also emerged as a top candidate for regulating adipose tissue phenotype in the HITS-CLIP analysis. With 8,131 normalized seed match total reads, miR-29 was among the most active miRNAs in adipose tissue. When compared to miRNA abundance, miR-29's seed match total read count was disproportionately high, suggesting that Ago:miR-29 complexes are more likely to be associated with targets than other miRNAs. Beyond miR-29, the HITS-CLIP data presented here provide a wealth of information about miRNA behavior in adipose tissue. The reads per peak and reads per gene analysis confirms that miRNA regulatory behavior differs significantly between iBAT and eWAT. The distribution of miRNA binding locations, however, appear to be fairly consistent between the two depots, with roughly 53% of peaks localized to mRNA 3'-UTRs and 41% localized to CDSs. Interestingly, many of the top ranked binding sites by match score analysis localized to mRNA coding sequences. These sites were roughly as likely as 3'-UTR sites to be well-conserved, suggesting that miRNAs may be more likely to bind coding sequences than was previously thought.

There are several limitations to the work performed in this chapter. First, the miRhub analysis relied on bioinformatic predictions of miRNA targets from TargetScan, many of which are false positives (Pinzon et al., 2017). Additionally, the miRNA sequencing and mRNA microarray data are from mice of different ages, which raises concerns about candidates that exhibit age-dependent expression, possibly including miR-29. For HITS-CLIP, efficiency of Ago immunoprecipitation can be influenced by the sequence and length of Ago-associated RNA, which could bias the results towards certain peaks. Also, read counts were significantly lower for eWAT samples than iBAT, which could have resulted in distortions during the PCR amplification of libraries prior to sequencing.

CHAPTER 4: MiR-29 regulates leptin

4.1 Introduction

High throughput Ago-crosslinking techniques reveal hundreds, or even thousands of targets per miRNA (Chi et al., 2009; Hafner et al., 2010), suggesting that miRNAs exert regulatory power by targeting a distributed network of mRNAs. However, these findings stand in contrast to some of the literature in miRNA biology that attributes the phenotypic impact of a miRNA to only one or a few targets. In *C. elegans*, repression of *nhl-2* by miR-35 is necessary for sex determination and viability. A mutation of the miR-35 binding site on *nhl-2* is lethal, demonstrating the significance of a single miRNA/target interaction for a miRNA with nearly 100 conserved potential binding sites (McJunkin and Ambros, 2017). In mice, miR-155 targets the gene encoding AID which promotes IgG diversification and acts as an oncogene by causing chromosomal translocations. A mutation in the miR-155 binding site in AID's 3'-UTR is sufficient to substantially increase chromosomal translocations, modeling the more extreme phenotype of miR-155 knockout mice (Dorsett et al., 2008). These findings underscore the importance of focusing on individual miRNA targets that significantly impact cellular function. For this reason, we decided to further investigate miR-29's role in regulating leptin, a top-ranked target by HITS-CLIP and a powerful modulator of energy homeostasis in mammals (Friedman and Halaas, 1998).

As discussed in chapter 1, AP-2β, SREBP1, Fosl2, and CEBPα have been described previously as regulators of leptin transcription (Fuke et al., 2010; Kim et al., 1998; Wrann et al., 2012; Miller et al., 1996). None of these factors, however, are necessary and sufficient for leptin transcription, and most only weakly impact leptin abundance. More recently,

PPARγ/RXRα and a long non-coding RNA (lncOb) were shown to powerfully promote leptin transcription by interacting with an enhancer 16 kb upstream of leptin's transcriptional start site (Dallner et al., 2019; Zhang et al., 2018). *In vitro* and *in vivo*, knockdown or knockout of lncOb caused a 5-6-fold reduction in leptin mRNA. By comparison, serum leptin concentrations were reduced by only ~50% in lncOb KO mice relative to Wt controls (Dallner et al., 2019). The discrepancy between leptin mRNA and protein levels suggest that post-transcriptional modes of regulation may be involved, perhaps acting to compensate for decreases in leptin mRNA. Here, we use a combination of luciferase assays, *in vitro* gain and loss-of-function, and *in vivo* correlative studies to characterize miR-29 as the first-identified post-transcriptional regulator of leptin.

4.2 Results: leptin is among the top ranked miR-29 targets

The miR-29 family consists of 3 members, of which miR-29a is 60-70-fold more abundant in adipose tissue than miR-29b and miR-29c. MiR-29a is enriched in iBAT compared to eWAT (Figure 4.1A) and is abundantly expressed in both mature adipocytes and the stromal

Table 6: Top ranked miR-29 targets

Target	Location	Match	PhastCons Enrichment	Peak Height	Match Score	Validation
Sparc	3'-UTR	7-mer	2.3	2,518	10,674	Previously validated[1]
Lpl	3'-UTR	8-mer	2.1	1,569	8,219	Previously validated[2]
Mcart1	3'-UTR	8-mer	0.67	1,600	5,870	Novel
Ptp4a1	3'-UTR	8-mer	2.5	790	4,416	Novel
Hmgcs1	3'-UTR	7-mer	1.7	1,004	3,765	Novel
Scd1	CDS	7-mer	0.92	941	2,909	Alternate site validated[3]
Cav2	3'-UTR	8-mer	7.2	336	2,774	Previously validated[4]
Lep	3'-UTR	7-mer	4.8	477	2,648	Novel
Sucla2	CDS	7-mer	1.6	720	2,638	Novel
Col3a1	3'-UTR	8-mer	1.3	543	2,417	Previously validated[5]

[1] (Zhou et al., 2019), [2] (Chen et al., 2011), [3] (Qiang et al., 2017), [4] (Hoeke et al., 2013), [5] (van Rooij et al., 2008)

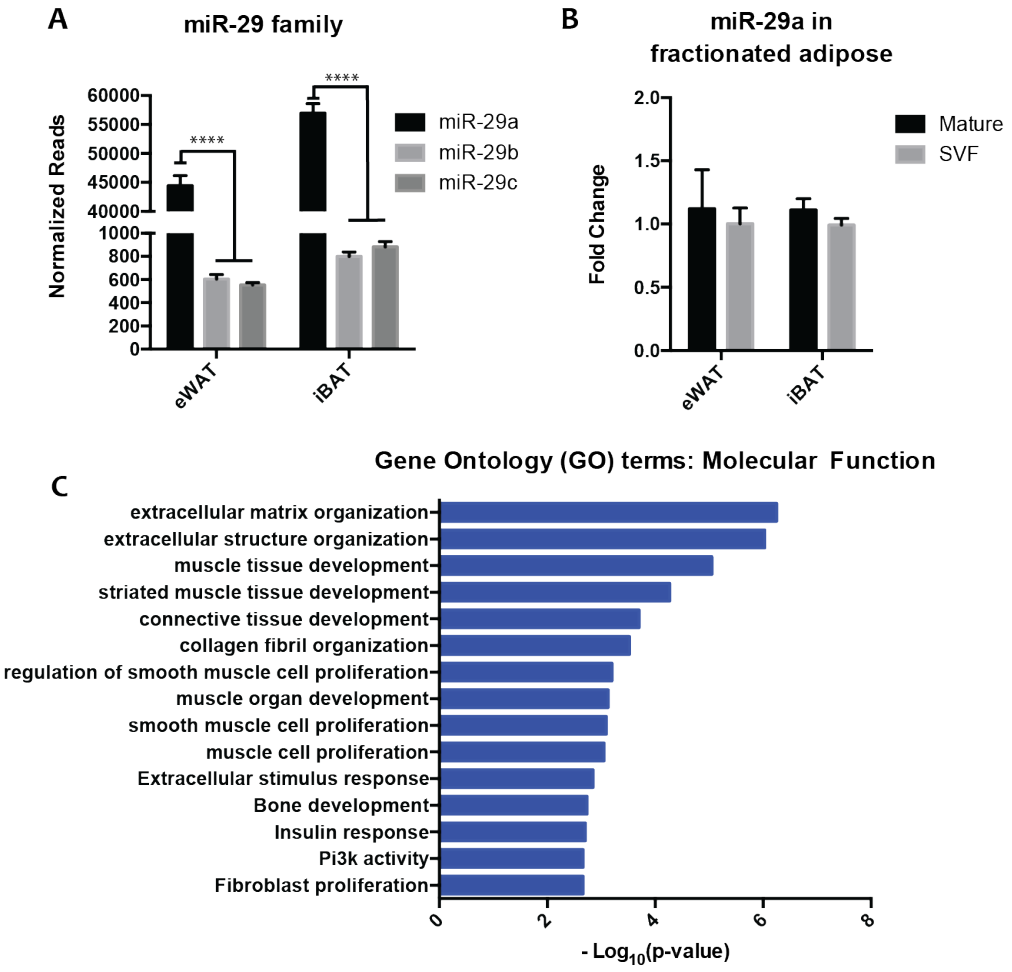

Figure 4.1 miR-29a is the predominant miR-29 family member in adipose tissue
(A) DEseq normalized read counts of miR29 from iBAT and eWAT of 13-week old male mice (n = 3).
(B) miR-29a levels in digested and fractionated iBAT and eWAT (n = 5).
(C) Gene ontology term enrichment of top 250 miR-29 3'-UTR targets.

All results are presented as mean ±SEM. 1-way ANOVA of DEseq normalized reads used for comparisons among miR-29 family members (*$p < 0.05$, **$p < 0.005$, ***$p < 0.0005$, ****$p < 0.00005$).

vascular fraction (SVF; Figure 4.1B). We performed a GO-term enrichment analysis of the top 250 3'-UTR miR-29 targets and found several pathways related to extracellular matrix organization and PI3K signaling, consistent with miR-29's previously described role in liver, cornea, muscle, and heart (Figure 4.1C; Roderburg et al., 2011; Toyono et al., 2016; Li et al.,

2017a; van Rooij et al., 2008). A closer examination of individual miR-29 targets, ranked by match score, reveals that 5 of the top 10 have been validated by luciferase assays in previous publications (Table 6).

To validate the 5 novel targets, miR-29a mimics were co-transfected into HEK-293A cells with a dual luciferase plasmid containing miRNA binding sites cloned into the 3'-UTR of firefly luciferase. For all 5 binding sites, normalized luminescence was significantly decreased with miR-29a, but not a scrambled control (Figures 4.2A – 4.2E). Mutations introduced within the miR-29 seed sequence binding sites were sufficient to block this effect.

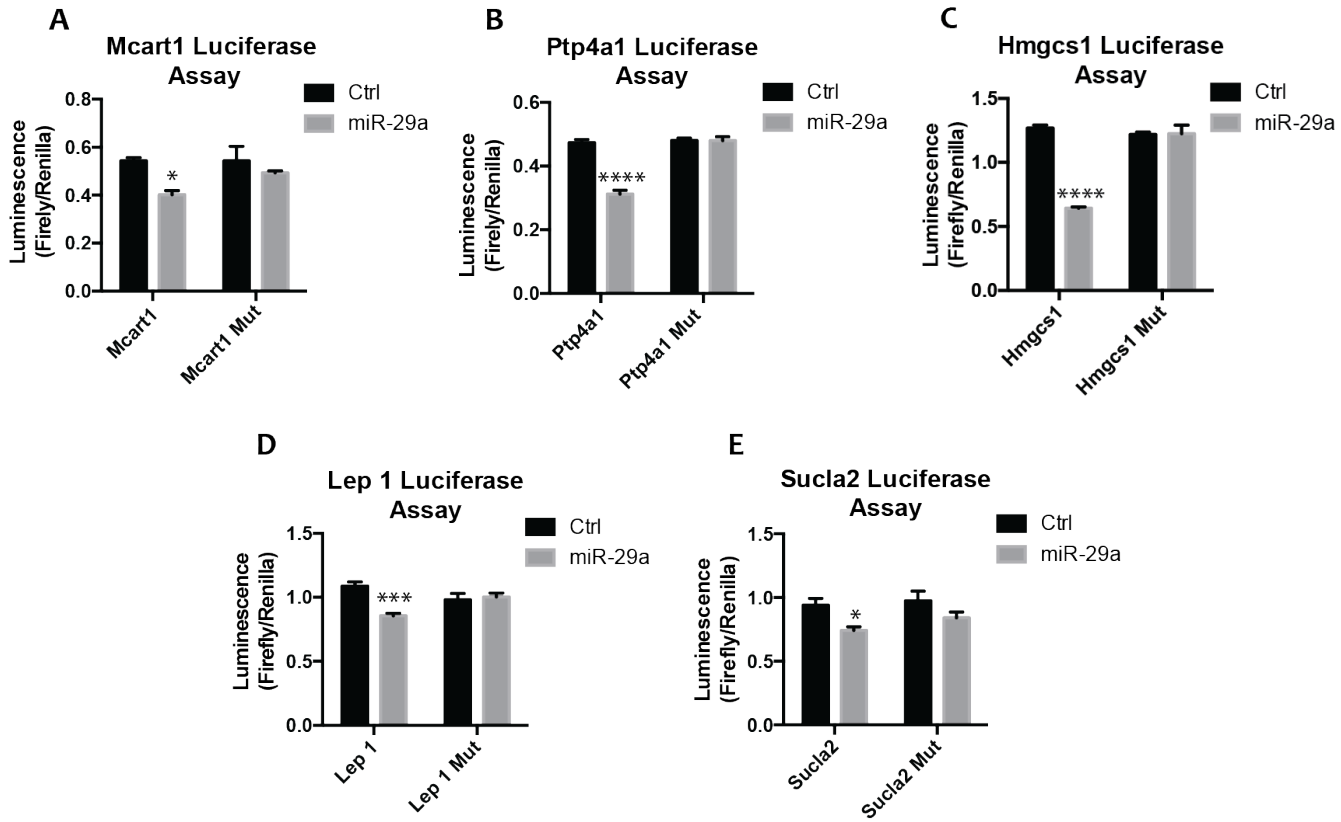

Figure 4.2 Five novel miR-29 targets validate by luciferase assay
(A - E) Dual luciferase assay validation. Luciferase activity is normalized to Renilla activity and presented as a ratio (n=4).

All results are presented as mean ±SEM. 2-way ANOVA used for miR-29a to ctrl comparisons (*$p < 0.05$, **$p < 0.005$, ***$p < 0.0005$, ****$p < 0.00005$).

Taken together, these findings demonstrate that 10/10 top predicted miR-29 targets validate, supporting the robustness of the HITS-CLIP match score analysis.

Among the 5 novel targets, only leptin contained multiple miR-29 binding sites, indicative of strong miRNA-based regulation (Grimson et al., 2007). A map of the leptin locus shows that HITS-CLIP reads fall almost exclusively within the 3'-UTR (Figure 4.3A). Normalized read counts cluster into 6 statistically significant peaks, 5 of which have complementarity with miRNA seeds, and several of which are marked by cross-linking

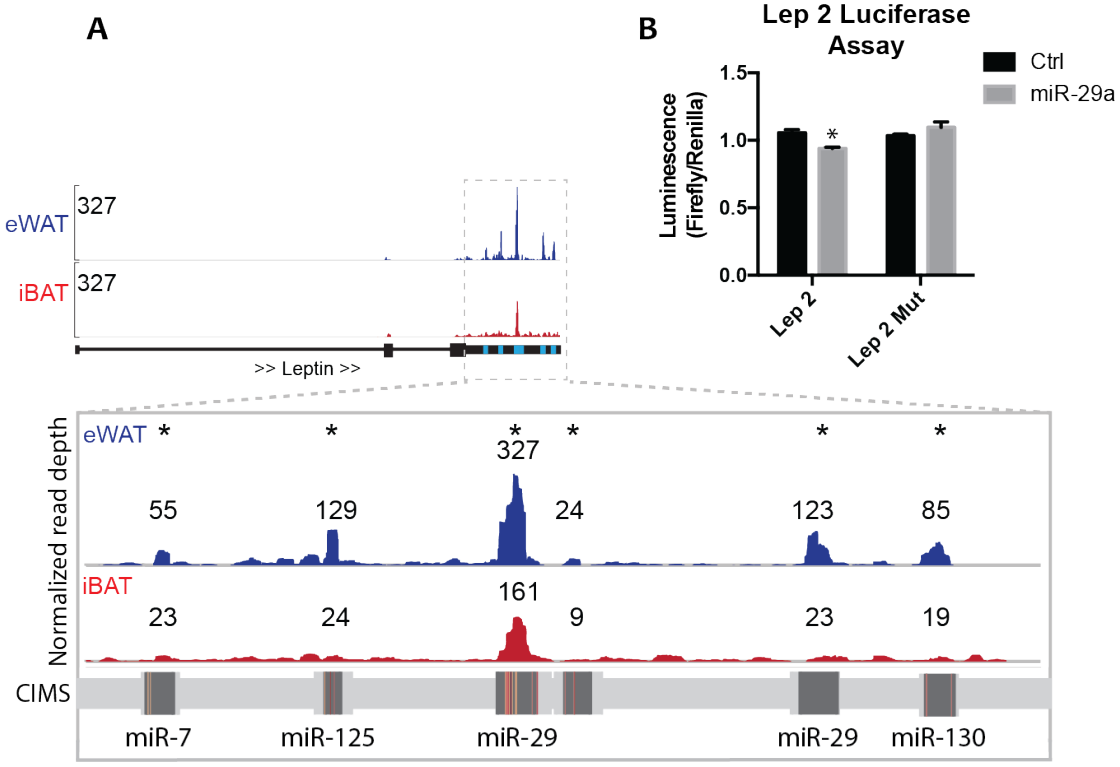

Figure 4.3 miR-29 binds two sites in the leptin 3'-UTR
(A) Gene track of the leptin locus showing reads plotted by genomic location relative to a maximum peak height of 327. Blue bars below peaks represent statistical significance. In insert, * represents statistically significant peaks and numbers indicate peak height. In the crosslinking induced mutation site (CIMS) track, red bars indicate robust mutation sites, and yellow bars indicate weak mutation sites.
(B) Dual luciferase assay validation. Luciferase activity is normalized to Renilla activity and presented as a ratio (n = 4).

All results are presented as mean ±SEM. 2-way ANOVA used for miR-29a vs. ctrl (*$p < 0.05$, **$p < 0.005$, ***$p < 0.0005$, ****$p < 0.00005$).

induced mutation sites (CIMS). In addition to the largest peak, which matches miR-29 (referred to here as the *Lep 1* binding site), a secondary miR-29 binding site (*Lep 2*) is located distal to the first and validates by luciferase assay (Figure 4.3B). There was a higher average read count in *Lep 1* and *Lep 2* for eWAT than iBAT; however, after normalizing to leptin mRNA abundance, both peaks had greater reads in iBAT (Figures 4.4A – 4.4C). The other peaks in the leptin 3'-UTR matched miRNA seed sites of miR-7, miR-125 and miR-30. The second tallest peak, corresponding to a potential miR-125 binding site, did not validate by luciferase assay (data not shown).

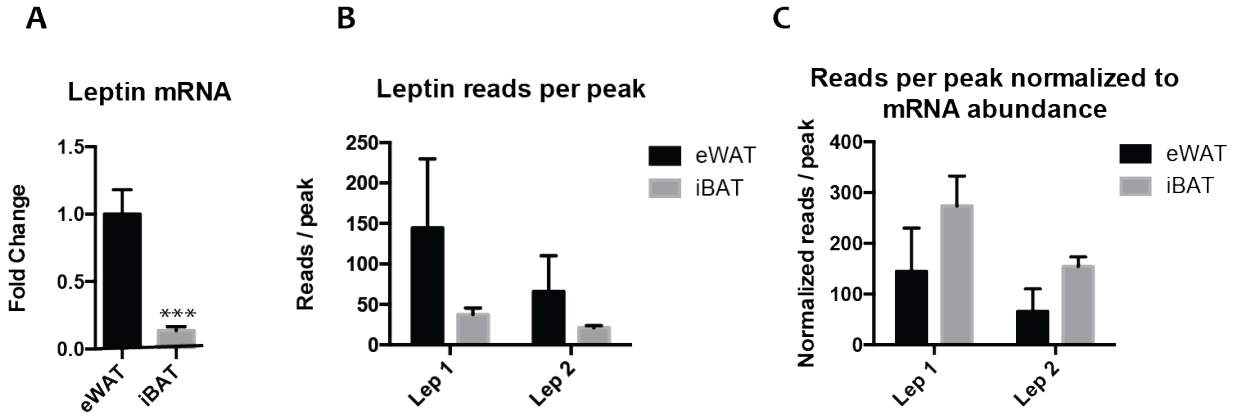

Figure 4.4 Leptin transcripts are more likely to be bound by miR-29 in iBAT than eWAT
(A) Leptin mRNA abundance in eWAT vs. iBAT from 15-week old male mice (n = 8)
(B and C) Average reads per peak in *Lep 1* and *Lep 2* binding sites, unnormalized (B) and normalized to leptin mRNA abundance (C) (2 mice pooled per group, n = 6 for BAT, n = 3 for eWAT).

All results are presented as mean ±SEM. Student's t test for eWAT vs. iBAT in (A) (*$p < 0.05$, **$p < 0.005$, ***$p < 0.0005$, ****$p < 0.00005$).

We next assessed whether miR-29 was capable of repressing leptin in primary adipocytes following transfection of a miR-29a mimic. 72 hours post-transduction, miR-29a levels were substantially increased in both iBAT and eWAT (Figures 4.5A and 4.5D). Leptin mRNA levels correspondingly decreased by 40% in iBAT and 80% in eWAT compared to cells transfected with a mutated miR-29a mimic (Figures 4.5B and 4.5E). Leptin secretion from primary cells is lower than that from adipocytes *in vivo*; however, the conditioned media (CM) of primary cells contains a sufficient amount of leptin to be detected by ELISA. We observed a 50%

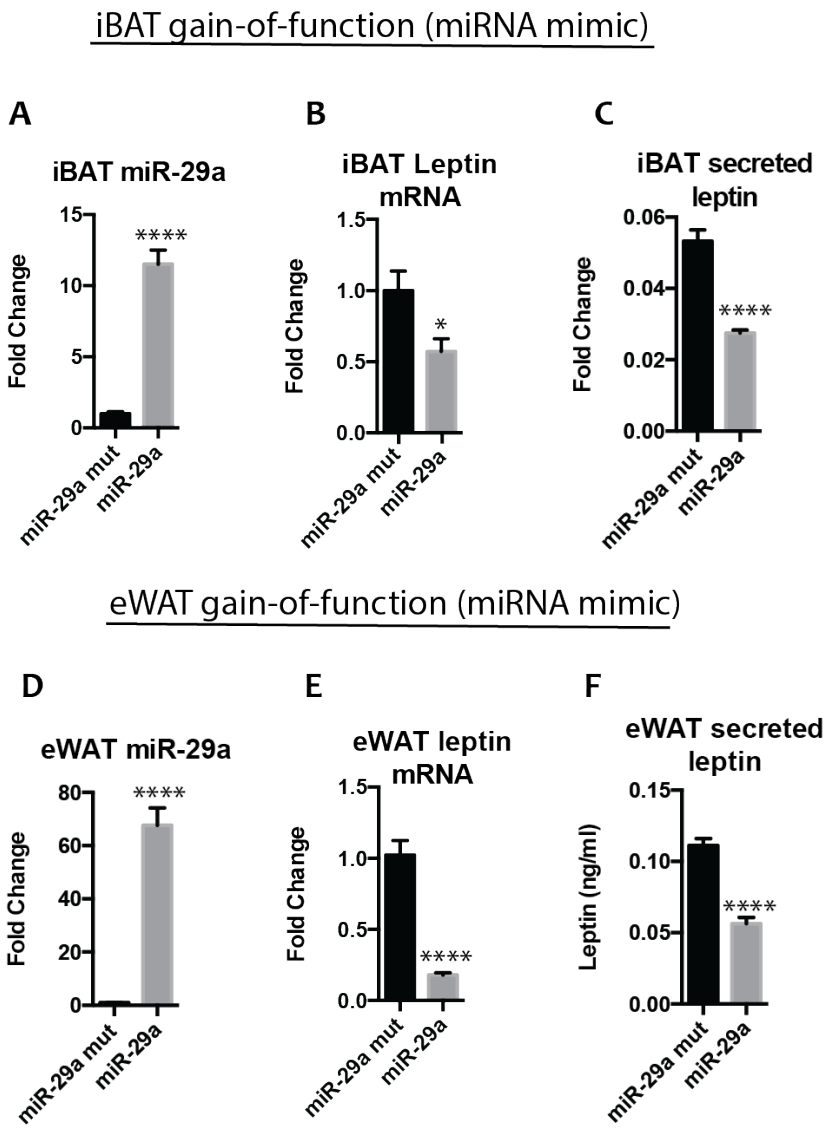

Figure 4.5 miR-29 gain-of-function represses leptin
(A - C) miR-29a (A), leptin mRNA (B), and CM leptin concentration (C) in primary iBAT cells transfected with a miR-29a mimic or a mutated miR-29 mimic (n = 6).
(D – F) miR-29a (D), leptin mRNA (E), and CM leptin concentration (F) in primary eWAT cells transfected with a miR-29a mimic or a mutated miR-29 mimic (n = 6).

All results are presented as mean ±SEM. Student's t test (*$p < 0.05$, **$p < 0.005$, ***$p < 0.0005$, ****$p < 0.00005$).

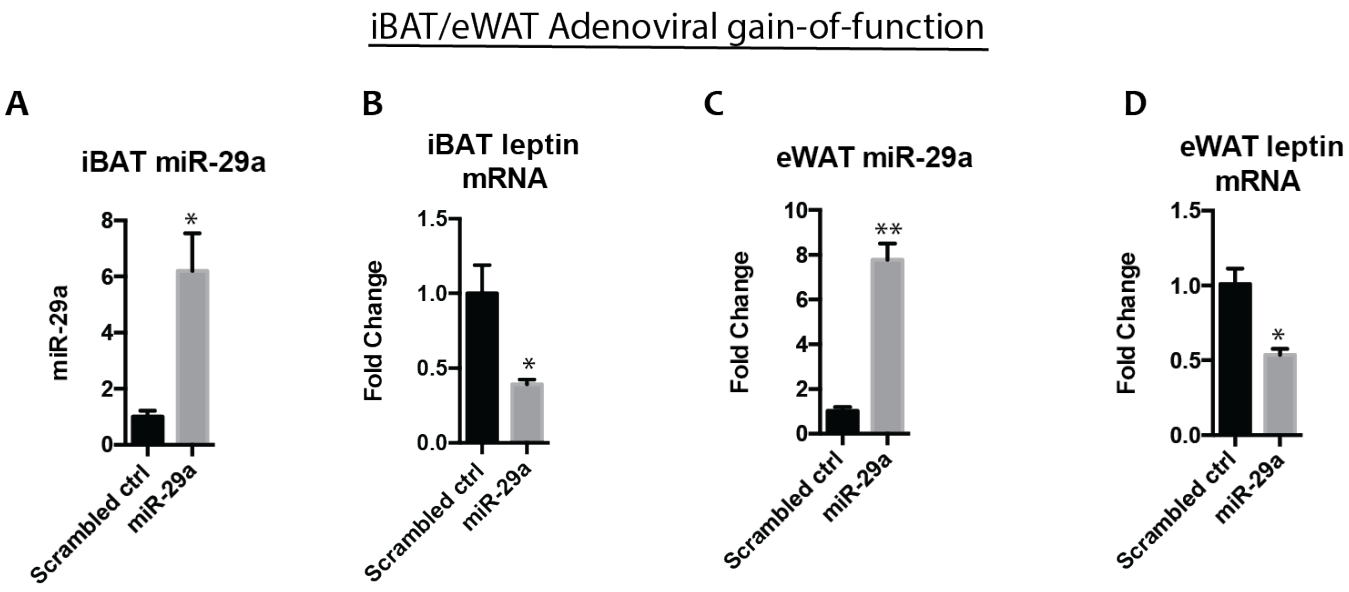

Figure 4.6 miR-29 adenoviral gain-of-function represses leptin mRNA
(A and B) miR-29a (A) and leptin mRNA (B) in primary iBAT cells transduced with adenovirus containing primary miR-29a or a scrambled sequence (n = 3).
(C and D) miR-29a (C) and leptin mRNA (D) in primary eWAT cells transduced with adenovirus containing primary miR-29a or a scrambled sequence (n = 3).

All results are presented as mean ±SEM. Student's t test (*$p < 0.05$, **$p < 0.005$, ***$p < 0.0005$, ****$p < 0.00005$).

decrease in leptin protein from both iBAT and eWAT CM (Figures 4.5C and 4.5F). As an alternative gain-of-function approach, primary cells were transduced with an adenovirus expressing miR-29a or a scrambled miRNA control. Consistent with the miRNA mimic experiments, an increase in miR-29a caused a significant decrease in leptin mRNA in both iBAT and eWAT (Figure 4.6A – 4.6D). Next, primary cells were transfected with a locked nucleic acid (LNA; Grunweller and Hartmann, 2007) to knockdown endogenous miR-29. Both iBAT and eWAT adipocytes showed a significant decrease in miR-29a levels (Figures 4.7A and 4.7D), and corresponding increases in leptin mRNA of 55% and 90%, respectively (Figures 4.7B and 4.7E). In CM from iBAT and eWAT, secreted leptin protein increased at comparable levels

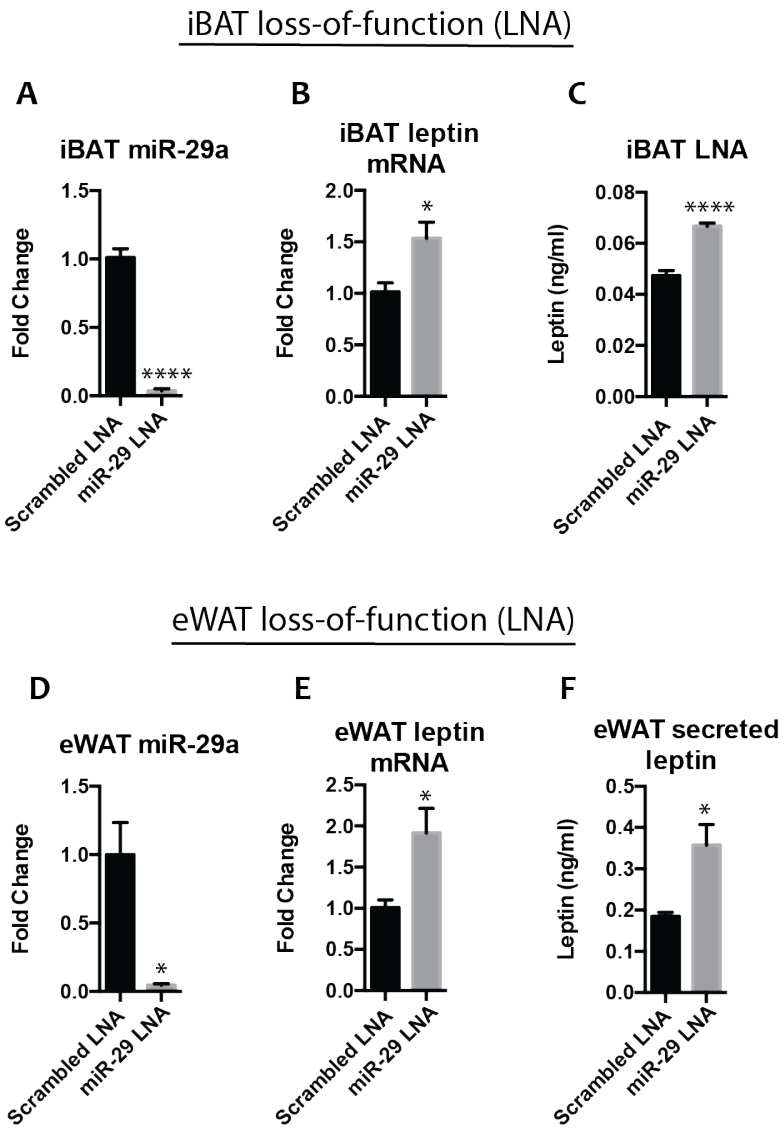

Figure 4.7 miR-29 loss-of-function increases leptin levels
(A-C) miR-29a (A), leptin mRNA (B), and CM leptin concentration (C) in primary iBAT cells transfected with a miR-29 LNA or a scrambled LNA (n = 6).
(D-F) miR-29a (E), leptin mRNA (E), and CM leptin concentration (C) in primary eWAT cells transfected with a miR-29 LNA or a scrambled LNA (n = 3).

All results are presented as mean ±SEM. Student's t test (*$p < 0.05$, **$p < 0.005$, ***$p < 0.0005$, ****$p < 0.00005$).

to leptin mRNA (Figures 4.7C and 4.7F). For each experiment, levels of the general adipocyte differentiation markers *Pparg2*, *Adiponectin*, and *aP2* were measured. Differentiation was moderately increased in iBAT and eWAT transfected with miRNA mimics (Figures 4.8A and 4.8B), consistent with previous reports that miR-29b promotes adipogenesis in human cells (Zhang et al., 2016). Adenoviral gain-of-function and LNA-based loss of function did not alter levels of differentiation markers (Figures 4.8C – 4.8F).

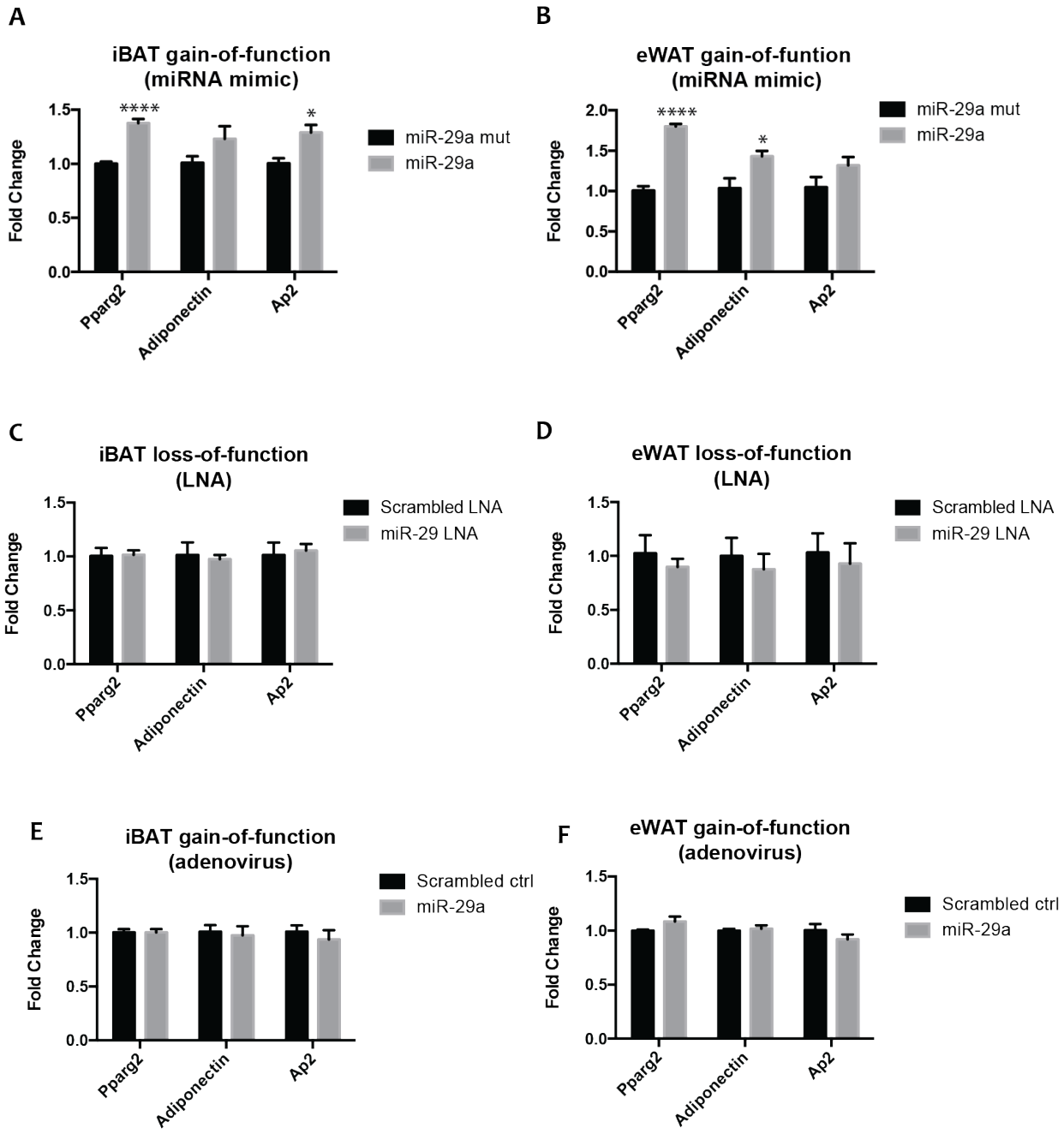

Figure 4.8 miR-29a mimic gain-of-function increases adipogenesis
(A-F) qPCR of differentiation markers in primary iBAT and eWAT cells transfected with miR-29a mimic (A and B), transfected with miR-29 LNA (C and D) or transduced with miR-29a adenovirus (E and F) (n = 3 for E, F and G, n = 6 for H, I, and J).

All results are presented as mean ±SEM. Student's t test for gain/loss of function versus control (*$p < 0.05$, **$p < 0.005$, ***$p < 0.0005$, ****$p < 0.00005$).

In addition to leptin, the other top miR-29 targets from Table 6 validated by luciferase assays, so we reasoned that these targets would also show miR-29 dependent changes in abundance. Surprisingly, only *Sparc* and *Col3a1* were repressed in miRNA mimic transfected iBAT (Figure 4.9A), and only *Hmgcs1* and *Cav2* were repressed in adenoviral transduced iBAT (Figure 4.9B). In iBAT loss-of-function, *Col3a1* was the only top 10 miR-29 target that significantly increased, along with *Eln*, a robust miR-29 target in liver (Figure 4.9C; van Rooij et al., 2008). In eWAT, mRNA levels of *Sparc*, *Hmgcs1*, *Col3a1,* and *Eln* were decreased in cells transfected with miRNA mimic, while *Lpl* and *Scd1* increased slightly (Figure 4.10A). No changes in mRNA abundance were observed in cells transduced with miR-29a adenovirus (Figure 4.10B). In eWAT loss-of-function, *Col3a1* and *Eln* were increased, mirroring the changes seen in iBAT (Figure 4.10C). The differences in effect between the two gain-of-function models may be due to inconsistencies in the magnitude of overexpression. Supraphysiological levels, especially those in the transfected eWAT cells, may be responsible for indirect changes in mRNA abundance. By comparison, the loss-of-function results were very similar between iBAT and eWAT. Regardless, in all 6 experiments performed, only a minority of mRNAs changed in the expected direction.

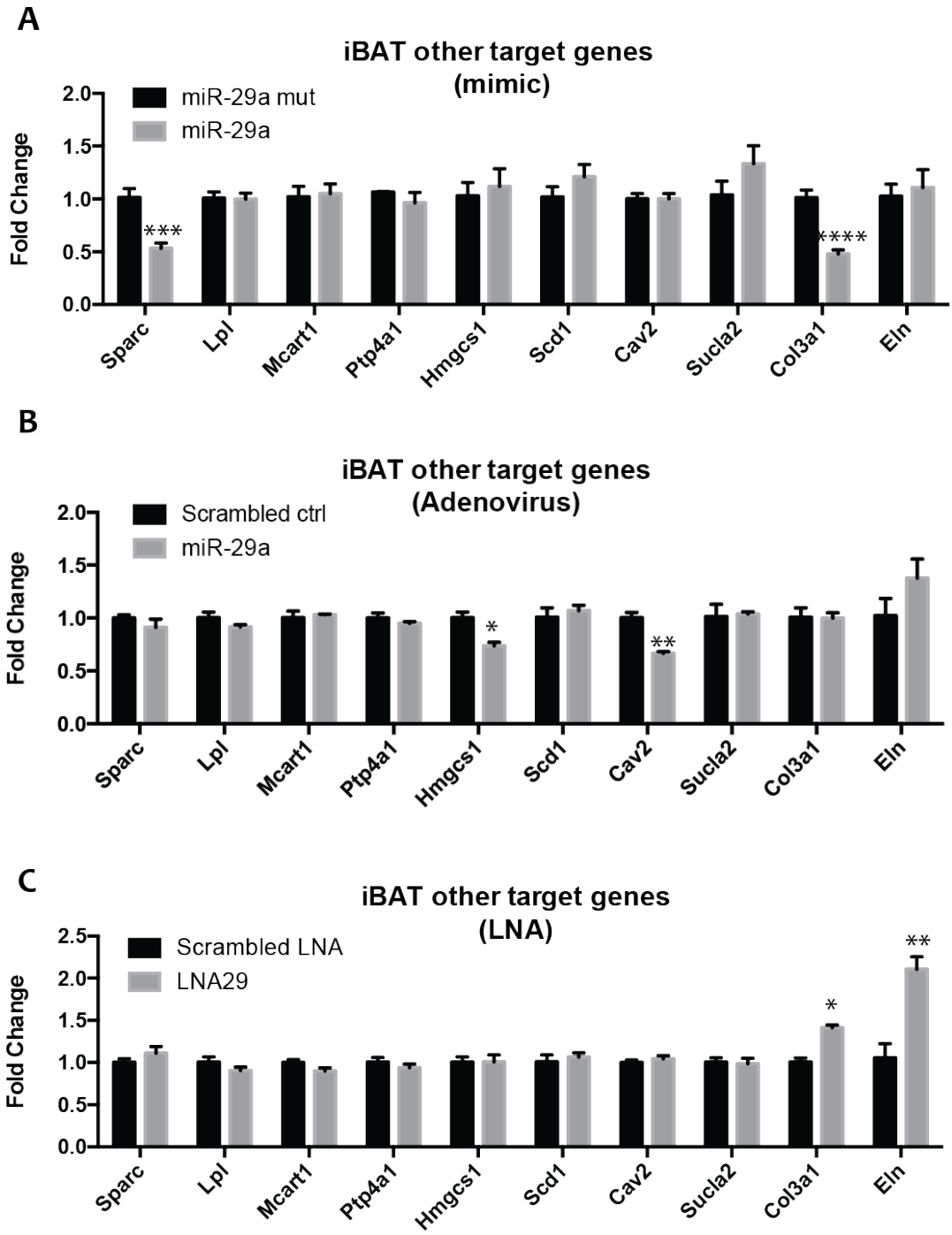

Figure 4.9 Most miR-29 targets are unaltered following gain/loss-of-function in iBAT
(A-C) qPCR of top 10 miR-29 targets and *Eln* following miRNA mimic transfection (A), adenoviral transduction (B) and LNA transfection (C).

All results are presented as mean ±SEM. Student's t test for gain/loss of function versus control (*$p < 0.05$, **$p < 0.005$, ***$p < 0.0005$, ****$p < 0.00005$).

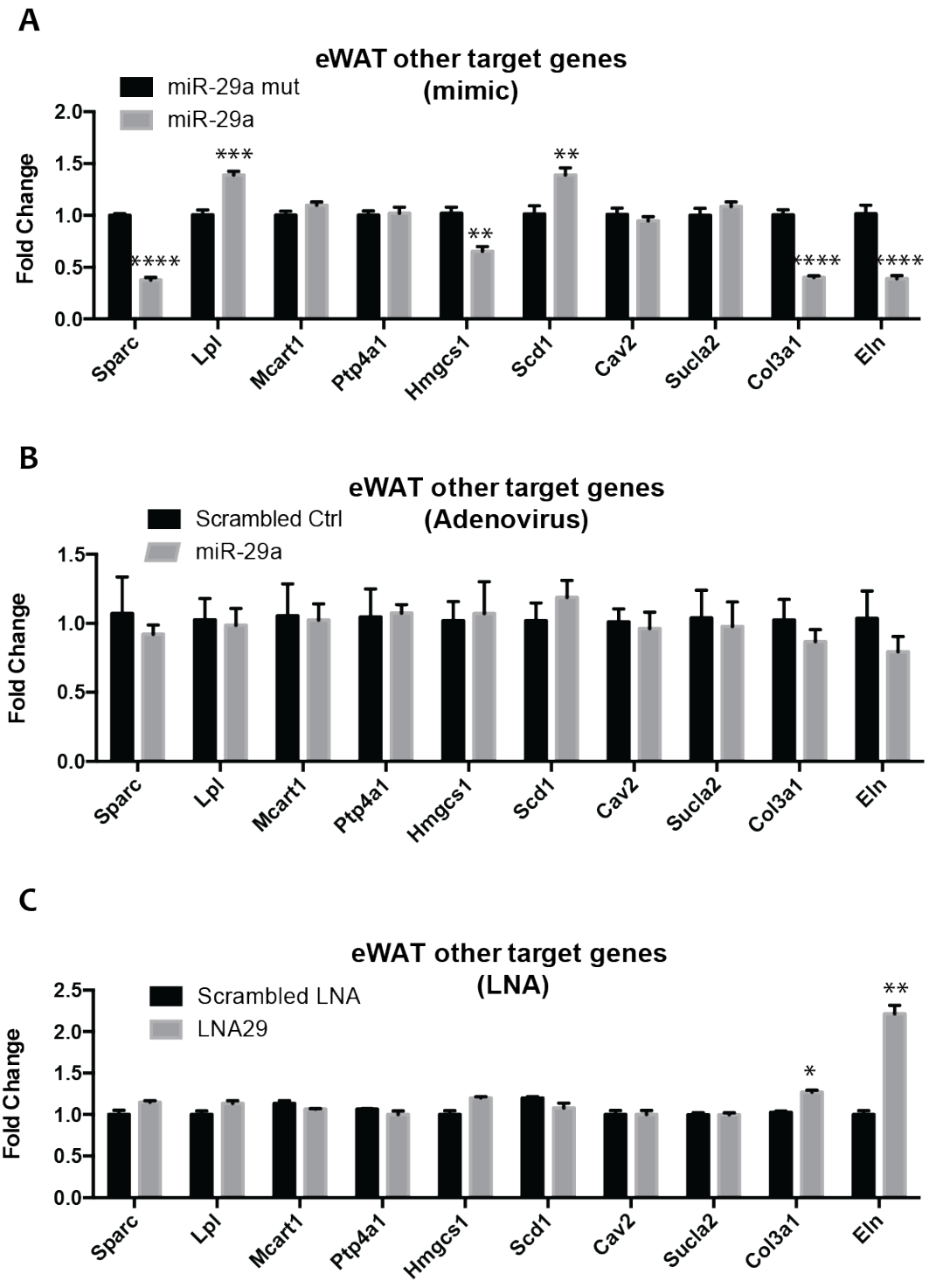

Figure 4.10 Most miR-29 targets are unaltered following gain/loss-of-function in eWAT
(A-C) qPCR of top 10 miR-29 targets and *Eln* following miRNA mimic transfection (A), adenoviral transduction (B) and LNA transfection (C).

All results are presented as mean ±SEM. Student's t test for gain/loss of function versus control (*$p < 0.05$, **$p < 0.005$, ***$p < 0.0005$, ****$p < 0.00005$).

4.4 Results: miR-29 abundance *in vivo* is inversely correlated with leptin

Leptin abundance increases in obese mice and humans compared to lean controls (Frederich et al., 1995), and we hypothesized that miR-29 levels would be inversely correlated. Mice fed a HFD for 15 weeks are 60% heavier than their chow-fed counterparts (Figure 4.11A) and have increased leptin mRNA in iBAT and eWAT, as well as increased serum leptin (Figures 4.11B and 4.11C). MiR-29a levels were correspondingly reduced by approximately 30% in iBAT and 60% in eWAT (Figure 4.11D). To confirm our findings, we next looked at miR-29 abundance in a genetic model of obesity. $Ob^{-/-}$ mice weigh 65% more than heterozygous controls (Figure 4.11E) due to a nonsense mutation in the leptin CDS that leads to high levels of leptin mRNA, but no functional protein (Figure 4.11F and 4.11G). MiR-29a in iBAT and eWAT of these mice was reduced by 24% and 31%, respectively (Figure 4.11H).

Human miR-29a is identical in sequence to murine miR-29a, and human leptin contains 2 TargetScan predicted binding sites (Agarwal et al., 2015), analogous to the two binding sites in mice. If miR-29a serves as a physiologically relevant regulator of leptin in humans, miR-29a should be reduced in obese patients. Indeed, previously published work demonstrates that in a cohort of 66 men and women, ranging from lean to obese, miR-29a in visceral and subcutaneous WAT is negatively correlated with BMI (Glantschnig et al., 2019). A second human study found an increase in miR-29a in subcutaneous WAT from 19 obese individuals following diet and exercise-induced weight loss (Kristensen et al., 2017).

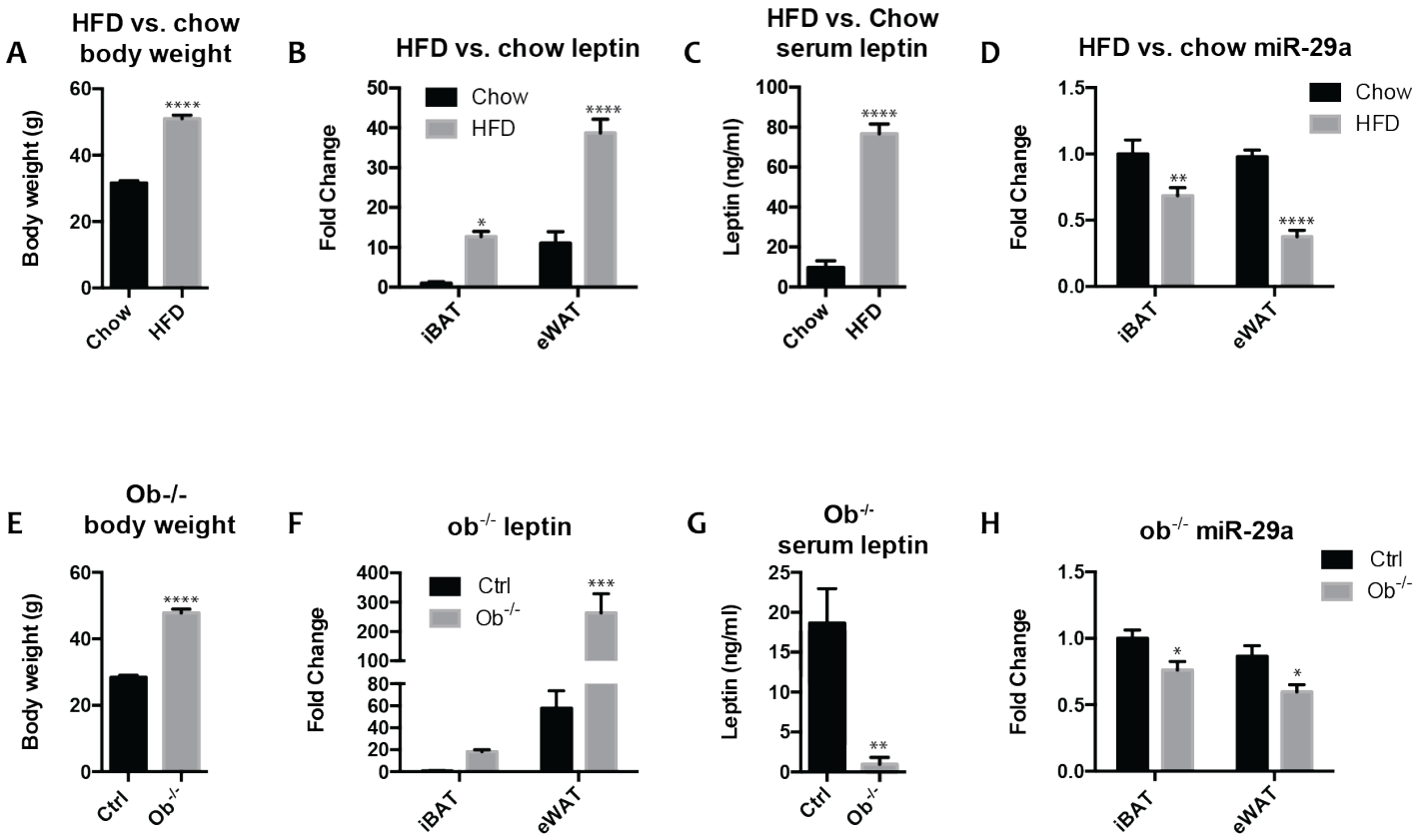

Figure 4.11 miR-29 abundance is inversely correlated with leptin in obese mice
(A-D) Body weights (A), leptin mRNA (B), serum leptin (C) and miR-29a levels (D) in 21-week old HFD vs. chow mice (n = 6).
(E-H) Body weights (E), leptin mRNA (F), serum leptin (G) and miR-29a levels (H) in 9-week old $ob^{-/-}$ vs. $ob^{+/-}$ mice (n = 9).

All results are presented as mean ±SEM. Student's t test used for serum leptin comparisons and 2-way ANOVA used for leptin and miR-29a comparisons (*$p < 0.05$, **$p < 0.005$, ***$p < 0.0005$, ****$p < 0.00005$).

4.5 Summary

In this chapter, we focused on miR-29 as a key miRNA regulator of adipocyte phenotype. GO term enrichment of miR-29 targets indicates that miR-29 regulates ECM structure and insulin signaling, consistent with its previously described role in heart, muscle, liver and other tissues (Li et al., 2017a; van Rooij et al., 2008; Roderburg et al., 2011). Novel top-ranked miR-29 targets were confirmed using luciferase assays, serving as validation of the

match score analysis ranking system. Among these targets, we decided to focus on leptin, a powerful hormone involved in energy homeostasis for which no post-transcriptional regulators have been previously identified. Despite lower expression levels in iBAT, we found major peaks corresponding to miR-29 binding sites in both iBAT and eWAT. When normalized to mRNA levels, peak reads were greater in iBAT, suggesting that suppression by miR-29 could be partly responsible for leptin's reduced abundance in brown adipocytes. *In vitro*, gain and loss-of-function in iBAT and eWAT primary adipocytes modulated leptin mRNA and protein secretion, and *in vivo*, miR-29 levels were inversely correlated with leptin production. Leptin binds to the Ob-Rb receptor in the hypothalamus and induces downstream IRS/PI3K signaling (Park and Ahima, 2014), a pathway that is directly regulated by miR-29 in adipose tissue. Adipocytes express leptin receptors, and although there is limited evidence of autocrine signaling (Harris, 2014), repression of both leptin and the pathways activated by leptin in adipocytes presents a potentially interesting model.

Beyond leptin, mRNA levels of most top-ranked miR-29 targets did not change as a result of miR-29 gain or loss-of-function. One possible explanation is that translational repression is more common in mouse adipose tissue than mRNA destabilization. This phenomenon was observed in mouse primary B cells where miR-17~92 modulates protein levels primarily via translational repression (Jin et al., 2017). Other work has shown that most miRNA targets, identified by either computational or high-throughput experimental methods, do not actually respond to changes in miRNA expression (Seitz, 2017; Baek et al., 2008). A miRNA binding to a target, even when that same target can be repressed in a luciferase assay, does not necessarily prove repression occurs. Another confounding factor is the *in vitro* model of transfecting primary adipocytes. Transfections of concentrated miRNA mimics can lead to

the formation of high molecular weight RNA species and mutations within miRNA mimics (Jin et al., 2015). Adenoviral transfection can also introduce non-specific effects, which we have observed in prior experiments with primary adipocyte transductions (data not published).

In addition to the gain and loss-of-function experiments, there are several other limitations to the work presented here. Luciferase assay validations rely on supraphysiological levels of miRNA mimics to inhibit targets that have been cloned into an artificial construct. Previous work has shown that the location of a miRNA binding site within a 3'-UTR and the sequences immediately flanking the binding site impact functional repression (Grimson et al., 2007). These conditions are not captured in the luciferase assays performed here. Additionally, the *in vivo* correlation between miR-29a and leptin levels is not conclusive evidence of regulation. Future studies with miR-29 cell type selective transgenic overexpression and KO in mice are necessary to fully probe miR-29's full regulatory role *in vivo*.

CHAPTER 5: Discussion

5.1 Significance of findings

In this thesis, I have presented 2 distinct approaches to identify miRNA regulators that influence adipose tissue phenotype. The first, more conventional approach, involved comprehensive profiling of miRNAs from various fat depots, *in vivo* and *in vitro*. While no candidate clearly imparted a strong pro-thermogenic or pro-inflammatory phenotype in gain-of-function experiments, several candidates did have modest effects. miR-335 may have inhibited adipogenesis, an effect that could become increasingly strong with higher levels of miR-335 gain-of-function. MiR-192 increased both pro-thermogenic and pro-inflammatory mRNA abundance. While unexpected, there are some conditions in which both of these

pathways can become upregulated, such as in subcutaneous fat following burn injury (Patsouris et al., 2015). The final candidate of interest, miR-338, increased the abundance of a variety of genes involved in both lipogenic and lipolytic/β-oxidative pathways, including *Pparα*, *Fasn,* and *Acc1*. Future experiments should focus on gain and loss-of-function in primary cells as opposed to immortalized cell lines. Long term studies should include characterizing the roles of these miRNA candidates *in vivo* with adipose-specific transgenic and KO mouse lines.

The latter two chapters of this thesis utilized network-based approaches to focus on miRNA targets rather than on differential abundance of miRNAs. Most notably, we employed the first-reported use of HITS-CLIP to map the miRNA targetome in adipose tissue. In comparison to purely computational methods of target prediction, there are several key advantages to this approach. First, while computational methods predict binding sites irrespective of cellular microenvironment, HITS-CLIP binding sites represent physiologically relevant Ago activity. Even when computationally predicted sites are validated by luciferase assays *in vitro*, the artificial, supraphysiological expression of miRNA and target *in vitro* do not necessarily indicate a biologically relevant binding event *in vivo.* Second, HITS-CLIP profiles Ago-associated miRNAs in addition to targets, providing relevant information about the abundance of Ago-loaded miRNAs. Lastly, HITS-CLIP identifies miRNA binding sites outside of the 3'-UTR, providing a more comprehensive picture of regulatory activity. Let-7, which targets the dicer CDS (Forman et al., 2008) and miR-103a, which targets the 5'-UTR of GPRC5A (Zhou and Rigoutsos, 2014), are examples of functional, non-3'-UTR target sites.

Our data indicate that abundant miRNAs associate with a vast array of targets, consistent with prior CLIP-based studies (Hafner et al., 2010; Chi et al., 2009). Recent work suggests that many of these Ago:RNA associations may be the result of weak, transient

interactions (Chandradoss et al., 2015), which may explain the low read counts of many miRNA binding peaks in our data. To address this, and to account for false-positive miRNA/target associations, we employed a match score system to rank miRNA targets. For miR-29, 5 of the top 10 targets had been validated in previous publications, and the remaining 5 were validated by luciferase assays in this study, indicating the predictive power of this analysis.

Among the top-ranked miR-29, targets we focused on leptin due to its central role in mammalian energy homeostasis. As discussed previously, prior work has characterized transcriptional regulators of leptin (Dallner et al., 2019; Lo et al., 2018), but until now, no post-transcriptional regulators have been identified. This is surprising given that miRNAs are estimated to regulate a majority of mRNAs in mammals (Friedman et al., 2009), and that leptin's 3'-UTR is about 3-fold longer than the average 3'-UTR in vertebrates (Mignone et al., 2002). Our HITS-CLIP data show a substantial association between Ago and the leptin 3'-UTR, with 6 peaks reaching statistical significance. Following normalization to leptin mRNA abundance, average reads for both *Lep 1* and *Lep 2* were greater in iBAT than eWAT, suggesting that miR-29 represses leptin more strongly in iBAT. Multiple binding sites within the same 3'-UTR can act together to enhance mRNA destabilization (Grimson et al., 2007), and while a single miRNA binding site can be more easily saturated, a second, lower affinity binding site allows for a more dynamic range of modulation. Indeed, this may explain how a relatively minor repression of luciferase in the binding-site validation experiments translates into a greater effect on leptin in gain and loss-of-function experiments.

In obese mice, one of the most prominent changes that occurs in adipose tissue is heightened leptin secretion (Frederich et al., 1995). We hypothesized that, as a negative

regulator of leptin, miR-29a levels would be correspondingly decreased in obesity. As expected, in two different mouse models of obesity, iBAT and eWAT miR-29a levels were lower than in lean controls. These results are consistent with the negative correlation between adipose miR-29 abundance and BMI in humans (Glantschnig et al., 2019). Given that the miR-29 family is 100% conserved between mice and humans, and that two analogous miR-29 binding sites are found within the human leptin 3'-UTR, it is likely that miR-29 plays a similar regulatory role in both species.

5.2 Future studies

5.2.1 Improving the match score analysis

Although HITS-CLIP provides a significantly improved map of miRNA behavior compared to computational predictions, false-positive binding events are still a concern. For example, there is a 1/92 chance of a random 6-nucleotide sequence matching a random 50 base pair peak. Summed across >20,000 peaks, a given miRNA is likely to have hundreds of false positives. Restricting to 7-mer and 8-mer sites as a requirement of matching brings the false match frequency to 1/309 and 1/1260, respectively, but risks overlooking many functional 6-mer miRNA matches. Additionally, for miRNA/target matches that are real, the strength of miRNA mediated repression is variable. The match score analysis described here prioritizes miRNAs with well-conserved binding sites and higher seed sequence complementarity; however, several improvements can be made to further increase accuracy of the ranking system. First, the location of each 3'-UTR binding site could be scored based on location. Specifically, miRNAs that bind close to the stop codon or within the center of a long 3'-UTR are less effective at mediating repression and should be de-emphasized in the ranking (Grimson

et al., 2007). This would be particularly relevant for miRNA targets, like leptin, where multiple peaks occur spaced throughout a long 3'-UTR. Next, the local context of miRNA binding should be considered. Higher AU content within 30 nucleotides of the miRNA binding site correlates with increased target repression and could be incorporated into the match score ranking (Grimson et al., 2007). A third factor which influences miRNA targeting is complementarity at nucleotides 12-17 of the miRNA, but interestingly, not other regions of the 3'end (Grimson et al., 2007). A slight preference for nucleotide pairing in this region could improve the match score analysis, both in terms of de-emphasizing false positives and predicting biologically relevant binding. There are also several features of miRNAs themselves that influence the strength of miRNA repression and prediction accuracy, which should be considered when comparing multiple miRNA regulators of the same target. These include the thermodynamic stability of miRNA seed pairing, which correlates with stronger repression of targets, and the number of targets within the tissue of interest, which is inversely correlated with repression (Garcia et al., 2011).

5.2.2 Alternative miR-29 regulated pathways

While improvements to the match score analysis would increase the value of the HITS-CLIP resource, the existing data are sufficient to continue to explore miR-29's regulatory function in adipose tissue. The data presented here suggest that miR-29 plays a central role in a variety of metabolic processes beyond leptin repression. In particular, a pathway analysis of miR-29 targets indicates involvement in insulin signaling and ECM structure. MiR-29 reduces insulin sensitivity by repressing *IRS-1* in myocytes (Yang et al., 2014), and by repressing *Dnmt3a* in liver (Hung et al., 2019). Both of these targets are highly ranked by the HITS-CLIP

match score analysis, along with other genes including *Myo1c* and *Cav2* which are involved in downstream propagation of *IRS-1* activation (Bose et al., 2002; Kwon et al., 2015). The second pathway, ECM organization and structure, is controlled in heart by miR-29 mediated repression of *Col3a1*, *Fbn1*, and *Eln* (van Rooij et al., 2008), and in liver by repression of *Col1a1*, *Col4a5* and *Col5a3* (Roderburg et al., 2011). In both heart and liver, down-regulation of miR-29 is associated with increased fibrosis. According to the HITS-CLIP dataset, 5/6 targets listed above contain 3'-UTR peaks matching miR-29, as do other fibrosis-related genes including *Hspg2* and *Cflar* (Lord et al., 2018; McCubbrey et al., 2018). These findings strongly suggest a role for miR-29 in regulating ECM and fibrosis in adipose tissue.

Future studies are needed to confirm the role of miR-29 in regulating these two pathways, beginning with luciferase assays to validate binding sites in newly identified targets. Following validation, *in vitro* gain and loss-of-function experiments, using a combination of viral transduction and miRNA mimic or LNA transfection, can be used to assess repression of relevant targets at the mRNA level. In addition, *in vitro* functional assays should be performed to assess changes in insulin signaling and ECM composition. These experiments might include stimulating primary adipocytes with recombinant insulin and measuring Akt phosphorylation and Glut4 translocation, or measuring levels of secreted ECM proteins, such as Col3a1, in primary cell conditioned media.

5.2.3 Developing *in vivo* models to study miR-29

Moving beyond *in vitro* work, a miR-29 floxed mouse line should be developed to create an adipose-specific miR-29 KO using an adiponectin-CRE driver. The KO line would provide the basis for studying several aspects of miR-29's regulatory function *in vivo*. To begin

with, leptin levels could be assessed in the KO mouse line, including leptin mRNA in eWAT, iWAT, and iBAT, as well as circulating leptin at baseline, and under fasted, refed and obesogenic conditions. Although the work performed here suggests that leptin levels would be elevated *in vivo*, compensatory mechanisms could prevent an increase in net circulating leptin, such as increased clearance from the circulation (Chan et al., 2008). If circulating leptin does in fact increase, however, weight loss is not necessarily guaranteed. While studies in leptin transgenic mice result in reduced body fat in young mice, mice still gain weight as they age (Qiu et al., 2001). Studies with long-term, exogenously administered leptin demonstrate a similar resistance to leptin-mediated weight loss in obese mice (Halaas et al., 1997; Roujeau et al., 2014), likely due to leptin resistance. To address these possibilities, different physiological conditions should be explored in miR-29 KO mice, including resistance to weight gain in lean mice and weight loss in response to caloric restriction in obese mice.

An adipocyte-specific miR-29 KO mouse line would also present an opportunity to more comprehensively, and accurately, explore miR-29's role in targeting mRNAs beyond leptin. This could be accomplished by first repeating HITS-CLIP using miR-29 KO and control mice. Peaks that are found exclusively within the control group would represent miR-29 targets in adipocytes with high confidence. This approach would be particularly valuable, since miR-29 is expressed in non-mature adipocytes, and the current HITS-CLIP data do not distinguish between binding sites in adipocytes compared to other cell types within adipose tissue. A pathway analysis of these adipose-specific peaks would provide more insight regarding miR-29's role in mature adipocytes *in vivo*.

A second advantage to a HITS-CLIP comparison between miR-29 KO and control mice would be the opportunity to identify non-canonical binding sites. Although most

physiologically relevant and effective miRNA binding sites seem to contain complementarity with miRNA seed regions (Bartel, 2018), previous HITS-CLIP studies have demonstrated that miRNAs associate with a surprisingly high number of non-canonical regions (Helwak et al., 2013). Peaks that are present exclusively within control mouse adipose tissue, but do not contain seed sequence matches with miR-29, would be likely candidates for non-canonical binding sites. Recent work has shown that miRNA 3'-end pairing can strengthen binding with a complementary seed or mitigate imperfect seed complementarity (Moore et al., 2015). Certain regions, including nucleotides 13-16, appear to be especially influential in this process (Bartel, 2009). A motif analysis on high-confidence, canonical and non-canonical binding sites would provide insight, specific to miR-29, regarding these 3'-end regions, and could be used to predict higher confidence miR-29 binding sites in tissues where Ago-CLIP techniques have not yet been used.

Without repeating HITS-CLIP, there is still ample opportunity to explore miR-29's role using a miR-29 KO mouse line. First, RNAseq of KO vs. control adipose tissue would provide a list of differentially abundant genes that are directly or indirectly regulated by miR-29. A comparison of these genes with HITS-CLIP predicted miR-29 targets would provide information about which targets are most likely to be physiologically repressed by miR-29 *in vivo*. Since many miRNA targets are not repressed at the mRNA or protein level despite Ago:miRNA binding (Pinzon et al., 2017), the expectation is that only a subset of predicted targets would be altered. Additionally, pathway analysis of the RNAseq results would provide additional insight into miR-29's role in fibrosis and insulin signaling, and perhaps reveal other pathways of interest. If these pathways are impacted as predicted, a number of experiments could be performed on miR-29 KO mice to more fully characterize the phenotypic effects.

Changes in insulin sensitivity could be measured by IP insulin injections, followed by an assessment of GLUT4 translocation and Akt phosphorylation in adipose tissue. Glucose and insulin tolerance tests would also provide insight regarding the whole-body metabolic impacts of the adipose-specific KO. Fibrosis could be assessed by quantifying collagens and other ECM proteins by western blot and histology in both lean and obese miR-29 KO mice.

The approach outlined above, using RNAseq to determine relevant miR-29 targets, relies on the assumption that miRNA-based repression occurs predominantly by mRNA destabilization rather than translational inhibition. While this assumption appears to be true in most cases for 3'-UTR binding sites (Eichhorn et al., 2014), sites located within the CDS exert most of their regulatory function through translational repression (Hausser et al., 2013). Even for 3'-UTR binding sites, there are several examples of miRNAs inhibiting translation. In Zebrafish blastulas, miR-430 was found to exert a substantial level of translational inhibition, and limited mRNA destabilization, 4 hours post-fertilization (Bazzini et al., 2012). A similar effect was seen with miR-17~92 in mouse B cells where translational repression accounts for a greater change in protein abundance than mRNA destabilization (Jin et al., 2017). To address this, ribosome profiling or SILAC of miR-29 KO adipose tissue or primary adipocytes would identify functionally relevant miR-29 targets that are impacted by both mRNA destabilization and translational inhibition. These data would provide a robust foundation on which to explore miR-29's role in regulating a variety of cellular processes. Additionally, no prior studies have combined a comprehensive catalog of HITS-CLIP predicted miRNA binding sites with RNAseq and ribosome profiling data from a miRNA KO animal or cell line. This would allow for an unprecedented look at the relative contributions of mRNA destabilization vs.

translational inhibition, compared across 3'-UTR, 5'-UTR, and CDS miR-29 targets, with broad implications for miRNA regulatory behavior.

One challenge in working with a miRNA KO mouse line is disentangling the direct and indirect actions of the miRNA. To address this, we previously used CRISPR to induce a double stranded break near the *Lep 1* binding site in mouse ES cells, followed by non-homologous end joining. The result was a 14 base pair deletion that removed 2 nucleotides from the miR-29 seed complementary region and the full miR-29 3' binding region. Future experiments will look at leptin mRNA levels and circulating protein in these mice under different physiological conditions. There are several advantages to using mutations in the miRNA binding site rather than altering levels of the miRNA itself. First, point mutations in the 3'-UTR should be sufficient to block miRNA binding without influencing mRNA stability or changing leptin's protein structure. Second, since leptin expression outside of adipocytes is very low, there is no need to make these mutations tissue specific. Lastly, changes in leptin abundance could be attributed to direct effects of miR-29 binding.

Since miR-29 sequences are identical in human and mouse, it is likely that miR-29 also regulates leptin in human adipocytes. Future experiments should be performed to confirm this, beginning with luciferase assay validation of the human miR-29 binding sites. Additionally, *in vitro* gain-and-loss of function studies could be performed using human adipose-derived stem cells, and if repression occurs at a physiologically relevant level, potential therapeutics could be explored. One option for a therapeutic modality would be a target site blocker that binds specifically to leptin's 3'-UTR and blocks miR-29 without recruiting RISC (Louloupi and Orom, 2018). While increasing circulating leptin may have limited effects in patients without

hypoleptinemia, a leptin promoting target site blocker could be combined with other leptin sensitizing drugs to create a powerful therapeutic (Coppari and Bjorbaek, 2012).

5.2.4 Alternative miRNA candidates

Beyond miR-29, our HITS-CLIP data hint at a variety of other, previously unexplored roles for miRNA in adipose tissue. The miR-101 family targets several genes involved in mitochondrial biogenesis, including *Gabpb2*, *Gabp,* and *Atf2*. MiR-101 also targets *Cidea*, a BAT enriched lipid-droplet associated protein (Barneda et al., 2015), and *Cebp1α*, a transcription factor that is essential for adipogenesis (Wang et al., 1995). MiR-16 regulates key members of several metabolic pathways, including the citric acid cycle, the electron transport chain, and cholesterol biosynthesis. Individual targets include *Ogdh*, *Sucla2*, *Cox11*, *Srebp1*, *Pparα* and *Fasn*, and many others. MiR-101 and miR-16 are also among the most abundant Ago-associated miRNAs in adipose tissue, ranking 5th and 4th, respectively, by total miRNA reads. miR-378, which has been previously characterized as a promoter of BAT expansion, binds the CDS of *UCP1* as its highest-ranked target. While seemingly paradoxical, this would explain the reduction of UCP1 protein in subcutaneous WAT seen with miR-378 transgenic mice (Pan et al., 2014).

Future studies should focus on validating key targets for these miRNAs, followed by gain-and-loss of function with miR-101 and miR-16 *in vitro*. For miR-101, changes in adipogenesis should be assessed by transfecting preadipocytes with miR-101 mimics and LNAs and measuring adipogenic markers by qPCR and Oil Red O staining. Mitochondrial density can be measured by quantifying mitochondrial DNA and staining with MitoTracker dyes following gain and loss-of-function in mature adipocytes. With miR-16, *in vitro*

experiments should focus on detecting changes in respiration and electron transport chain dysfunction. Changes in lipid and cholesterol processing can be assessed by measuring lipid accumulation, FFA secretion, and cholesterol production and uptake. Further *in vivo* experiments with adipose-specific transgenic overexpression or KO for miR-16 and miR-101 would allow for a more in-depth analysis of these pathways.

CHAPTER 6: Materials and methods

6.1 Methods

Mouse models

Animal care and experimentation were performed according to procedures approved by the Institutional Animal Care and Use Committee at the Rockefeller University. All mice used in the study were purchased from Jackson Labs on a C57BL/6J background, including $ob^{-/-}$ (stock no. 000632), Wt (stock no. 000664) and HFD (stock no. 380050). For consistency, all mice used were male. Controls for $ob^{-/-}$ mice were heterozygous littermates. Mice were group housed at 5 mice per cage at 23° C and maintained on 12-hour light:dark cycles. HFD mice were fed a diet composed of 60% dietary fat from 6 weeks of age, and all other animals were maintained on a chow diet. Cold exposed mice were individually house at 4° C for 1 week prior to sacrifice.

HEK-293A and Phoenix cell lines

HEK-293A cells (Invitrogen) and Phoenix cells (ATCC) were maintained at 37° C with 5% CO2 in DMEM (4.5g/L glucose, L-glutamine, 110 mg/L sodium pyruvate) supplemented with 10% FBS and 1% penicillin-streptomycin.

Adenovirus cloning, amplification and transduction

Adenoviruses for miR-29a and the scrambled miRNA control were cloned using the AdEasy system (Agilent) according to the protocol provided. Briefly, primary miRNAs for miR-29a and miR-16 were amplified from genomic DNA by PCR and cloned the pAdTrack shuttle. The miR-16 pAdTrack plasmid was then mutated by site-directed mutagenesis to induce 3 point mutations into the miR-16 seed sequence, creating the scrambled control. Both the miR-29a and the scrambled control pAdTrack plasmids were linearized with PmeI and transformed into BJ5183-AD-1 competent cells for recombination with the adenoviral backbone. Successful clones were amplified in the XL10-Gold bacterial strain. Generation of the initial adenoviral stock was performed by digesting the adenoviral plasmid with PacI, then transfecting HEK-293A cells. For adenoviruses expressing miR-10b, miR-375, miR-338 or GFP only, viruses were purchased from Applied Biological Materials. Several rounds of amplification were performed by infecting HEK-293A cells with low titer adenovirus. For transduction of primary adipocytes, iBAT and eWAT cells were treated with a final adenoviral concentration of 7 x 10^7 IFU/ml on the 4^{th} day of differentiation. 72 hours post-transduction, adipocytes were inspected for GFP expression, then total RNA was collected.

Retrovirus cloning, amplification and transduction

The primary miRNA sequences for miR-335 and miR-192 were amplified by PCR from genomic DNA and cloned into the pMSCV retroviral vector. Retroviral plasmids were transfected into Phoenix cells (ATCC) using FuGene HD (Promega), and after 48 hours supernatant was collected and filtered at 0.45 um. Stable preadipocyte cell lines were generated

by transducing 3T3-F442A cells with 50% viral supernatant and 50% media with 8 ug/ml polybrene. Cells were passaged and transduced 3-4 times, until >95% of cells expressed GFP.

Primary adipocyte culture

Primary adipocytes were isolated from 6-week old male C57BL/6J eWAT and iBAT adipose depots. Adipose depots were diced with spring scissors, then placed in 10 ml digestion buffer for 16 minutes (eWAT) or 40 minutes (iBAT) and incubated in a 37°C shaking water bath (140 RPM). iBAT digestion buffer was prepared as follows: 15 mg collagenase B was dissolved in 5 ml of 2X master mix (125nM NaCl, 5mM KCl, 1.3 mM CaCl2, 5mM glucose, 1% penicillin-streptomycin, 4% BSA in H2O) and 5 ml PBS. eWAT digestion buffer was prepared as follows: 100 mg collagenase D was dissolved in a solution of 10 ml PBS, 200 ul of 120 mg/ml dispase II and 40 ul 2.5M $CaCl_2$. Following digestion, the stromal vascular fraction was isolated by centrifugation and filtration at 100 um and 70 um, then plated in 12-well collagen coated plates.

All primary adipocyte cultures were maintained at 37° C with 10% CO_2. Prior to differentiation, iBAT cells were cultured in GlutaMAX media (GlutaMAX media: DMEM / F12 + GlutaMAX (2.438 g/L sodium bicarbonate, sodium pyruvate) supplemented with 10% FBS and 1% penicillin-streptomycin) and eWAT cells were cultured in ITS media (ITS media: 56.5% low glucose DMEM, 37.5% 1X MCDB210 pH 7.25, 2% FBS, 2% ITS premix, 1% 10 mM L-ascorbic acid 2-phosphate in DMEM, 0.01% 100ug/ml bFGF, 0.5% penicillin-streptomycin, and 0.2% primocin). Following induction of differentiation, iBAT cells and eWAT cells were cultured in GlutaMAX media.

When iBAT preadipocytes reached 100% confluency and eWAT preadipocytes reached 95% confluency, differentiation was induced using a standard cocktail of 0.5 mM isobutylmethylxanthine, 1 mM dexamethasone, 850 nM insulin, and 1 mM rosiglitazone dissolved in GlutaMAX media. After 48 hours, isobutylmethylxanthine and dexamethasone were removed, and after 96 hours rosiglitazone was removed.

Small RNAseq

For *in vivo* sequencing, total RNA was extracted from inguinal, epididymal, brown, axillary, and mesenteric fat pads of 13-week old C57BL/6J male mice housed at room temperature and from inguinal fat pads of 13-week old mice housed at 4° C for 1 week prior to sacrifice. RNA extraction was performed using Qiagen's RNeasy kit (modified protocol for miRNAs as described in RNA extraction section), then RNA was pooled into groups of 3 mice for inguinal, epididymal, brown and axillary fat. The TruSeq Small RNA Library Prep Kit (Illumina) was used to prepare libraries for sequencing, which was performed by LC Sciences.

For *in vitro* sequencing, total RNA was extracted from primary eWAT and sWAT preadipocytes immediately prior to differentiation and from mature adipocytes on the 7th day of differentiation. CL-316,243 treatment of sWAT adipocytes was performed 24 hours prior to RNA collection (10 uM final concentration). Biological replicates consisted of separate adipocyte preparations from different cohorts of 6-week old C57BL/6J mice. The TruSeq Small RNA Library Prep Kit (Illumina) was used to prepare libraries for sequencing, which was performed by LC Sciences.

HITS-CLIP Protocol

iBAT and eWAT tissues were dissected from 15-week old C57BL/6J male mice and immediately flash frozen in liquid nitrogen. Frozen iBAT and eWAT pairs were then pooled into groups of 2 and ground while still frozen with a Cellcrusher tissue pulverizer (Cellcrusher) cooled in liquid nitrogen. Frozen samples were spread to a thin layer on petri dishes pre-cooled on dry ice and UV-crosslinked at 400 mJ/cm^2 3X using a Stratalinker 2400 (Stratagene). All samples were stored at -80C until tissue lysis.

For each sample, 400 ul Protein A Dynabeads (Invitrogen) were pooled, then prepared by washing with 1 ml antibody binding (AB) buffer (AB: PBS, 0.02% tween) 3X. Following the final wash, beads were resuspended in 400 ul AB per sample and 50 ul of rabbit anti-mouse bridging antibody (Jackson ImmunoResearch) was added. Beads were rotated at RT for 1 hour, washed 3X with 1 ml AB, resuspended in AB, and incubated for 2 hours at RT with either 12 ul pan-Ago antibody (clone A28), or 12 ul mouse normal IgG (Santa Cruz Biotechnology).

Tissue pellets were lysed with 800µl PXL+ lysis buffer (PXL+: 1x PBS; 0.1% SDS; 0.5% Na-DOC; 0.5% NP-40, one Complete EDTA-Free Protease Inhibitor Cocktail tablet (Roche) per 10ml) and subject to DNase treatment by incubating for 5 minutes at 37°C, 1100 rpm, with DNAse (Promega). Samples were then centrifuged at 20,000 x g for 20 minutes, and a needle was used to withdraw 800 ul of aqueous protein lysate while avoiding the lipid layer and pellet. Lysates were then treated with RNase A (Affymetrix, 20U/mL) by first diluting the RNAse to the indicated concentration by volume (i.e., 1:100 for “High RNase,” or 1:10,000 for “Low

RNase) then treating samples with 8µl diluted RNAse per mL of lysate and digesting for 5 minutes at 37°C, 1100 rpm. Immediately following RNAse digestion, samples were added to prepared antibody bound beads and rotated for 3 hours at 4°C.

After IP, the following washes were performed: twice with lysis buffer, twice with high salt lysis buffer (5X PBS, 1% Igepal, 0.5% deoxycholate and 0.1% SDS), twice with stringent wash buffer (15 mM Tris pH 7.5, 5 mM EDTA, 2.5 mM EGTA, 1% TritonX-100, 1% NaDOC, 0.1% SDS, 120 mM NaCl, 25 mM KCl), twice with high salt wash buffer (15 mM Tris pH 7.5, 5 mM EDTA, 2.5 mM EGTA, 1% TritonX-100, 1% NaDOC, 0.1% SDS, 1M NaCl), twice with low salt wash buffer (15 mM Tris pH 7.5, 5 mM EDTA), and twice with PNK wash buffer (50 mM Tris pH 7.4, 10 mM MgCl2, 0.5% NP-40). The second of each wash was rotated for 2-3 minutes at room temperature. Tags were dephosphorylated as described (Moore et al., 2014) and subject to overnight 3' ligation at 16°C with a pre-adenylated linker (Moore et al., 2018) with the following ligation reaction: 2 ul of 25 uM linker, 2 ul of T4 RNA Ligase 2, truncated K227Q (NEB), 1X ligation buffer (supplied with ligase), 2 ul Superasin RNase inhibitor (Promega), and 8 ul PEG8000 (supplied with ligase). The resulting beads were washed, ^{32}P-labeled, and subject to SDS-PAGE and transfer as described (Moore et al., 2014).

Tags were collected from nitrocellulose as described (Zarnegar et al., 2016) with the following exceptions: Phenol:Chloroform:IAA, 25:24:1 pH 6.6 was used for extraction, and tags were precipitated with a standard NaOAC precipitation. Cloning was performed using the BrdU-CLIP protocol as described (Moore et al., 2018) with a few exceptions. Briefly, the RT primer contains a 14-nt degenerate linker (a 3-nt degenerate sequence, a 4-nt multiplexing index, and

a 7-nt unique molecular identifier), a 5′linker for PCR amplification, a spacer to prevent rolling circle amplification after circularization, and the reverse-complementary sequence of the 3′linker for reverse transcription. BrdUTP-labeled cDNA was specifically isolated via two sequential BrdUTP immunoprecipitations (Abcam AB8955) and circularized with CircLigase II (Epicenter CL9025K). Ago-CLIP libraries were sequenced by MiSeq (Illumina) to obtain 75-nt single end reads.

Western blot analysis

Samples and beads were prepared as described above. Following immunoprecipitation and washes, samples were immediately eluted, fractionated by SDS-PAGE, transferred to a nitrocellulose membrane and incubated with anti-Ago 2A8. The Ago positive control was prepared from cell lysate of HEK-293T cells transfected with a plasmid expressing mouse Ago2. Protein was detected by incubation with HRP-conjugated sheep anti-mouse secondary antibody (Jackson ImmunoResearch) and blots were imaged on a Biorad Chemidoc Imaging System.

Ckt analysis

Sequencing files were demultiplexed (barcode.txt), linkers were trimmed and reads were collapsed. Reads were aligned to mm10 genome assembly using Novoalign. All raw CLIP read processing and significant peak calling was performed using the Ckt software package (Shah et al., 2017). CLIP peaks and CIMS analysis was carried out as previously described (Moore et al., 2014).

Analysis performed in R

CLIP peak and unique tag output files were analyzed in R (www.r-project.org; Ihaka and Gentleman, 1996) using Bioconductor (Gentleman et al., 2004). using packages, "AnnotationDbi", "annotatr", "Biobase", "BiocGenerics", "BiocManager", "BiocParallel", "Biostrings", "BSgenome", "BSgenome.Mmusculus.UCSC.mm10", "DelayedArray", "DESeq2", "dplyr", "edgeR", "GenomeInfoDb", "GenomicFeatures", "GenomicRanges", "ggplot2", "ggpubr", "ggsignif", "gridExtra", "IRanges", "limma", "magrittr", "matrixStats", "mirbase.db", "org.Mm.eg.db", "plyr", "Rsamtools", "rtracklayer", "S4Vectors", "stringr", "SummarizedExperiment", "tibble", "tidyr", "TxDb.Mmusculus.UCSC.mm10.knownGene", "tximport", "VariantAnnotation", "wesanderson", "XVector". R version 3.6.1 Patched (2019-08-29 r77095).

Ago-associated miRNA mapping and analysis

All HITS-CLIP reads were mapped to a catalog of mature murine miRNAs from miRbase, and miRNAs that were not detected in adipose tissue by small RNAseq were discarded. Next, reads were normalized by RPM, then grouped into families based on shared 6-mer seed sequences. miRNAs were then matched to peaks by scanning for 6-mer, 7-mer (including 1-7 and 2-8 matching base pairs) and 8-mer seed sequences among peaks, limited to miRNAs with average normalized reads > 10.

Match score analysis

To select for single miRNA/peak matches, peaks were scanned for seed sequence matches with the 18 most abundant miRNA families. When two miRNAs matched a single peak, the miRNA

seed with greater complementarity was chosen (8-mer > 7-mer > 6-mer), and if two miRNA seeds had equivalent complementarity, the more abundant miRNA was chosen. A complementarity score was then assigned (6-mer = 1 point, 7-mer = 2 points, 8-mer = 3 points). Adjusted complementarity score = 1 + $\log_2$(raw complementarity score). Raw PhastCons scores (Siepel et al., 2005) were calculated for each miRNA 6-mer seed binding site, then divided by the average PhastCons score for 100 nucleotides upstream and downstream of the 22-nucleotide miRNA binding site. Adjusted PhastCons score = $\log_2$(raw PhastCons + 2). Match scores were calculated for each miRNA/peak pair according to the following formula: Match score = (peak height)*(adjusted PhastCons score)*(adjusted complementarity score)

Dual-luciferase assays

5'-phosphorylated oligonucleotides containing the predicted binding sites of miR-29 target genes, 6 bp of flanking DNA, and SacI/XhoI restriction site overhands were annealed then ligated into the dual luciferase reporter plasmid (Promega). For mutated sequences, 3-4-point mutations were induced in the miR-29a seed binding site using the Q5 Site Directed Mutagenesis Kit (NEB). 20 ug of recombinant dual-luciferase plasmid and 6 pmol of either miR-29a mimic or scrambled control were mixed with 100 ul Opti-MEM containing 1 ul lipofectamine RNAiMax in 24-well plate wells. Reverse transfection was initiated by adding 90,000 HEK293A cells/well in 500 ul. After 48 hours, firefly activity was measured by luminescence and normalized to Renilla activity.

RNA extraction, reverse transcriptase PCR, and quantitative PCR

RNA was extracted from tissues and cells using a TRIzol (Invitrogen)/chloroform extraction, followed by purification with RNeasy mini kits (Qiagen). To retain small RNAs during RNA purification, 1.5X volumes of 100% ethanol was used to precipitate RNA prior to column loading and RW1 buffer was substituted with RWT (Qiagen). For cDNA synthesis of mRNAs, the Applied Biosystems high capacity cDNA synthesis kit was used with 1000 ng of purified RNA. For cDNA synthesis of miRNAs, reverse transcription using the universal primer 5' - CAGGTCCAGTTTTTTTTTTTTTTVN - 3' was used as previously reported (Balcells et al., 2011). qPCR for both mRNAs and miRNAs was performed on a QuantStudio 6 Flex machine (Applied Biosystems) using SYBR-green fluorescent dye (Applied Biosystems). qPCR reactions were carried out in 384-well plates with a volume of 10 ul containing 0.5 uM forward and reverse primers, 1X qPCR master mix and 5 ng of mRNA-based cDNA or 1 ng of miRNA-based cDNA. MiRprimer2.0 was used to design primers for miRNA qPCR (Busk, 2014).

LNA and miRNA mimic transfections

All cells were transfected on 12-well plates 4 days after inducing differentiation. For each well, 3 ul of 10 uM miRNA mimic or 20 uM LNA was mixed with 3 ul lipofectamine RNAiMAX (Invitrogen) in 100 ul Opti-MEM reduced serum media and added to cells following a 15-minute incubation. RNA was collected in TRIzol (Invitrogen) 72 hours after transfection.

Leptin ELISA

The mouse leptin ELISA kit (Crystal Chem) was used to measure leptin concentration in serum (5 ul per assay) and CM (100 ul per assay).

Adipose fractionation

iBAT and eWAT were dissected from 6-week old male C57BL/6J mice, then pooled into groups (iBAT or eWAT from 2 mice per pool) and minced with spring scissors until only fine chunks remained. Diced tissue was then placed in 4 ml digestion buffer for 16 minutes (eWAT) or 40 minutes (iBAT) and incubated in a 37°C shaking water bath (140 RPM). Following digestion, the stromal vascular fraction and mature adipocyte fraction were separated by centrifugation (10 minutes at 500 x g). Fractions were added directly to TRIzol for total RNA extraction.

miRNAseq analysis

Data analysis for the *in vitro* and *in vivo* miRNA sequencing presented in chapter one was performed by LC Sciences. Briefly, reads were mapped to a catalogue of mature miRNAs from miRbase and sorted by species. Read counts were normalized by DEseq (Anders and Huber, 2010) across all 6 tissues. Data anlysis for the *in vivo* analysis in chapter 2 was analyzed using miRquant2.0 (Kanke et al., 2016), which includes adapter trimming, alignment to the mouse genome (mm9), quantification, identification of iso-miRs, and differential miRNA analysis.

miR-hub

Differentially expressed gene lists, either up or down regulated, ($|\log_2$ fold change$| > 2$; p-adjusted < 0.05) were examined for enrichment of miR binding sites, considering only well-expressed and significant miRs (DESeq normalized counts > 100; p-value < 0.01) that were

differentially expressed in the opposite direction of the gene list using miRhub (Baran-Gale et al., 2013).

6.2 Key materials

REAGENT or RESOURCE	SOURCE	IDENTIFIER
Antibodies		
Mouse mono-clonal anti-pan-Ago	Rockefeller University Antibody and Bioresource Core Facility	N/A
Rabbit anti-mouse IgG	Jackson ImmunoResearch Labs	Cat#315005008
Normal mouse IgG	Santa Cruz Biotechnology	Cat#sc-2343
Bacterial and Virus Strains		
AdEasy bacteria BJ5183-AD-1 cells	Agilent	Cat#240010 (included in kit)
Adenovirus: miR-338/GFP	Applied Biological Materials	Cat#mm0367
Adenovirus: miR-375/GFP	Applied Biological Materials	Cat#0408
Adenovirus: miR-10b/GFP	Applied Biological Materials	Cat#mm0022
Adenovirus: GFP	Applied Biological Materials	Cat#mm009
Chemicals, Peptides, and Recombinant Proteins		
RQ1 DNAse	Promega	M610A
RNase A (20 U/ml)	Affymetrix	Discontinued
Critical Commercial Assays		
Mouse Leptin ELISA	Crystal Chem	Cat#90030
AdEasy System	Agilent	Cat#240010
Dual-luciferase plasmid and kit	Promega	Cat#E1960
Q5® Site-Directed Mutagenesis Kit	NEB	Cat#E0554S
RWT buffer	Qiagen	Cat.#1067933
ABI high capacity cDNA synthesis kit	Applied Biosystems	Cat.# 4368814
Mouse Leptin ELISA kit	Crystal Chem	Cat.# 90030
PowerUp SYBR Green Master Mix	Applied Biosystems	Cat.# 4367659
Lipofectamine RNAiMax	Invitrogen	Cat.#13778
Experimental Models: Cell Lines		
Phoenix cell line	ATCC	Cat#CRL-3213
HEK-293A cell line	Invitrogen	Cat#R70507
Experimental Models: Organisms/Strains		
Lean C57BL/6J mice (chow-fed)	Jackson Labs	Cat#000664
Obese C57BL/6J mice (HFD-fed)	Jackson Labs	Cat#380050
$ob^{-/-}$ mice	Jackson Labs	Cat#000632

Oligonucleotides		
miR-29a miRNA mimic	Dharmacon	Cat# C-310521-07-0005
Scrambled miRNA mimic	Dharmacon	Cat# CN-001000-01-05
Mutated miR-29a miRNA mimic	Dharmacon	Cat# BUTMJ-000001 (seq UUGGAGCAUCUGAAAUCGGUUA)
Recombinant DNA		
Plasmid: pAdTrack	Addgene	Plasmid#16404
Plasmid: pMSCV	Clonetech	Cat#K1062-1
Software and Algorithms		
miRprimer2	Busk, 2014	https://sourceforge.net/projects/mirprimer/
mirHub	Baren-Gale et al., 2013	N/A
Ckt HITS-CLIP analysis	Shah et al., 2017	https://zhanglab.c2b2.columbia.edu/index.php/CTK_Documentation
Data processing in R	Ihaka and Gentleman, 1996	www.r-project.org
Bioconducter	Gentleman et al., 2004	https://www.bioconductor.org/
Other		
Collagenase B	Roche	Cat#11088831001
Collagenase D	Roche	Cat#11088882001
Dispase II	Roche	Cat#04942078001
MCDB210	Sigma	Cat# M6770-1L
ITS premix	BD Bio	Cat# 354352
L-ascorbic acid 2-phosphate	Sigma	Cat# A8960
bFGF	BD Bio	Cat# 13256-029

qPCR primers		
mRNA qPCR	**Oligo 1**	**Oligo 2**
TBP	GGGTATCTGCTGGCGGTTT	TGAAATAGTGATGCTGGGCACT
Leptin	TGACACCAAAACCCTCATCA	TGAAGCCCAGGAATGAAGTC
Pparg2	GCATGGTGCCTTCGCTGA	TGGCATCTCTGTGTCAACCATG
Adiponectin	GCACTGGCAAGTTCTACTGCA	GTAGGTGAAGAGAACGGCCTTGT
Ap2	ACACCGAGATTTCCTTCAAACTG	CCATCTAGGGTTATGATGCTCTTCA
PRDM16	GACTTGGACACTACCACGGG	AGATGCACCCCCAAACTCAG
PGC1α	CCCTGCCATTGTTAAGACC	TGCTGCTGTTCCTGTTTTC
Cidea	GCCGTGTTAAGGAATCTGCTG	TGCTCTTCTGTATCGCCCAGT
UCP1	ACTGCCACACCTCCAGTCATT	CTTTGCCTCACTCAGGATTGG
Angiotensinogen	GTCTGTGCCCATGATCTCCGGC	GCACGCACGTCACGGAGAAGT
Saa3	GAAAGAAGCTGGTCAAGGGTC	TCCGGGCAGCATCATAGTTC
Opgn	TTAGCTAGACAGGCAGGGGT	GTCAGCTTAGTCCAATACAGAGGA
Bnc1	CGCTTCAGGATTACATCCCTG	TGCTGCAAGGTAGCCACTTC
Hif1α	GCCTAGGAACCCGAGCCGGA	TCGGTGCCCGCGTTGTCTTC

Resistin	CCCAGAAGGCACAGCAGTC	CCCCGTCCCTGTCAACATAAG
Dio2	CAGTGTGGTGCACGTCTCCAATC	TGAACCAAAGTTGACCACCAG
Cox8b	GAACCATGAAGCCAACGACT	GCGAAGTTCACAGTGGTTCC
EHMT1	TGCAGCCAGCAAAGACCATA	CAAGCAAGCTGTCTGGGACT
Ebf2	CTCGTGTCTCTAACGCAGGG	AAGCATCACCTGTTCTTTGCAG
Elovl3	GGACCTGATGCAACCCTATGA	TCCGCGTTCTCATGTAGGTCT
Ckmt1	TGACCCCTATTTTGGCTCCAG	CGCAAGTCAGGAACTAGGAGG
Gatm	TGAAGACAAGGCCACCCATC	GCATTTTCAGCTCTGCCCAC
SERCA2B	GGCCCGAAACTACCTGGAAC	AGCACAAACGGCCAGGAAAT
Wt1	GAGAGCCAGCCTACCATCC	GGGTCCTCGTGTTTGAAGGAA
Raldh2	TGCTGACTTGGACTACGCTG	TCCACAAAGATGCGAGACCC
Tnfα	TAGCCCACGTCGTAGCAAAC	GCAGCCTTGTCCCTTGAAGA
TLE3	TGGTGAGCTTTGGAGCTGTT	CGGTTTCCCTCCAGGAAT
Pparα	GTGTTCGCAGCTGTTTTGGGG	GGACTTTCCAGGTCATCTGCC
SCD1	GTACCGCTGGCACATCAACT	AACTCAGAAGCCCAAAGCTCA
Acox1	CTCACTCGAAGCCAGCGTTA	CGGTGCACAGAGTTTTTAAACCA
Fsp27	GATGGCACAATCGTGGAGACAG	TCTTAGTTGGCTTCTGGGAAAGG
FASN	TGCACCTCACAGGCATCAAT	GTCCCACTTGATGTGAGGGG
ACC1	GCATGTCTGGCTTGCACCTA	CACCGACGGATAGATCGCAT
ATGL	GACAGCTCCACCAACATCCA	GCAAAGGGTTGGGTTGGTTC
Eln	TAGGGTGCAAAGGGTTGTGT	CCAAAGAGCACACCAACAATCA
Sparc	ACCTGGACTACATCGGACCA	CCAGGCGCTTCTCATTCTCA
Lpl	TCCAGAGTTTGACCGCCTTC	ATTCCCGTTACCGTCCATCC
Mcart1	GGGCCGTGGGTTAAAGAAACTC	TTGGGGGCCTCTTCTCATGT
Ptp4a1	CTGTGGTGTTCTCGGTCACA	CACGCCTGTGTCCAGGTTAT
Hmgcs1	GTCTGCGGTCTCCTTGCTTT	GGCACTATGCAAATCAATGGCT
Cav2	TGCCTTCCGTGCAGACAATA	GGTCTGAGTGGTCAGTCGTG
Sucla2	CGGCGTCCATGTTCTACGG	ACCCGCTTCCTGCAATAACT
Col3a1	ACGTAAGCACTGGTGGACAG	CAGGAGGGCCATAGCTGAAC
miRNA qPCR	**Oligo 1**	**Oligo 2**
snoRNA 202	GGCTGTACTGACTTGTAGAAAG	TCCAGTTTTTTTTTTTTTTTCATCAGA
miR-29a	CGCAGTAGCACCATCTGA	GGTCCAGTTTTTTTTTTTTTTTAACC
miR-183	GCAGTATGGCACTGGTAGA	GGTCCAGTTTTTTTTTTTTTTTAGTGA
miR-96	GCAGTTTGGCACTAGCAC	GGTCCAGTTTTTTTTTTTTTTTAGCA
miR-182	GTTTGGCAATGGTAGAACTCA	GTCCAGTTTTTTTTTTTTTTTCGGT
miR-338	GCAGTCCAGCATCAGTG	GGTCCAGTTTTTTTTTTTTTTTCAAC
miR-10b	CAGTACCCTGTAGAACCGA	GGTCCAGTTTTTTTTTTTTTTTCAC
miR-192	CAGCTGACCTATGAATTGACA	TCCAGTTTTTTTTTTTTTTTGGCT
miR-375	AGTTTGTTCGTTCGGCTC	GGTCCAGTTTTTTTTTTTTTTTCAC
miR-335	GCAGTCAAGAGCAATAACGA	CAGGTCCAGTTTTTTTTTTTTTTTACA

Cloning PCR primers		
Cloned gene	**Primer 1**	**Primer 2**
miR-29a	(BgI11) ctaagatctATAGCTGATTAGTCAACCACC	(NotI) taagcggccgcCCACCATCACTATGTGAATAG
miR-16	(XhoI) attctcgagCCTTGGAGTAAAGTAGCAGC	(HindIII) cacaagcttCAGACACAATATGTAGAGCG

miR-16 SDM (scrambled)	aaatattggcgTTAAGATTCTGAAATTACCT CCAGTATTGAC	acgtgttacaaAGGCACCGCTGACATTGC
miR-335	(Bg1II) cagagatctCACTTAATTTTTACAACAGC	(XhoI) aagctcgagATCATATACTGGATTTAACC
miR-192	(HpaI) gaagttaacAGGAAGAGGAGCCACAG	(EcoRI) tatgaattcAACTGGAAACAGGAAGGAG

Luciferase assay oligonucleotides		
Cloning gene	**Oligo 1 (IDT)**	**Oligo 2 (IDT)**
Lep 1	/5Phos/cAGTTTCGTGCTCAGCTCTGTC TGGTGCTGTGAGCc	/5Phos/tcgagGCTCACAGCACCAGACAGAG CTGAGCACGAAACTgagct
Lep 2	/5Phos/cTGAGCGGGATCAGGTTTTGTG GTGCTAAGAGAc	/5Phos/tcgagTCTCTTAGCACCACAAAACCT GATCCCGCTCAgagct
Mcart1	/5Phos/cGTTTGTTTATTTTTTTAAATGG TGCTAGGGATc	/5Phos/tcgagATCCCTAGCACCATTTAAAAA AATAAACAAACgagct
Ptp4a1	/5Phos/cCTTTATTAGGTTGTATATATG GTGCTAGAAGTc	/5Phos/tcgagACTTCTAGCACCATATATACA ACCTAATAAAGgagct
Sucla2	(/5Phos/cAGCATAGGATGTCTAGTAAA TGGTGCTGGCTTc	/5Phos/tcgagAAGCCAGCACCATTTACTAGA CATCCTATGCTgagct
Hmgcs1	/5Phos/cCAAGTTCTCTGGATGATTTTT GGTGCTGAACAATc	/5Phos/tcgagATTGTTCAGCACCAAAAATCA TCCAGAGAACTTGgagct
Lep 1 SDM	GCTCTGTCTGtgtaTGTGAGCCTCGAGT C	TGAGCACGAAACTGAGCT
Lep 2 SDM	AGGTTTTGTGtgtaTAAGAGACTCGAG TCTAGAGTCGAC	GATCCCGCTCAGAGCTCG
Mcart 1 SDM	TTTTTAAATGtgtaTAGGGATCTCGAGT CTAGAG	AATAAACAAACGAGCTCG
Ptp4a1 SDM	TGTATATATGtgtaTAGAAGTCTCGAGT CTAGAG	ACCTAATAAAGGAGCTCG
Hmgcs1 SDM	ATGATTTTTGtgtaTGAACAATCTCGAG TCTAGAGTC	CCAGAGAACTTGGAGCTC

REFERENCES

Acharya, A., Berry, D.C., Zhang, H., Jiang, Y., Jones, B.T., Hammer, R.E., Graff, J.M., and Mendell, J.T. (2019). miR-26 suppresses adipocyte progenitor differentiation and fat production by targeting Fbxl19. Genes Dev.

Agarwal, V., Bell, G.W., Nam, J.W., and Bartel, D.P. (2015). Predicting effective microRNA target sites in mammalian mRNAs. Elife *4*.

Ahima, R.S. (2008). Revisiting leptin's role in obesity and weight loss. J Clin Invest *118*, 2380-2383.

Ailhaud, G., Fukamizu, A., Massiera, F., Negrel, R., Saint-Marc, P., and Teboul, M. (2000). Angiotensinogen, angiotensin II and adipose tissue development. Int J Obes Relat Metab Disord *24 Suppl 4*, S33-35.

Anders, S., and Huber, W. (2010). Differential expression analysis for sequence count data. Genome Biol *11*, R106.

Armellini, F., Zamboni, M., Rigo, L., Bergamo-Andreis, I.A., Robbi, R., De Marchi, M., and Bosello, O. (1991). Sonography detection of small intra-abdominal fat variations. Int J Obes *15*, 847-852.

Aronis, K.N., Foo, J.P., Chamberland, J.P., and Mantzoros, C.S. (2012). Secretion patterns of circulating osteoprotegerin and response to acute and chronic energy deprivation in young healthy adults. J Clin Endocrinol Metab *97*, 2765-2772.

Baek, D., Villen, J., Shin, C., Camargo, F.D., Gygi, S.P., and Bartel, D.P. (2008). The impact of microRNAs on protein output. Nature *455*, 64-71.

Bail, S., Swerdel, M., Liu, H., Jiao, X., Goff, L.A., Hart, R.P., and Kiledjian, M. (2010). Differential regulation of microRNA stability. RNA *16*, 1032-1039.

Balcells, I., Cirera, S., and Busk, P.K. (2011). Specific and sensitive quantitative RT-PCR of miRNAs with DNA primers. BMC Biotechnol *11*, 70.

Baran-Gale, J., Fannin, E.E., Kurtz, C.L., and Sethupathy, P. (2013). Beta cell 5'-shifted isomiRs are candidate regulatory hubs in type 2 diabetes. PLoS One *8*, e73240.

Barneda, D., Planas-Iglesias, J., Gaspar, M.L., Mohammadyani, D., Prasannan, S., Dormann, D., Han, G.S., Jesch, S.A., Carman, G.M., Kagan, V.*, et al.* (2015). The brown adipocyte protein CIDEA promotes lipid droplet fusion via a phosphatidic acid-binding amphipathic helix. Elife *4*, e07485.

Bartel, D.P. (2009). MicroRNAs: target recognition and regulatory functions. Cell *136*, 215-233.

Bartel, D.P. (2018). Metazoan MicroRNAs. Cell *173*, 20-51.

Bazzini, A.A., Lee, M.T., and Giraldez, A.J. (2012). Ribosome profiling shows that miR-430 reduces translation before causing mRNA decay in zebrafish. Science *336*, 233-237.

Berry, D.C., Jacobs, H., Marwarha, G., Gely-Pernot, A., O'Byrne, S.M., DeSantis, D., Klopfenstein, M., Feret, B., Dennefeld, C., Blaner, W.S.*, et al.* (2013). The STRA6 receptor is essential for retinol-binding protein-induced insulin resistance but not for maintaining vitamin A homeostasis in tissues other than the eye. J Biol Chem *288*, 24528-24539.

Biener, A., Cawley, J., and Meyerhoefer, C. (2017). The High and Rising Costs of Obesity to the US Health Care System. J Gen Intern Med *32*, 6-8.

Bitetti, A., Mallory, A.C., Golini, E., Carrieri, C., Carreno Gutierrez, H., Perlas, E., Perez-Rico, Y.A., Tocchini-Valentini, G.P., Enright, A.J., Norton, W.H.J.*, et al.* (2018). MicroRNA degradation by a conserved target RNA regulates animal behavior. Nat Struct Mol Biol *25*, 244-251.

Bjorntorp, P. (2000). [Metabolic difference between visceral fat and subcutaneous abdominal fat]. Diabetes Metab *26 Suppl 3*, 10-12.

Boele, J., Persson, H., Shin, J.W., Ishizu, Y., Newie, I.S., Sokilde, R., Hawkins, S.M., Coarfa, C., Ikeda, K., Takayama, K.*, et al.* (2014). PAPD5-mediated 3' adenylation and subsequent degradation of miR-21 is disrupted in proliferative disease. Proc Natl Acad Sci U S A *111*, 11467-11472.

Bose, A., Guilherme, A., Robida, S.I., Nicoloro, S.M., Zhou, Q.L., Jiang, Z.Y., Pomerleau, D.P., and Czech, M.P. (2002). Glucose transporter recycling in response to insulin is facilitated by myosin Myo1c. Nature *420*, 821-824.

Boudreau, R.L., Jiang, P., Gilmore, B.L., Spengler, R.M., Tirabassi, R., Nelson, J.A., Ross, C.A., Xing, Y., and Davidson, B.L. (2014). Transcriptome-wide discovery of microRNA binding sites in human brain. Neuron *81*, 294-305.

Brendle, C., Werner, M.K., Schmadl, M., la Fougere, C., Nikolaou, K., Stefan, N., and Pfannenberg, C. (2018). Correlation of Brown Adipose Tissue with Other Body Fat Compartments and Patient Characteristics: A Retrospective Analysis in a Large Patient Cohort Using PET/CT. Acad Radiol *25*, 102-110.

Bruun, J.M., Lihn, A.S., Pedersen, S.B., and Richelsen, B. (2005). Monocyte chemoattractant protein-1 release is higher in visceral than subcutaneous human adipose tissue (AT): implication of macrophages resident in the AT. J Clin Endocrinol Metab *90*, 2282-2289.

Busk, P.K. (2014). A tool for design of primers for microRNA-specific quantitative RT-qPCR. BMC Bioinformatics *15*, 29.

Cao, H., Gerhold, K., Mayers, J.R., Wiest, M.M., Watkins, S.M., and Hotamisligil, G.S. (2008). Identification of a lipokine, a lipid hormone linking adipose tissue to systemic metabolism. Cell *134*, 933-944.

Cawley, J., Rizzo, J.A., and Haas, K. (2007). Occupation-specific absenteeism costs associated with obesity and morbid obesity. J Occup Environ Med *49*, 1317-1324.

Cawthorn, W.P., Scheller, E.L., Learman, B.S., Parlee, S.D., Simon, B.R., Mori, H., Ning, X., Bree, A.J., Schell, B., Broome, D.T., *et al.* (2014). Bone marrow adipose tissue is an endocrine organ that contributes to increased circulating adiponectin during caloric restriction. Cell Metab *20*, 368-375.

Cawthorn, W.P., and Sethi, J.K. (2008). TNF-alpha and adipocyte biology. FEBS Lett *582*, 117-131.

Chan, J.L., Wong, S.L., and Mantzoros, C.S. (2008). Pharmacokinetics of subcutaneous recombinant methionyl human leptin administration in healthy subjects in the fed and fasting states: regulation by gender and adiposity. Clin Pharmacokinet *47*, 753-764.

Chan, K.L., Pillon, N.J., Sivaloganathan, D.M., Costford, S.R., Liu, Z., Theret, M., Chazaud, B., and Klip, A. (2015). Palmitoleate Reverses High Fat-induced Proinflammatory Macrophage Polarization via AMP-activated Protein Kinase (AMPK). J Biol Chem *290*, 16979-16988.

Chandradoss, S.D., Schirle, N.T., Szczepaniak, M., MacRae, I.J., and Joo, C. (2015). A Dynamic Search Process Underlies MicroRNA Targeting. Cell *162*, 96-107.

Chang, H.M., Triboulet, R., Thornton, J.E., and Gregory, R.I. (2013). A role for the Perlman syndrome exonuclease Dis3l2 in the Lin28-let-7 pathway. Nature *497*, 244-248.

Chau, Y.Y., and Hastie, N. (2015). Wt1, the mesothelium and the origins and heterogeneity of visceral fat progenitors. Adipocyte *4*, 217-221.

Chen, L., Hou, J., Ye, L., Chen, Y., Cui, J., Tian, W., Li, C., and Liu, L. (2014a). MicroRNA-143 regulates adipogenesis by modulating the MAP2K5-ERK5 signaling. Sci Rep *4*, 3819.

Chen, T., Li, Z., Tu, J., Zhu, W., Ge, J., Zheng, X., Yang, L., Pan, X., Yan, H., and Zhu, J. (2011). MicroRNA-29a regulates pro-inflammatory cytokine secretion and scavenger receptor expression by targeting LPL in oxLDL-stimulated dendritic cells. FEBS Lett *585*, 657-663.

Chen, Y.W., Song, S., Weng, R., Verma, P., Kugler, J.M., Buescher, M., Rouam, S., and Cohen, S.M. (2014b). Systematic study of Drosophila microRNA functions using a collection of targeted knockout mutations. Dev Cell *31*, 784-800.

Chi, J., Wu, Z., Choi, C.H.J., Nguyen, L., Tegegne, S., Ackerman, S.E., Crane, A., Marchildon, F., Tessier-Lavigne, M., and Cohen, P. (2018). Three-Dimensional Adipose

Tissue Imaging Reveals Regional Variation in Beige Fat Biogenesis and PRDM16-Dependent Sympathetic Neurite Density. Cell Metab *27*, 226-236 e223.

Chi, S.W., Zang, J.B., Mele, A., and Darnell, R.B. (2009). Argonaute HITS-CLIP decodes microRNA-mRNA interaction maps. Nature *460*, 479-486.

Christian, M. (2015). Transcriptional fingerprinting of "browning" white fat identifies NRG4 as a novel adipokine. Adipocyte *4*, 50-54.

Cimen, I., Kocaturk, B., Koyuncu, S., Tufanli, O., Onat, U.I., Yildirim, A.D., Apaydin, O., Demirsoy, S., Aykut, Z.G., Nguyen, U.T.*, et al.* (2016). Prevention of atherosclerosis by bioactive palmitoleate through suppression of organelle stress and inflammasome activation. Sci Transl Med *8*, 358ra126.

Cioffi, M., Vallespinos-Serrano, M., Trabulo, S.M., Fernandez-Marcos, P.J., Firment, A.N., Vazquez, B.N., Vieira, C.R., Mulero, F., Camara, J.A., Cronin, U.P.*, et al.* (2015). MiR-93 Controls Adiposity via Inhibition of Sirt7 and Tbx3. Cell Rep *12*, 1594-1605.

Cohen, P., Levy, J.D., Zhang, Y., Frontini, A., Kolodin, D.P., Svensson, K.J., Lo, J.C., Zeng, X., Ye, L., Khandekar, M.J.*, et al.* (2014). Ablation of PRDM16 and beige adipose causes metabolic dysfunction and a subcutaneous to visceral fat switch. Cell *156*, 304-316.

Coleman, D.L. (1978). Obese and diabetes: two mutant genes causing diabetes-obesity syndromes in mice. Diabetologia *14*, 141-148.

Cook, K.S., Min, H.Y., Johnson, D., Chaplinsky, R.J., Flier, J.S., Hunt, C.R., and Spiegelman, B.M. (1987). Adipsin: a circulating serine protease homolog secreted by adipose tissue and sciatic nerve. Science *237*, 402-405.

Coppari, R., and Bjorbaek, C. (2012). Leptin revisited: its mechanism of action and potential for treating diabetes. Nat Rev Drug Discov *11*, 692-708.

Corrales, P., Vidal-Puig, A., and Medina-Gomez, G. (2018). PPARs and Metabolic Disorders Associated with Challenged Adipose Tissue Plasticity. Int J Mol Sci *19*.

Cypess, A.M., Lehman, S., Williams, G., Tal, I., Rodman, D., Goldfine, A.B., Kuo, F.C., Palmer, E.L., Tseng, Y.H., Doria, A.*, et al.* (2009). Identification and importance of brown adipose tissue in adult humans. N Engl J Med *360*, 1509-1517.

Dallner, O.S., Marinis, J.M., Lu, Y.H., Birsoy, K., Werner, E., Fayzikhodjaeva, G., Dill, B.D., Molina, H., Moscati, A., Kutalik, Z.*, et al.* (2019). Dysregulation of a long noncoding RNA reduces leptin leading to a leptin-responsive form of obesity. Nat Med *25*, 507-516.

de Jesus, L.A., Carvalho, S.D., Ribeiro, M.O., Schneider, M., Kim, S.W., Harney, J.W., Larsen, P.R., and Bianco, A.C. (2001). The type 2 iodothyronine deiodinase is essential for adaptive thermogenesis in brown adipose tissue. J Clin Invest *108*, 1379-1385.

Deshmane, S.L., Kremlev, S., Amini, S., and Sawaya, B.E. (2009). Monocyte chemoattractant protein-1 (MCP-1): an overview. J Interferon Cytokine Res *29*, 313-326.

Despres, J.P., Allard, C., Tremblay, A., Talbot, J., and Bouchard, C. (1985). Evidence for a regional component of body fatness in the association with serum lipids in men and women. Metabolism *34*, 967-973.

Dorsett, Y., McBride, K.M., Jankovic, M., Gazumyan, A., Thai, T.H., Robbiani, D.F., Di Virgilio, M., Reina San-Martin, B., Heidkamp, G., Schwickert, T.A.*, et al.* (2008). MicroRNA-155 suppresses activation-induced cytidine deaminase-mediated Myc-Igh translocation. Immunity *28*, 630-638.

Drolet, R., Richard, C., Sniderman, A.D., Mailloux, J., Fortier, M., Huot, C., Rheaume, C., and Tchernof, A. (2008). Hypertrophy and hyperplasia of abdominal adipose tissues in women. Int J Obes (Lond) *32*, 283-291.

Eder, K., Baffy, N., Falus, A., and Fulop, A.K. (2009). The major inflammatory mediator interleukin-6 and obesity. Inflamm Res *58*, 727-736.

Eheim, A., Medrikova, D., and Herzig, S. (2014). Immune cells and metabolic dysfunction. Semin Immunopathol *36*, 13-25.

Eichhorn, S.W., Guo, H., McGeary, S.E., Rodriguez-Mias, R.A., Shin, C., Baek, D., Hsu, S.H., Ghoshal, K., Villen, J., and Bartel, D.P. (2014). mRNA destabilization is the dominant effect of mammalian microRNAs by the time substantial repression ensues. Mol Cell *56*, 104-115.

Faggioni, R., Fantuzzi, G., Fuller, J., Dinarello, C.A., Feingold, K.R., and Grunfeld, C. (1998). IL-1 beta mediates leptin induction during inflammation. Am J Physiol *274*, R204-208.

Fang, H., and Judd, R.L. (2018). Adiponectin Regulation and Function. Compr Physiol *8*, 1031-1063.

Fei, H., Okano, H.J., Li, C., Lee, G.H., Zhao, C., Darnell, R., and Friedman, J.M. (1997). Anatomic localization of alternatively spliced leptin receptors (Ob-R) in mouse brain and other tissues. Proc Natl Acad Sci U S A *94*, 7001-7005.

Fernandez-Riejos, P., Najib, S., Santos-Alvarez, J., Martin-Romero, C., Perez-Perez, A., Gonzalez-Yanes, C., and Sanchez-Margalet, V. (2010). Role of leptin in the activation of immune cells. Mediators Inflamm *2010*, 568343.

Ferrante, S.C., Nadler, E.P., Pillai, D.K., Hubal, M.J., Wang, Z., Wang, J.M., Gordish-Dressman, H., Koeck, E., Sevilla, S., Wiles, A.A.*, et al.* (2015). Adipocyte-derived exosomal miRNAs: a novel mechanism for obesity-related disease. Pediatr Res *77*, 447-454.

Fischer, A.W., Shabalina, I.G., Mattsson, C.L., Abreu-Vieira, G., Cannon, B., Nedergaard, J., and Petrovic, N. (2017). UCP1 inhibition in Cidea-overexpressing mice is physiologically

counteracted by brown adipose tissue hyperrecruitment. Am J Physiol Endocrinol Metab *312*, E72-E87.

Flowers, M.T., and Ntambi, J.M. (2008). Role of stearoyl-coenzyme A desaturase in regulating lipid metabolism. Curr Opin Lipidol *19*, 248-256.

Forman, J.J., Legesse-Miller, A., and Coller, H.A. (2008). A search for conserved sequences in coding regions reveals that the let-7 microRNA targets Dicer within its coding sequence. Proc Natl Acad Sci U S A *105*, 14879-14884.

Frederich, R.C., Hamann, A., Anderson, S., Lollmann, B., Lowell, B.B., and Flier, J.S. (1995). Leptin levels reflect body lipid content in mice: evidence for diet-induced resistance to leptin action. Nat Med *1*, 1311-1314.

Freedland, E.S. (2004). Role of a critical visceral adipose tissue threshold (CVATT) in metabolic syndrome: implications for controlling dietary carbohydrates: a review. Nutr Metab (Lond) *1*, 12.

Friedman, J.M., and Halaas, J.L. (1998). Leptin and the regulation of body weight in mammals. Nature *395*, 763-770.

Friedman, R.C., Farh, K.K., Burge, C.B., and Bartel, D.P. (2009). Most mammalian mRNAs are conserved targets of microRNAs. Genome Res *19*, 92-105.

Fuchs Wightman, F., Giono, L.E., Fededa, J.P., and de la Mata, M. (2018). Target RNAs Strike Back on MicroRNAs. Front Genet *9*, 435.

Fuke, T., Yoshizaki, T., Kondo, M., Morino, K., Obata, T., Ugi, S., Nishio, Y., Maeda, S., Kashiwagi, A., and Maegawa, H. (2010). Transcription factor AP-2beta inhibits expression and secretion of leptin, an insulin-sensitizing hormone, in 3T3-L1 adipocytes. Int J Obes (Lond) *34*, 670-678.

Gantier, M.P., McCoy, C.E., Rusinova, I., Saulep, D., Wang, D., Xu, D., Irving, A.T., Behlke, M.A., Hertzog, P.J., Mackay, F.*, et al.* (2011). Analysis of microRNA turnover in mammalian cells following Dicer1 ablation. Nucleic Acids Res *39*, 5692-5703.

Gao, Y., Cao, Y., Cui, X., Wang, X., Zhou, Y., Huang, F., Wang, X., Wen, J., Xie, K., Xu, P.*, et al.* (2018). miR-199a-3p regulates brown adipocyte differentiation through mTOR signaling pathway. Mol Cell Endocrinol *476*, 155-164.

Garcia, D.M., Baek, D., Shin, C., Bell, G.W., Grimson, A., and Bartel, D.P. (2011). Weak seed-pairing stability and high target-site abundance decrease the proficiency of lsy-6 and other microRNAs. Nat Struct Mol Biol *18*, 1139-1146.

Garcia, R.A., Roemmich, J.N., and Claycombe, K.J. (2016). Evaluation of markers of beige adipocytes in white adipose tissue of the mouse. Nutr Metab (Lond) *13*, 24.

Gates, D.M., Succop, P., Brehm, B.J., Gillespie, G.L., and Sommers, B.D. (2008). Obesity and presenteeism: the impact of body mass index on workplace productivity. J Occup Environ Med *50*, 39-45.

Gentleman, R.C., Carey, V.J., Bates, D.M., Bolstad, B., Dettling, M., Dudoit, S., Ellis, B., Gautier, L., Ge, Y., Gentry, J.*, et al.* (2004). Bioconductor: open software development for computational biology and bioinformatics. Genome Biol *5*, R80.

Giroud, M., Karbiener, M., Pisani, D.F., Ghandour, R.A., Beranger, G.E., Niemi, T., Taittonen, M., Nuutila, P., Virtanen, K.A., Langin, D.*, et al.* (2016). Let-7i-5p represses brite adipocyte function in mice and humans. Sci Rep *6*, 28613.

Glantschnig, C., Koenen, M., Gil-Lozano, M., Karbiener, M., Pickrahn, I., Williams-Dautovich, J., Patel, R., Cummins, C.L., Giroud, M., Hartleben, G.*, et al.* (2019). A miR-29a-driven negative feedback loop regulates peripheral glucocorticoid receptor signaling. FASEB J *33*, 5924-5941.

Goodpaster, B.H., Delany, J.P., Otto, A.D., Kuller, L., Vockley, J., South-Paul, J.E., Thomas, S.B., Brown, J., McTigue, K., Hames, K.C.*, et al.* (2010). Effects of diet and physical activity interventions on weight loss and cardiometabolic risk factors in severely obese adults: a randomized trial. JAMA *304*, 1795-1802.

Goody, D., and Pfeifer, A. (2019). MicroRNAs in brown and beige fat. Biochim Biophys Acta Mol Cell Biol Lipids *1864*, 29-36.

Grahn, T.H., Kaur, R., Yin, J., Schweiger, M., Sharma, V.M., Lee, M.J., Ido, Y., Smas, C.M., Zechner, R., Lass, A.*, et al.* (2014). Fat-specific protein 27 (FSP27) interacts with adipose triglyceride lipase (ATGL) to regulate lipolysis and insulin sensitivity in human adipocytes. J Biol Chem *289*, 12029-12039.

Grimson, A., Farh, K.K., Johnston, W.K., Garrett-Engele, P., Lim, L.P., and Bartel, D.P. (2007). MicroRNA targeting specificity in mammals: determinants beyond seed pairing. Mol Cell *27*, 91-105.

Grosswendt, S., Filipchyk, A., Manzano, M., Klironomos, F., Schilling, M., Herzog, M., Gottwein, E., and Rajewsky, N. (2014). Unambiguous identification of miRNA:target site interactions by different types of ligation reactions. Mol Cell *54*, 1042-1054.

Grunweller, A., and Hartmann, R.K. (2007). Locked nucleic acid oligonucleotides: the next generation of antisense agents? BioDrugs *21*, 235-243.

Guo, K., McMinn, J.E., Ludwig, T., Yu, Y.H., Yang, G., Chen, L., Loh, D., Li, C., Chua, S., Jr., and Zhang, Y. (2007). Disruption of peripheral leptin signaling in mice results in hyperleptinemia without associated metabolic abnormalities. Endocrinology *148*, 3987-3997.

Guo, X., Li, H., Xu, H., Halim, V., Zhang, W., Wang, H., Ong, K.T., Woo, S.L., Walzem, R.L., Mashek, D.G.*, et al.* (2012). Palmitoleate induces hepatic steatosis but suppresses liver inflammatory response in mice. PLoS One *7*, e39286.

Ha, M., and Kim, V.N. (2014). Regulation of microRNA biogenesis. Nat Rev Mol Cell Biol *15*, 509-524.

Hafner, M., Landthaler, M., Burger, L., Khorshid, M., Hausser, J., Berninger, P., Rothballer, A., Ascano, M., Jr., Jungkamp, A.C., Munschauer, M.*, et al.* (2010). Transcriptome-wide identification of RNA-binding protein and microRNA target sites by PAR-CLIP. Cell *141*, 129-141.

Halaas, J.L., Boozer, C., Blair-West, J., Fidahusein, N., Denton, D.A., and Friedman, J.M. (1997). Physiological response to long-term peripheral and central leptin infusion in lean and obese mice. Proc Natl Acad Sci U S A *94*, 8878-8883.

Halaas, J.L., Gajiwala, K.S., Maffei, M., Cohen, S.L., Chait, B.T., Rabinowitz, D., Lallone, R.L., Burley, S.K., and Friedman, J.M. (1995). Weight-reducing effects of the plasma protein encoded by the obese gene. Science *269*, 543-546.

Hales, C.M., Carroll, M.D., Fryar, C.D., and Ogden, C.L. (2017). Prevalence of Obesity Among Adults and Youth: United States, 2015-2016. NCHS Data Brief, 1-8.

Harman-Boehm, I., Bluher, M., Redel, H., Sion-Vardy, N., Ovadia, S., Avinoach, E., Shai, I., Kloting, N., Stumvoll, M., Bashan, N.*, et al.* (2007). Macrophage infiltration into omental versus subcutaneous fat across different populations: effect of regional adiposity and the comorbidities of obesity. J Clin Endocrinol Metab *92*, 2240-2247.

Harms, M., and Seale, P. (2013). Brown and beige fat: development, function and therapeutic potential. Nat Med *19*, 1252-1263.

Harris, R.B. (2014). Direct and indirect effects of leptin on adipocyte metabolism. Biochim Biophys Acta *1842*, 414-423.

Hausser, J., Syed, A.P., Bilen, B., and Zavolan, M. (2013). Analysis of CDS-located miRNA target sites suggests that they can effectively inhibit translation. Genome Res *23*, 604-615.

He, L., Tang, M., Xiao, T., Liu, H., Liu, W., Li, G., Zhang, F., Xiao, Y., Zhou, Z., Liu, F.*, et al.* (2018). Obesity-Associated miR-199a/214 Cluster Inhibits Adipose Browning via PRDM16-PGC-1alpha Transcriptional Network. Diabetes *67*, 2585-2600.

Heidersbach, A., Saxby, C., Carver-Moore, K., Huang, Y., Ang, Y.S., de Jong, P.J., Ivey, K.N., and Srivastava, D. (2013). microRNA-1 regulates sarcomere formation and suppresses smooth muscle gene expression in the mammalian heart. Elife *2*, e01323.

Helwak, A., Kudla, G., Dudnakova, T., and Tollervey, D. (2013). Mapping the human miRNA interactome by CLASH reveals frequent noncanonical binding. Cell *153*, 654-665.

Herbert, K.M., Pimienta, G., DeGregorio, S.J., Alexandrov, A., and Steitz, J.A. (2013). Phosphorylation of DGCR8 increases its intracellular stability and induces a progrowth miRNA profile. Cell Rep *5*, 1070-1081.

Hervey, G.R. (1959). The effects of lesions in the hypothalamus in parabiotic rats. J Physiol *145*, 336-352.

Himms-Hagen, J., Cui, J., Danforth, E., Jr., Taatjes, D.J., Lang, S.S., Waters, B.L., and Claus, T.H. (1994). Effect of CL-316,243, a thermogenic beta 3-agonist, on energy balance and brown and white adipose tissues in rats. Am J Physiol *266*, R1371-1382.

Hoeke, L., Sharbati, J., Pawar, K., Keller, A., Einspanier, R., and Sharbati, S. (2013). Intestinal Salmonella typhimurium infection leads to miR-29a induced caveolin 2 regulation. PLoS One *8*, e67300.

Hotamisligil, G.S., Shargill, N.S., and Spiegelman, B.M. (1993). Adipose expression of tumor necrosis factor-alpha: direct role in obesity-linked insulin resistance. Science *259*, 87-91.

Hu, F., Wang, M., Xiao, T., Yin, B., He, L., Meng, W., Dong, M., and Liu, F. (2015). miR-30 promotes thermogenesis and the development of beige fat by targeting RIP140. Diabetes *64*, 2056-2068.

Huang, Z., Zhong, L., Lee, J.T.H., Zhang, J., Wu, D., Geng, L., Wang, Y., Wong, C.M., and Xu, A. (2017). The FGF21-CCL11 Axis Mediates Beiging of White Adipose Tissues by Coupling Sympathetic Nervous System to Type 2 Immunity. Cell Metab *26*, 493-508 e494.

Hummel, K.P., Dickie, M.M., and Coleman, D.L. (1966). Diabetes, a new mutation in the mouse. Science *153*, 1127-1128.

Hung, Y.H., Kanke, M., Kurtz, C.L., Cubitt, R., Bunaciu, R.P., Miao, J., Zhou, L., Graham, J.L., Hussain, M.M., Havel, P.*, et al.* (2019). Acute suppression of insulin resistance-associated hepatic miR-29 in vivo improves glycemic control in adult mice. Physiol Genomics *51*, 379-389.

Huppertz, I., Attig, J., D'Ambrogio, A., Easton, L.E., Sibley, C.R., Sugimoto, Y., Tajnik, M., Konig, J., and Ule, J. (2014). iCLIP: protein-RNA interactions at nucleotide resolution. Methods *65*, 274-287.

Ibrahim, M.M. (2010). Subcutaneous and visceral adipose tissue: structural and functional differences. Obes Rev *11*, 11-18.

Iikuni, N., Lam, Q.L., Lu, L., Matarese, G., and La Cava, A. (2008). Leptin and Inflammation. Curr Immunol Rev *4*, 70-79.

Ikeda, K., Kang, Q., Yoneshiro, T., Camporez, J.P., Maki, H., Homma, M., Shinoda, K., Chen, Y., Lu, X., Maretich, P.*, et al.* (2017). UCP1-independent signaling involving SERCA2b-mediated calcium cycling regulates beige fat thermogenesis and systemic glucose homeostasis. Nat Med *23*, 1454-1465.

Imbeault, P., Couillard, C., Tremblay, A., Despres, J.P., and Mauriege, P. (2000). Reduced alpha(2)-adrenergic sensitivity of subcutaneous abdominal adipocytes as a modulator of fasting and postprandial triglyceride levels in men. J Lipid Res *41*, 1367-1375.

Inagaki, T., Sakai, J., and Kajimura, S. (2016). Transcriptional and epigenetic control of brown and beige adipose cell fate and function. Nat Rev Mol Cell Biol *17*, 480-495.

Ingalls, A.M., Dickie, M.M., and Snell, G.D. (1950). Obese, a new mutation in the house mouse. J Hered *41*, 317-318.

Janochova, K., Haluzik, M., and Buzga, M. (2019). Visceral fat and insulin resistance - what we know? Biomed Pap Med Fac Univ Palacky Olomouc Czech Repub *163*, 19-27.

Jin, H.Y., Gonzalez-Martin, A., Miletic, A.V., Lai, M., Knight, S., Sabouri-Ghomi, M., Head, S.R., Macauley, M.S., Rickert, R.C., and Xiao, C. (2015). Transfection of microRNA Mimics Should Be Used with Caution. Front Genet *6*, 340.

Jin, H.Y., Oda, H., Chen, P., Yang, C., Zhou, X., Kang, S.G., Valentine, E., Kefauver, J.M., Liao, L., Zhang, Y.*, et al.* (2017). Differential Sensitivity of Target Genes to Translational Repression by miR-17~92. PLoS Genet *13*, e1006623.

Jung, E., Seong, Y., Jeon, B., Song, H., and Kwon, Y.S. (2017). Global analysis of AGO2-bound RNAs reveals that miRNAs induce cleavage of target RNAs with limited complementarity. Biochim Biophys Acta Gene Regul Mech *1860*, 1148-1158.

Kamenska, A., Lu, W.T., Kubacka, D., Broomhead, H., Minshall, N., Bushell, M., and Standart, N. (2014). Human 4E-T represses translation of bound mRNAs and enhances microRNA-mediated silencing. Nucleic Acids Res *42*, 3298-3313.

Kamenska, A., Simpson, C., Vindry, C., Broomhead, H., Benard, M., Ernoult-Lange, M., Lee, B.P., Harries, L.W., Weil, D., and Standart, N. (2016). The DDX6-4E-T interaction mediates translational repression and P-body assembly. Nucleic Acids Res *44*, 6318-6334.

Kanke, M., Baran-Gale, J., Villanueva, J., and Sethupathy, P. (2016). miRquant 2.0: an Expanded Tool for Accurate Annotation and Quantification of MicroRNAs and their isomiRs from Small RNA-Sequencing Data. J Integr Bioinform *13*, 307.

Kanter, M. (2018). High-Quality Carbohydrates and Physical Performance: Expert Panel Report. Nutr Today *53*, 35-39.

Karbiener, M., Pisani, D.F., Frontini, A., Oberreiter, L.M., Lang, E., Vegiopoulos, A., Mossenbock, K., Bernhardt, G.A., Mayr, T., Hildner, F.*, et al.* (2014). MicroRNA-26 family is required for human adipogenesis and drives characteristics of brown adipocytes. Stem Cells *32*, 1578-1590.

Katoh, T., Sakaguchi, Y., Miyauchi, K., Suzuki, T., Kashiwabara, S., Baba, T., and Suzuki, T. (2009). Selective stabilization of mammalian microRNAs by 3' adenylation mediated by the cytoplasmic poly(A) polymerase GLD-2. Genes Dev *23*, 433-438.

Kazak, L., Chouchani, E.T., Jedrychowski, M.P., Erickson, B.K., Shinoda, K., Cohen, P., Vetrivelan, R., Lu, G.Z., Laznik-Bogoslavski, D., Hasenfuss, S.C*., et al.* (2015). A creatine-driven substrate cycle enhances energy expenditure and thermogenesis in beige fat. Cell *163*, 643-655.

Kelesidis, T., Kelesidis, I., Chou, S., and Mantzoros, C.S. (2010). Narrative review: the role of leptin in human physiology: emerging clinical applications. Ann Intern Med *152*, 93-100.

Khaodhiar, L., McCowen, K.C., and Blackburn, G.L. (1999). Obesity and its comorbid conditions. Clin Cornerstone *2*, 17-31.

Khvorova, A., Reynolds, A., and Jayasena, S.D. (2003). Functional siRNAs and miRNAs exhibit strand bias. Cell *115*, 209-216.

Kiefer, F.W. (2017). The significance of beige and brown fat in humans. Endocr Connect *6*, R70-R79.

Kim, C., Lee, H., Cho, Y.M., Kwon, O.J., Kim, W., and Lee, E.K. (2013). TNFalpha-induced miR-130 resulted in adipocyte dysfunction during obesity-related inflammation. FEBS Lett *587*, 3853-3858.

Kim, J.B., Sarraf, P., Wright, M., Yao, K.M., Mueller, E., Solanes, G., Lowell, B.B., and Spiegelman, B.M. (1998). Nutritional and insulin regulation of fatty acid synthetase and leptin gene expression through ADD1/SREBP1. J Clin Invest *101*, 1-9.

Kloting, N., Graham, T.E., Berndt, J., Kralisch, S., Kovacs, P., Wason, C.J., Fasshauer, M., Schon, M.R., Stumvoll, M., Bluher, M*., et al.* (2007). Serum retinol-binding protein is more highly expressed in visceral than in subcutaneous adipose tissue and is a marker of intra-abdominal fat mass. Cell Metab *6*, 79-87.

Kmiec, Z., Pokrywka, L., Kotlarz, G., Kubasik, J., Szutowicz, A., and Mysliwski, A. (2005). Effects of fasting and refeeding on serum leptin, adiponectin and free fatty acid concentrations in young and old male rats. Gerontology *51*, 357-362.

Koh, E.H., Chernis, N., Saha, P.K., Xiao, L., Bader, D.A., Zhu, B., Rajapakshe, K., Hamilton, M.P., Liu, X., Perera, D*., et al.* (2018). miR-30a Remodels Subcutaneous Adipose Tissue Inflammation to Improve Insulin Sensitivity in Obesity. Diabetes *67*, 2541-2553.

Krishnan, J., Danzer, C., Simka, T., Ukropec, J., Walter, K.M., Kumpf, S., Mirtschink, P., Ukropcova, B., Gasperikova, D., Pedrazzini, T*., et al.* (2012). Dietary obesity-associated Hif1alpha activation in adipocytes restricts fatty acid oxidation and energy expenditure via suppression of the Sirt2-NAD+ system. Genes Dev *26*, 259-270.

Kristensen, M.M., Davidsen, P.K., Vigelso, A., Hansen, C.N., Jensen, L.J., Jessen, N., Bruun, J.M., Dela, F., and Helge, J.W. (2017). miRNAs in human subcutaneous adipose tissue: Effects of weight loss induced by hypocaloric diet and exercise. Obesity (Silver Spring) *25*, 572-580.

Krol, J., Sobczak, K., Wilczynska, U., Drath, M., Jasinska, A., Kaczynska, D., and Krzyzosiak, W.J. (2004). Structural features of microRNA (miRNA) precursors and their relevance to miRNA biogenesis and small interfering RNA/short hairpin RNA design. J Biol Chem *279*, 42230-42239.

Kuzuoglu-Ozturk, D., Bhandari, D., Huntzinger, E., Fauser, M., Helms, S., and Izaurralde, E. (2016). miRISC and the CCR4-NOT complex silence mRNA targets independently of 43S ribosomal scanning. EMBO J *35*, 1186-1203.

Kwon, H., Lee, J., Jeong, K., Jang, D., and Pak, Y. (2015). Fatty acylated caveolin-2 is a substrate of insulin receptor tyrosine kinase for insulin receptor substrate-1-directed signaling activation. Biochim Biophys Acta *1853*, 1022-1034.

La Rocca, G., Olejniczak, S.H., Gonzalez, A.J., Briskin, D., Vidigal, J.A., Spraggon, L., DeMatteo, R.G., Radler, M.R., Lindsten, T., Ventura, A.*, et al.* (2015). In vivo, Argonaute-bound microRNAs exist predominantly in a reservoir of low molecular weight complexes not associated with mRNA. Proc Natl Acad Sci U S A *112*, 767-772.

Lagos-Quintana, M., Rauhut, R., Lendeckel, W., and Tuschl, T. (2001). Identification of novel genes coding for small expressed RNAs. Science *294*, 853-858.

Lau, N.C., Lim, L.P., Weinstein, E.G., and Bartel, D.P. (2001). An abundant class of tiny RNAs with probable regulatory roles in Caenorhabditis elegans. Science *294*, 858-862.

Lee, P., Greenfield, J.R., Ho, K.K., and Fulham, M.J. (2010). A critical appraisal of the prevalence and metabolic significance of brown adipose tissue in adult humans. Am J Physiol Endocrinol Metab *299*, E601-606.

Lee, R.C., Feinbaum, R.L., and Ambros, V. (1993). The C. elegans heterochronic gene lin-4 encodes small RNAs with antisense complementarity to lin-14. Cell *75*, 843-854.

Lee, Y., Jeon, K., Lee, J.T., Kim, S., and Kim, V.N. (2002). MicroRNA maturation: stepwise processing and subcellular localization. EMBO J *21*, 4663-4670.

Lee, Y., Kim, M., Han, J., Yeom, K.H., Lee, S., Baek, S.H., and Kim, V.N. (2004). MicroRNA genes are transcribed by RNA polymerase II. EMBO J *23*, 4051-4060.

Li, J., Chan, M.C., Yu, Y., Bei, Y., Chen, P., Zhou, Q., Cheng, L., Chen, L., Ziegler, O., Rowe, G.C.*, et al.* (2017a). miR-29b contributes to multiple types of muscle atrophy. Nat Commun *8*, 15201.

Li, Y.L., Li, X., Jiang, T.T., Fan, J.M., Zheng, X.L., Shi, X.E., Yu, T.Y., Chu, G.Y., and Yang, G.S. (2017b). An Additive Effect of Promoting Thermogenic Gene Expression in Mice Adipose-Derived Stromal Vascular Cells by Combination of Rosiglitazone and CL316,243. Int J Mol Sci *18*.

Liang, H., and Ward, W.F. (2006). PGC-1alpha: a key regulator of energy metabolism. Adv Physiol Educ *30*, 145-151.

Liu, W., Bi, P., Shan, T., Yang, X., Yin, H., Wang, Y.X., Liu, N., Rudnicki, M.A., and Kuang, S. (2013). miR-133a regulates adipocyte browning in vivo. PLoS Genet *9*, e1003626.

Lo, J.C., Ljubicic, S., Leibiger, B., Kern, M., Leibiger, I.B., Moede, T., Kelly, M.E., Chatterjee Bhowmick, D., Murano, I., Cohen, P.*, et al.* (2014). Adipsin is an adipokine that improves beta cell function in diabetes. Cell *158*, 41-53.

Lo, K.A., Huang, S., Walet, A.C.E., Zhang, Z.C., Leow, M.K., Liu, M., and Sun, L. (2018). Adipocyte Long-Noncoding RNA Transcriptome Analysis of Obese Mice Identified Lnc-Leptin, Which Regulates Leptin. Diabetes *67*, 1045-1056.

Lord, M.S., Tang, F., Rnjak-Kovacina, J., Smith, J.G.W., Melrose, J., and Whitelock, J.M. (2018). The multifaceted roles of perlecan in fibrosis. Matrix Biol *68-69*, 150-166.

Louloupi, A., and Orom, U.A.V. (2018). Inhibiting Pri-miRNA Processing with Target Site Blockers. Methods Mol Biol *1823*, 63-68.

Lund, E., and Dahlberg, J.E. (2006). Substrate selectivity of exportin 5 and Dicer in the biogenesis of microRNAs. Cold Spring Harb Symp Quant Biol *71*, 59-66.

Lynes, M.D., Leiria, L.O., Lundh, M., Bartelt, A., Shamsi, F., Huang, T.L., Takahashi, H., Hirshman, M.F., Schlein, C., Lee, A.*, et al.* (2017). The cold-induced lipokine 12,13-diHOME promotes fatty acid transport into brown adipose tissue. Nat Med *23*, 631-637.

Mao, L., Liu, S., Hu, L., Jia, L., Wang, H., Guo, M., Chen, C., Liu, Y., and Xu, L. (2018). miR-30 Family: A Promising Regulator in Development and Disease. Biomed Res Int *2018*, 9623412.

Marzi, M.J., Ghini, F., Cerruti, B., de Pretis, S., Bonetti, P., Giacomelli, C., Gorski, M.M., Kress, T., Pelizzola, M., Muller, H.*, et al.* (2016). Degradation dynamics of microRNAs revealed by a novel pulse-chase approach. Genome Res *26*, 554-565.

McCubbrey, A.L., Barthel, L., Mohning, M.P., Redente, E.F., Mould, K.J., Thomas, S.M., Leach, S.M., Danhorn, T., Gibbings, S.L., Jakubzick, C.V.*, et al.* (2018). Deletion of c-FLIP from CD11b(hi) Macrophages Prevents Development of Bleomycin-induced Lung Fibrosis. Am J Respir Cell Mol Biol *58*, 66-78.

McJunkin, K., and Ambros, V. (2017). A microRNA family exerts maternal control on sex determination in C. elegans. Genes Dev *31*, 422-437.

Mignone, F., Gissi, C., Liuni, S., and Pesole, G. (2002). Untranslated regions of mRNAs. Genome Biol *3*, REVIEWS0004.

Miller, S.G., De Vos, P., Guerre-Millo, M., Wong, K., Hermann, T., Staels, B., Briggs, M.R., and Auwerx, J. (1996). The adipocyte specific transcription factor C/EBPalpha modulates human ob gene expression. Proc Natl Acad Sci U S A *93*, 5507-5511.

Min, S.Y., Kady, J., Nam, M., Rojas-Rodriguez, R., Berkenwald, A., Kim, J.H., Noh, H.L., Kim, J.K., Cooper, M.P., Fitzgibbons, T.*, et al.* (2016). Human 'brite/beige' adipocytes develop from capillary networks, and their implantation improves metabolic homeostasis in mice. Nat Med *22*, 312-318.

Miranda, K., Yang, X., Bam, M., Murphy, E.A., Nagarkatti, P.S., and Nagarkatti, M. (2018). MicroRNA-30 modulates metabolic inflammation by regulating Notch signaling in adipose tissue macrophages. Int J Obes (Lond) *42*, 1140-1150.

Misra, A., and Vikram, N.K. (2003). Clinical and pathophysiological consequences of abdominal adiposity and abdominal adipose tissue depots. Nutrition *19*, 457-466.

Monteys, A.M., Spengler, R.M., Wan, J., Tecedor, L., Lennox, K.A., Xing, Y., and Davidson, B.L. (2010). Structure and activity of putative intronic miRNA promoters. RNA *16*, 495-505.

Moore, M.J., Blachere, N.E., Fak, J.J., Park, C.Y., Sawicka, K., Parveen, S., Zucker-Scharff, I., Moltedo, B., Rudensky, A.Y., and Darnell, R.B. (2018). ZFP36 RNA-binding proteins restrain T cell activation and anti-viral immunity. Elife *7*.

Moore, M.J., Scheel, T.K., Luna, J.M., Park, C.Y., Fak, J.J., Nishiuchi, E., Rice, C.M., and Darnell, R.B. (2015). miRNA-target chimeras reveal miRNA 3'-end pairing as a major determinant of Argonaute target specificity. Nat Commun *6*, 8864.

Moore, M.J., Zhang, C., Gantman, E.C., Mele, A., Darnell, J.C., and Darnell, R.B. (2014). Mapping Argonaute and conventional RNA-binding protein interactions with RNA at single-nucleotide resolution using HITS-CLIP and CIMS analysis. Nat Protoc *9*, 263-293.

Moraes-Vieira, P.M., Castoldi, A., Aryal, P., Wellenstein, K., Peroni, O.D., and Kahn, B.B. (2016). Antigen Presentation and T-Cell Activation Are Critical for RBP4-Induced Insulin Resistance. Diabetes *65*, 1317-1327.

Morak, M., Schmidinger, H., Riesenhuber, G., Rechberger, G.N., Kollroser, M., Haemmerle, G., Zechner, R., Kronenberg, F., and Hermetter, A. (2012). Adipose triglyceride lipase (ATGL) and hormone-sensitive lipase (HSL) deficiencies affect expression of lipolytic activities in mouse adipose tissues. Mol Cell Proteomics *11*, 1777-1789.

Mori, M., Nakagami, H., Rodriguez-Araujo, G., Nimura, K., and Kaneda, Y. (2012). Essential role for miR-196a in brown adipogenesis of white fat progenitor cells. PLoS Biol *10*, e1001314.

Mori, M.A., Thomou, T., Boucher, J., Lee, K.Y., Lallukka, S., Kim, J.K., Torriani, M., Yki-Jarvinen, H., Grinspoon, S.K., Cypess, A.M.*, et al.* (2014). Altered miRNA processing disrupts brown/white adipocyte determination and associates with lipodystrophy. J Clin Invest *124*, 3339-3351.

Morris, D.L., and Rui, L. (2009). Recent advances in understanding leptin signaling and leptin resistance. Am J Physiol Endocrinol Metab *297*, E1247-1259.

Mueller, E., Drori, S., Aiyer, A., Yie, J., Sarraf, P., Chen, H., Hauser, S., Rosen, E.D., Ge, K., Roeder, R.G.*, et al.* (2002). Genetic analysis of adipogenesis through peroxisome proliferator-activated receptor gamma isoforms. J Biol Chem *277*, 41925-41930.

Mulyadi, L., Stevens, C., Munro, S., Lingard, J., and Bermingham, M. (2001). Body fat distribution and total body fat as risk factors for microalbuminuria in the obese. Ann Nutr Metab *45*, 67-71.

Nam, H.Y., and Jun, S. (2017). Association between active brown adipose tissue and coronary artery calcification in healthy men. Nuklearmedizin *56*, 184-190.

Nugroho, D.B., Ikeda, K., Kajimoto, K., Hirata, K.I., and Emoto, N. (2018). Activation of neuregulin-4 in adipocytes improves metabolic health by enhancing adipose tissue angiogenesis. Biochem Biophys Res Commun *504*, 427-433.

O'Brien, J., Hayder, H., Zayed, Y., and Peng, C. (2018). Overview of MicroRNA Biogenesis, Mechanisms of Actions, and Circulation. Front Endocrinol (Lausanne) *9*, 402.

Ohno, H., Shinoda, K., Ohyama, K., Sharp, L.Z., and Kajimura, S. (2013). EHMT1 controls brown adipose cell fate and thermogenesis through the PRDM16 complex. Nature *504*, 163-167.

Oliverio, M., Schmidt, E., Mauer, J., Baitzel, C., Hansmeier, N., Khani, S., Konieczka, S., Pradas-Juni, M., Brodesser, S., Van, T.M.*, et al.* (2016). Dicer1-miR-328-Bace1 signalling controls brown adipose tissue differentiation and function. Nat Cell Biol *18*, 328-336.

Olzmann, J.A., and Carvalho, P. (2019). Dynamics and functions of lipid droplets. Nat Rev Mol Cell Biol *20*, 137-155.

Orava, J., Nuutila, P., Noponen, T., Parkkola, R., Viljanen, T., Enerback, S., Rissanen, A., Pietilainen, K.H., and Virtanen, K.A. (2013). Blunted metabolic responses to cold and insulin stimulation in brown adipose tissue of obese humans. Obesity (Silver Spring) *21*, 2279-2287.

Ottaviani, E., Malagoli, D., and Franceschi, C. (2011). The evolution of the adipose tissue: a neglected enigma. Gen Comp Endocrinol *174*, 1-4.

Pan, D., Mao, C., Quattrochi, B., Friedline, R.H., Zhu, L.J., Jung, D.Y., Kim, J.K., Lewis, B., and Wang, Y.X. (2014). MicroRNA-378 controls classical brown fat expansion to counteract obesity. Nat Commun *5*, 4725.

Pan, Y., Hui, X., Hoo, R.L.C., Ye, D., Chan, C.Y.C., Feng, T., Wang, Y., Lam, K.S.L., and Xu, A. (2019). Adipocyte-secreted exosomal microRNA-34a inhibits M2 macrophage polarization to promote obesity-induced adipose inflammation. J Clin Invest *129*, 834-849.

Panee, J. (2012). Monocyte Chemoattractant Protein 1 (MCP-1) in obesity and diabetes. Cytokine *60*, 1-12.

Park, H.K., and Ahima, R.S. (2014). Leptin signaling. F1000Prime Rep *6*, 73.

Park, J.H., and Shin, C. (2014). MicroRNA-directed cleavage of targets: mechanism and experimental approaches. BMB Rep *47*, 417-423.

Patsouris, D., Qi, P., Abdullahi, A., Stanojcic, M., Chen, P., Parousis, A., Amini-Nik, S., and Jeschke, M.G. (2015). Burn Induces Browning of the Subcutaneous White Adipose Tissue in Mice and Humans. Cell Rep *13*, 1538-1544.

Pedersen, S.B., Hansen, P.S., Lund, S., Andersen, P.H., Odgaard, A., and Richelsen, B. (1996). Identification of oestrogen receptors and oestrogen receptor mRNA in human adipose tissue. Eur J Clin Invest *26*, 262-269.

Penzkofer, D., Bonauer, A., Fischer, A., Tups, A., Brandes, R.P., Zeiher, A.M., and Dimmeler, S. (2014). Phenotypic characterization of miR-92a-/- mice reveals an important function of miR-92a in skeletal development. PLoS One *9*, e101153.

Perdikari, A., Leparc, G.G., Balaz, M., Pires, N.D., Lidell, M.E., Sun, W., Fernandez-Albert, F., Muller, S., Akchiche, N., Dong, H.*, et al.* (2018). BATLAS: Deconvoluting Brown Adipose Tissue. Cell Rep *25*, 784-797 e784.

Pinzon, N., Li, B., Martinez, L., Sergeeva, A., Presumey, J., Apparailly, F., and Seitz, H. (2017). microRNA target prediction programs predict many false positives. Genome Res *27*, 234-245.

Planas, A., Clara, A., Pou, J.M., Vidal-Barraquer, F., Gasol, A., de Moner, A., Contreras, C., and Marrugat, J. (2001). Relationship of obesity distribution and peripheral arterial occlusive disease in elderly men. Int J Obes Relat Metab Disord *25*, 1068-1070.

Prostek, A., Gajewska, M., and Balasinska, B. (2016). The influence of eicosapentaenoic acid and docosahexaenoic acid on expression of genes connected with metabolism and secretory functions of ageing 3T3-L1 adipocytes. Prostaglandins Other Lipid Mediat *125*, 48-56.

Qi, C., Surapureddi, S., Zhu, Y.J., Yu, S., Kashireddy, P., Rao, M.S., and Reddy, J.K. (2003). Transcriptional coactivator PRIP, the peroxisome proliferator-activated receptor gamma (PPARgamma)-interacting protein, is required for PPARgamma-mediated adipogenesis. J Biol Chem *278*, 25281-25284.

Qiang, J., Tao, Y.F., He, J., Sun, Y.L., and Xu, P. (2017). miR-29a modulates SCD expression and is regulated in response to a saturated fatty acid diet in juvenile genetically improved farmed tilapia (Oreochromis niloticus). J Exp Biol *220*, 1481-1489.

Qiu, J., Ogus, S., Lu, R., and Chehab, F.F. (2001). Transgenic mice overexpressing leptin accumulate adipose mass at an older, but not younger, age. Endocrinology *142*, 348-358.

Rajakumari, S., Wu, J., Ishibashi, J., Lim, H.W., Giang, A.H., Won, K.J., Reed, R.R., and Seale, P. (2013). EBF2 determines and maintains brown adipocyte identity. Cell Metab *17*, 562-574.

Rebuffe-Scrive, M., Lundholm, K., and Bjorntorp, P. (1985). Glucocorticoid hormone binding to human adipose tissue. Eur J Clin Invest *15*, 267-271.

Reis, F.C., Branquinho, J.L., Brandao, B.B., Guerra, B.A., Silva, I.D., Frontini, A., Thomou, T., Sartini, L., Cinti, S., Kahn, C.R.*, et al.* (2016). Fat-specific Dicer deficiency accelerates aging and mitigates several effects of dietary restriction in mice. Aging (Albany NY) *8*, 1201-1222.

Ricquier, D., and Kader, J.C. (1976). Mitochondrial protein alteration in active brown fat: a soidum dodecyl sulfate-polyacrylamide gel electrophoretic study. Biochem Biophys Res Commun *73*, 577-583.

Roderburg, C., Urban, G.W., Bettermann, K., Vucur, M., Zimmermann, H., Schmidt, S., Janssen, J., Koppe, C., Knolle, P., Castoldi, M.*, et al.* (2011). Micro-RNA profiling reveals a role for miR-29 in human and murine liver fibrosis. Hepatology *53*, 209-218.

Roos, J., Enlund, E., Funcke, J.B., Tews, D., Holzmann, K., Debatin, K.M., Wabitsch, M., and Fischer-Posovszky, P. (2016). miR-146a-mediated suppression of the inflammatory response in human adipocytes. Sci Rep *6*, 38339.

Rosen, E.D., and Spiegelman, B.M. (2014). What we talk about when we talk about fat. Cell *156*, 20-44.

Ross, S.E., Hemati, N., Longo, K.A., Bennett, C.N., Lucas, P.C., Erickson, R.L., and MacDougald, O.A. (2000). Inhibition of adipogenesis by Wnt signaling. Science *289*, 950-953.

Roujeau, C., Jockers, R., and Dam, J. (2014). New pharmacological perspectives for the leptin receptor in the treatment of obesity. Front Endocrinol (Lausanne) *5*, 167.

Runtsch, M.C., Nelson, M.C., Lee, S.H., Voth, W., Alexander, M., Hu, R., Wallace, J., Petersen, C., Panic, V., Villanueva, C.J.*, et al.* (2019). Anti-inflammatory microRNA-146a protects mice from diet-induced metabolic disease. PLoS Genet *15*, e1007970.

Rutledge, H., Baran-Gale, J., de Villena, F.P., Chesler, E.J., Churchill, G.A., Sethupathy, P., and Kelada, S.N. (2015). Identification of microRNAs associated with allergic airway disease using a genetically diverse mouse population. BMC Genomics *16*, 633.

Rytka, J.M., Wueest, S., Schoenle, E.J., and Konrad, D. (2011). The portal theory supported by venous drainage-selective fat transplantation. Diabetes *60*, 56-63.

Sanada, Y., Yamamoto, T., Satake, R., Yamashita, A., Kanai, S., Kato, N., van de Loo, F.A., Nishimura, F., Scherer, P.E., and Yanaka, N. (2016). Serum Amyloid A3 Gene Expression in Adipocytes is an Indicator of the Interaction with Macrophages. Sci Rep *6*, 38697.

Sanuki, R., Onishi, A., Koike, C., Muramatsu, R., Watanabe, S., Muranishi, Y., Irie, S., Uneo, S., Koyasu, T., Matsui, R.*, et al.* (2011). miR-124a is required for hippocampal axogenesis and retinal cone survival through Lhx2 suppression. Nat Neurosci *14*, 1125-1134.

Sassi, Y., Avramopoulos, P., Ramanujam, D., Gruter, L., Werfel, S., Giosele, S., Brunner, A.D., Esfandyari, D., Papadopoulou, A.S., De Strooper, B.*, et al.* (2017). Cardiac myocyte miR-29 promotes pathological remodeling of the heart by activating Wnt signaling. Nat Commun *8*, 1614.

Schaffer, J.E. (2003). Lipotoxicity: when tissues overeat. Curr Opin Lipidol *14*, 281-287.

Scheja, L., and Heeren, J. (2019). The endocrine function of adipose tissues in health and cardiometabolic disease. Nat Rev Endocrinol *15*, 507-524.

Scherer, P.E., Williams, S., Fogliano, M., Baldini, G., and Lodish, H.F. (1995). A novel serum protein similar to C1q, produced exclusively in adipocytes. J Biol Chem *270*, 26746-26749.

Schwartz, D.R., and Lazar, M.A. (2011). Human resistin: found in translation from mouse to man. Trends Endocrinol Metab *22*, 259-265.

Seale, P., Conroe, H.M., Estall, J., Kajimura, S., Frontini, A., Ishibashi, J., Cohen, P., Cinti, S., and Spiegelman, B.M. (2011). Prdm16 determines the thermogenic program of subcutaneous white adipose tissue in mice. J Clin Invest *121*, 96-105.

Seitz, H. (2017). Issues in current microRNA target identification methods. RNA Biol *14*, 831-834.

Shah, A., Qian, Y., Weyn-Vanhentenryck, S.M., and Zhang, C. (2017). CLIP Tool Kit (CTK): a flexible and robust pipeline to analyze CLIP sequencing data. Bioinformatics *33*, 566-567.

Shamsi, F., Zhang, H., and Tseng, Y.H. (2017). MicroRNA Regulation of Brown Adipogenesis and Thermogenic Energy Expenditure. Front Endocrinol (Lausanne) *8*, 205.

Shapira, S.N., and Seale, P. (2019). Transcriptional Control of Brown and Beige Fat Development and Function. Obesity (Silver Spring) *27*, 13-21.

Sharma, A.M., Engeli, S., and Pischon, T. (2001). New developments in mechanisms of obesity-induced hypertension: role of adipose tissue. Curr Hypertens Rep *3*, 152-156.

Shibata, M., Nakao, H., Kiyonari, H., Abe, T., and Aizawa, S. (2011). MicroRNA-9 regulates neurogenesis in mouse telencephalon by targeting multiple transcription factors. J Neurosci *31*, 3407-3422.

Shin, C., Nam, J.W., Farh, K.K., Chiang, H.R., Shkumatava, A., and Bartel, D.P. (2010). Expanding the microRNA targeting code: functional sites with centered pairing. Mol Cell *38*, 789-802.

Siepel, A., Bejerano, G., Pedersen, J.S., Hinrichs, A.S., Hou, M., Rosenbloom, K., Clawson, H., Spieth, J., Hillier, L.W., Richards, S.*, et al.* (2005). Evolutionarily conserved elements in vertebrate, insect, worm, and yeast genomes. Genome Res *15*, 1034-1050.

Skurk, T., Alberti-Huber, C., Herder, C., and Hauner, H. (2007). Relationship between adipocyte size and adipokine expression and secretion. J Clin Endocrinol Metab *92*, 1023-1033.

Smith, R.E., and Horwitz, B.A. (1969). Brown fat and thermogenesis. Physiol Rev *49*, 330-425.

Smith, S., Witkowski, A., and Joshi, A.K. (2003). Structural and functional organization of the animal fatty acid synthase. Prog Lipid Res *42*, 289-317.

Song, R., Walentek, P., Sponer, N., Klimke, A., Lee, J.S., Dixon, G., Harland, R., Wan, Y., Lishko, P., Lize, M.*, et al.* (2014). miR-34/449 miRNAs are required for motile ciliogenesis by repressing cp110. Nature *510*, 115-120.

Spengler, R.M., Zhang, X., Cheng, C., McLendon, J.M., Skeie, J.M., Johnson, F.L., Davidson, B.L., and Boudreau, R.L. (2016). Elucidation of transcriptome-wide microRNA binding sites in human cardiac tissues by Ago2 HITS-CLIP. Nucleic Acids Res *44*, 7120-7131.

Stanford, K.I., Lynes, M.D., Takahashi, H., Baer, L.A., Arts, P.J., May, F.J., Lehnig, A.C., Middelbeek, R.J.W., Richard, J.J., So, K.*, et al.* (2018). 12,13-diHOME: An Exercise-Induced Lipokine that Increases Skeletal Muscle Fatty Acid Uptake. Cell Metab *27*, 1357.

Steppan, C.M., and Lazar, M.A. (2004). The current biology of resistin. J Intern Med *255*, 439-447.

Sun, L., Nicholson, A.C., Hajjar, D.P., Gotto, A.M., Jr., and Han, J. (2003). Adipogenic differentiating agents regulate expression of fatty acid binding protein and CD36 in the J744 macrophage cell line. J Lipid Res *44*, 1877-1886.

Sun, L., Xie, H., Mori, M.A., Alexander, R., Yuan, B., Hattangadi, S.M., Liu, Q., Kahn, C.R., and Lodish, H.F. (2011). Mir193b-365 is essential for brown fat differentiation. Nat Cell Biol *13*, 958-965.

Takanabe, R., Ono, K., Abe, Y., Takaya, T., Horie, T., Wada, H., Kita, T., Satoh, N., Shimatsu, A., and Hasegawa, K. (2008). Up-regulated expression of microRNA-143 in association with obesity in adipose tissue of mice fed high-fat diet. Biochem Biophys Res Commun *376*, 728-732.

Tan, Y., Jin, X.L., Lao, W., Kim, J., Xiao, L., and Qu, X. (2015). Antiresistin RNA Oligonucleotide Ameliorates Diet-Induced Nonalcoholic Fatty Liver Disease in Mice through Attenuating Proinflammatory Cytokines. Biomed Res Int *2015*, 414860.

Tang, X., Zhang, Y., Tucker, L., and Ramratnam, B. (2010). Phosphorylation of the RNase III enzyme Drosha at Serine300 or Serine302 is required for its nuclear localization. Nucleic Acids Res *38*, 6610-6619.

Tchoukalova, Y.D., Votruba, S.B., Tchkonia, T., Giorgadze, N., Kirkland, J.L., and Jensen, M.D. (2010). Regional differences in cellular mechanisms of adipose tissue gain with overfeeding. Proc Natl Acad Sci U S A *107*, 18226-18231.

Thomou, T., Mori, M.A., Dreyfuss, J.M., Konishi, M., Sakaguchi, M., Wolfrum, C., Rao, T.N., Winnay, J.N., Garcia-Martin, R., Grinspoon, S.K.*, et al.* (2017). Adipose-derived circulating miRNAs regulate gene expression in other tissues. Nature *542*, 450-455.

Thompson, B.R., Lobo, S., and Bernlohr, D.A. (2010). Fatty acid flux in adipocytes: the in's and out's of fat cell lipid trafficking. Mol Cell Endocrinol *318*, 24-33.

Thompson, H.J., Sedlacek, S.M., Wolfe, P., Paul, D., Lakoski, S.G., Playdon, M.C., McGinley, J.N., and Matthews, S.B. (2015). Impact of Weight Loss on Plasma Leptin and Adiponectin in Overweight-to-Obese Post Menopausal Breast Cancer Survivors. Nutrients *7*, 5156-5176.

Timper, K., Denson, J.L., Steculorum, S.M., Heilinger, C., Engstrom-Ruud, L., Wunderlich, C.M., Rose-John, S., Wunderlich, F.T., and Bruning, J.C. (2017). IL-6 Improves Energy and Glucose Homeostasis in Obesity via Enhanced Central IL-6 trans-Signaling. Cell Rep *19*, 267-280.

Tong, L. (2005). Acetyl-coenzyme A carboxylase: crucial metabolic enzyme and attractive target for drug discovery. Cell Mol Life Sci *62*, 1784-1803.

Tontonoz, P., Hu, E., Graves, R.A., Budavari, A.I., and Spiegelman, B.M. (1994). mPPAR gamma 2: tissue-specific regulator of an adipocyte enhancer. Genes Dev *8*, 1224-1234.

Toyono, T., Usui, T., Villarreal, G., Jr., Kallay, L., Matthaei, M., Vianna, L.M., Zhu, A.Y., Kuroda, M., Amano, S., and Jun, A.S. (2016). MicroRNA-29b Overexpression Decreases Extracellular Matrix mRNA and Protein Production in Human Corneal Endothelial Cells. Cornea *35*, 1466-1470.

Trajkovski, M., Ahmed, K., Esau, C.C., and Stoffel, M. (2012). MyomiR-133 regulates brown fat differentiation through Prdm16. Nat Cell Biol *14*, 1330-1335.

Treede, I., Braun, A., Jeliaskova, P., Giese, T., Fullekrug, J., Griffiths, G., Stremmel, W., and Ehehalt, R. (2009). TNF-alpha-induced up-regulation of pro-inflammatory cytokines is reduced by phosphatidylcholine in intestinal epithelial cells. BMC Gastroenterol *9*, 53.

Treiber, T., Treiber, N., Plessmann, U., Harlander, S., Daiss, J.L., Eichner, N., Lehmann, G., Schall, K., Urlaub, H., and Meister, G. (2017). A Compendium of RNA-Binding Proteins that Regulate MicroRNA Biogenesis. Mol Cell *66*, 270-284 e213.

Trim, W., Turner, J.E., and Thompson, D. (2018). Parallels in Immunometabolic Adipose Tissue Dysfunction with Ageing and Obesity. Front Immunol *9*, 169.

Vaisse, C., Halaas, J.L., Horvath, C.M., Darnell, J.E., Jr., Stoffel, M., and Friedman, J.M. (1996). Leptin activation of Stat3 in the hypothalamus of wild-type and ob/ob mice but not db/db mice. Nat Genet *14*, 95-97.

van Rooij, E., Sutherland, L.B., Thatcher, J.E., DiMaio, J.M., Naseem, R.H., Marshall, W.S., Hill, J.A., and Olson, E.N. (2008). Dysregulation of microRNAs after myocardial infarction reveals a role of miR-29 in cardiac fibrosis. Proc Natl Acad Sci U S A *105*, 13027-13032.

Varanasi, U., Chu, R., Chu, S., Espinosa, R., LeBeau, M.M., and Reddy, J.K. (1994). Isolation of the human peroxisomal acyl-CoA oxidase gene: organization, promoter analysis, and chromosomal localization. Proc Natl Acad Sci U S A *91*, 3107-3111.

Ventayol, M., Vinas, J.L., Sola, A., Jung, M., Brune, B., Pi, F., Mastora, C., and Hotter, G. (2014). miRNA let-7e targeting MMP9 is involved in adipose-derived stem cell differentiation toward epithelia. Cell Death Dis *5*, e1048.

Villanueva, C.J., Vergnes, L., Wang, J., Drew, B.G., Hong, C., Tu, Y., Hu, Y., Peng, X., Xu, F., Saez, E.*, et al.* (2013). Adipose subtype-selective recruitment of TLE3 or Prdm16 by PPARgamma specifies lipid storage versus thermogenic gene programs. Cell Metab *17*, 423-435.

Wada, T., Kikuchi, J., and Furukawa, Y. (2012). Histone deacetylase 1 enhances microRNA processing via deacetylation of DGCR8. EMBO Rep *13*, 142-149.

Wang, G.X., Zhao, X.Y., and Lin, J.D. (2015). The brown fat secretome: metabolic functions beyond thermogenesis. Trends Endocrinol Metab *26*, 231-237.

Wang, G.X., Zhao, X.Y., Meng, Z.X., Kern, M., Dietrich, A., Chen, Z., Cozacov, Z., Zhou, D., Okunade, A.L., Su, X.*, et al.* (2014). The brown fat-enriched secreted factor Nrg4 preserves metabolic homeostasis through attenuation of hepatic lipogenesis. Nat Med *20*, 1436-1443.

Wang, H., Moyano, A.L., Ma, Z., Deng, Y., Lin, Y., Zhao, C., Zhang, L., Jiang, M., He, X., Ma, Z.*, et al.* (2017). miR-219 Cooperates with miR-338 in Myelination and Promotes Myelin Repair in the CNS. Dev Cell *40*, 566-582 e565.

Wang, N.D., Finegold, M.J., Bradley, A., Ou, C.N., Abdelsayed, S.V., Wilde, M.D., Taylor, L.R., Wilson, D.R., and Darlington, G.J. (1995). Impaired energy homeostasis in C/EBP alpha knockout mice. Science *269*, 1108-1112.

Weisberg, S.P., McCann, D., Desai, M., Rosenbaum, M., Leibel, R.L., and Ferrante, A.W., Jr. (2003). Obesity is associated with macrophage accumulation in adipose tissue. J Clin Invest *112*, 1796-1808.

WHO (2018). Obesity and Overweight. World Health Organization.

Wightman, B., Ha, I., and Ruvkun, G. (1993). Posttranscriptional regulation of the heterochronic gene lin-14 by lin-4 mediates temporal pattern formation in C. elegans. Cell *75*, 855-862.

Wrann, C.D., Eguchi, J., Bozec, A., Xu, Z., Mikkelsen, T., Gimble, J., Nave, H., Wagner, E.F., Ong, S.E., and Rosen, E.D. (2012). FOSL2 promotes leptin gene expression in human and mouse adipocytes. J Clin Invest *122*, 1010-1021.

Yang, W.M., Jeong, H.J., Park, S.Y., and Lee, W. (2014). Induction of miR-29a by saturated fatty acids impairs insulin signaling and glucose uptake through translational repression of IRS-1 in myocytes. FEBS Lett *588*, 2170-2176.

Ye, L., Wu, J., Cohen, P., Kazak, L., Khandekar, M.J., Jedrychowski, M.P., Zeng, X., Gygi, S.P., and Spiegelman, B.M. (2013). Fat cells directly sense temperature to activate thermogenesis. Proc Natl Acad Sci U S A *110*, 12480-12485.

Ying, W., Riopel, M., Bandyopadhyay, G., Dong, Y., Birmingham, A., Seo, J.B., Ofrecio, J.M., Wollam, J., Hernandez-Carretero, A., Fu, W*., et al.* (2017). Adipose Tissue Macrophage-Derived Exosomal miRNAs Can Modulate In Vivo and In Vitro Insulin Sensitivity. Cell *171*, 372-384 e312.

Yun, U.J., Song, N.J., Yang, D.K., Kwon, S.M., Kim, K., Kim, S., Jo, D.G., Park, W.J., Park, K.W., and Kang, H. (2015). miR-195a inhibits adipocyte differentiation by targeting the preadipogenic determinator Zfp423. J Cell Biochem *116*, 2589-2597.

Zarnegar, B.J., Flynn, R.A., Shen, Y., Do, B.T., Chang, H.Y., and Khavari, P.A. (2016). irCLIP platform for efficient characterization of protein-RNA interactions. Nat Methods *13*, 489-492.

Zhang, X.M., Wang, L.H., Su, D.J., Zhu, D., Li, Q.M., and Chi, M.H. (2016). MicroRNA-29b promotes the adipogenic differentiation of human adipose tissue-derived stromal cells. Obesity (Silver Spring) *24*, 1097-1105.

Zhang, Y., Dallner, O.S., Nakadai, T., Fayzikhodjaeva, G., Lu, Y.H., Lazar, M.A., Roeder, R.G., and Friedman, J.M. (2018). A noncanonical PPARgamma/RXRalpha-binding sequence regulates leptin expression in response to changes in adipose tissue mass. Proc Natl Acad Sci U S A *115*, E6039-E6047.

Zhang, Y., Li, H., Cao, R., Sun, L., Wang, Y., Fan, S., Zhao, Y., Kong, D., Cui, L., Lin, L*., et al.* (2017). Suppression of miR-708 inhibits the Wnt/beta-catenin signaling pathway by activating DKK3 in adult B-all. Oncotarget *8*, 64114-64128.

Zhang, Y., Proenca, R., Maffei, M., Barone, M., Leopold, L., and Friedman, J.M. (1994). Positional cloning of the mouse obese gene and its human homologue. Nature *372*, 425-432.

Zhou, H., and Rigoutsos, I. (2014). MiR-103a-3p targets the 5' UTR of GPRC5A in pancreatic cells. RNA *20*, 1431-1439.

Zhou, S., Lei, D., Bu, F., Han, H., Zhao, S., and Wang, Y. (2019). MicroRNA-29b-3p Targets SPARC Gene to Protect Cardiocytes against Autophagy and Apoptosis in Hypoxic-Induced H9c2 Cells. J Cardiovasc Transl Res *12*, 358-365.

Zhou, Y., and Rui, L. (2013). Leptin signaling and leptin resistance. Front Med *7*, 207-222.

Ziegler, A.K., Damgaard, A., Mackey, A.L., Schjerling, P., Magnusson, P., Olesen, A.T., Kjaer, M., and Scheele, C. (2019). An anti-inflammatory phenotype in visceral adipose tissue of old lean mice, augmented by exercise. Sci Rep *9*, 12069.

Zisoulis, D.G., Kai, Z.S., Chang, R.K., and Pasquinelli, A.E. (2012). Autoregulation of microRNA biogenesis by let-7 and Argonaute. Nature *486*, 541-544.